1 **Radiation Belt Radial Diffusion at Earth and Beyond**

2 Solène Lejosne[1] and Peter Kollmann[2]

3

4   1. Space Sciences Laboratory, University of California, Berkeley, CA, USA
5   2. Johns Hopkins University, Applied Physics Laboratory, 11100 Johns Hopkins Road,
6   Laurel, MD 20723-6099, USA.

7 Corresponding author: solene@berkeley.edu

8

9 ORCID LEJOSNE: 0000-0003-4238-8579
10 ORCID KOLLMANN: 0000-0002-4274-9760

11

12 **ABSTRACT**

13 The year 2019 marks the 60th anniversary of the concept of radial diffusion in magnetospheric
14 research. This makes it one of the oldest research topics in radiation belt science. While first
15 introduced to account for the existence of the Earth's outer belt, radial diffusion is now applied
16 to the radiation belts of all strongly magnetized Planets.
17 But for all its study and application, radial diffusion remains an elusive process. As the
18 theoretical picture evolved over time, so too did the definitions of various related concepts, such
19 as the notion of radial transport. Whether data is scarce or not, doubts in the efficacy of the
20 process remain because of the use of various unchecked assumptions. As a result, quantifying
21 radial diffusion still represents a major challenge to tackle in order to advance our understanding
22 and abilities to model radiation belt dynamics.
23 The core objective of this review is to address the confusion that emerges from the coexistence
24 of various definitions for radial diffusion, and to highlight the complexity and subtleties of the
25 problem. To contextualize, we provide an historical perspective on radial diffusion research: why
26 and how the concept of radial diffusion was introduced at Earth, how it evolved, and how it was
27 transposed to the radiation belts of the Giant Planets. Then, we discuss the necessary theoretical
28 tools to unify the evolving image of radial diffusion, to describe radiation belt drift dynamics,
29 and to carry contemporary radial diffusion research.

30

31 **KEYWORDS**

34

35 **ACKNOWLEDGEMENTS**

TABLE OF CONTENTS

123 **FREQUENTLY USED SYMBOLS**
124

125	α	local pitch angle
126	α_{eq}	pitch angle at the magnetic equator
127	$\boldsymbol{A}$	magnetic vector potential
128	A	proportionality coefficient for the asymmetry of the disturbance magnetic field $\boldsymbol{b}$
129	$\boldsymbol{b}$	disturbance magnetic field
130	$\mathcal{b}$	geocentric stand-off distance to the subsolar point on the magnetopause
131	$\boldsymbol{B}$	magnetic field
132	ΔB	asymmetric perturbation of the dipole field, in the model of Fei et al (2006)
133	B_E , B_P	magnetic equatorial field at the surface of the Earth (E) or the planet (P)
134	B_d	amplitude of the dipole field
135	B_m	magnetic field at the mirror point
136	c	speed of light in vacuum
137	D_1, D_2, D_{ij}	Fokker-Planck coefficients
138	D_{LL}	radial diffusion coefficient
139	$D_{LL,m}$	D_{LL} due to magnetic fluctuations, including the effect of the induced electric fields
140	$D_{LL,b}$	D_{LL} due to magnetic fluctuations, in the absence of any kind of electric fields
141	$D_{LL,e}$	D_{LL} due to electric potential fluctuations
142	$D_{LL,\epsilon}$	D_{LL} due to electric field fluctuations, regardless of their nature
143	ds	infinitesimal displacement along a field line
144	dl	infinitesimal displacement along a guiding drift contour (Γ)
145	ε	total energy of the guiding center (kinetic and potential)
146	E_o	rest mass energy (511 keV for an electron, 938 MeV for a proton)
147	$\boldsymbol{E}$	electric field
148	$\boldsymbol{E_{ind}}$	induced rotational electric field
149	η	flux tube content per magnetic flux
150	f, f_o, F	drift-averaged distribution functions; different notations correspond to different
151		set of variables: $f(J_1, J_2, J_3, t)$; $f_o(M, J, L, t)$; $F(M, J, \Phi, t)$
152	φ	magnetic local time
153	Φ	magnetic flux through a particle drift shell; proportional to J_3
154	γ	Lorentz factor
155	Γ	guiding drift contour
156	$\Gamma(\alpha_{eq})$	pitch angle factor for $D_{LL,m}$ ($\Gamma(\alpha_{eq}) = D_{LL,m}/D_{LL,m,eq}$)
157	H	Hamiltonian function
158	I	geometric integral ($= J/2p$)
159	J	second adiabatic invariant
160	J_3	third adiabatic invariant
161	(J_i, φ_i)	action-angle variables associated with the ith quasi-periodic motion (1$^{\text{st}}$: gyration;
162		2$^{\text{nd}}$: bounce; 3$^{\text{rd}}$: drift)
163	K	adiabatic constant ($=I\sqrt{B_m}$)

164	Kp	3-hour geomagnetic activity index
165	Λ	quantity approx. conserved in case of strong pitch angle scattering ($=p^3 \oint ds/B$)
166	L	normalized equatorial radial distance
167	L^*	Roederer's parameter (proportional to $1/\Phi$)
168	M	first adiabatic invariant
169	m_o	particle rest mass
170	$N, d\mathcal{N}$	number of particles
171	n	particle number density
172	r	radial distance
173	r_0	unperturbed equatorial radius of a drift contour
174	ν	drift frequency ($= \Omega/2\pi$)
175	Ω	angular drift velocity
176	$\boldsymbol{p}$	particle momentum
177	$\boldsymbol{p}_\perp, p_\parallel$	$\boldsymbol{p}$ components perpendicular ($\perp$) and parallel ($\parallel$) to the magnetic field direction
178	P	transition probability – for example from J_3 to $J_3 + \Delta J_3$
179	P_X	power spectrum of the signal X
180	Π	probability
181	q	electric charge of a particle
182	R_E, R_P	Earth/planetary equatorial radius
183	S	proportionality coefficient for the symmetry of the disturbance magnetic field $\boldsymbol{b}$
184	Σ	height-integrated Pedersen conductivity
185	θ	magnetic colatitude
186	$t, \Delta t$	time, time interval
187	τ_C	characteristic time for the variation of the fields
188	τ_G	gyration period
189	τ_B	bounce period
190	τ_D	drift period
191	T, E, W	kinetic energy of the guiding center
192	U	electrostatic potential
193	$\boldsymbol{V_D}$	bounce-averaged drift velocity
194	V_L	dL^*/dt: bounce-averaged Lagrangian velocity of the guiding center in L^*
195	$[\ ]$	square brackets = expected value (average value) of the bracketed quantity
196	$\langle\ \rangle$	angle brackets = average change per unit time of the bracketed quantity
197	$\sim$	symbol for "approximately equal"
198	$\propto$	symbol for "directly proportional"
199		

200 **1.   MOTIVATION**

201

202 1.1.   What is radial diffusion, and why this review?

203

204 *Radial diffusion in a nutshell*

205 If trapped radiation belt particles were experiencing constant magnetic and electric fields, they

206 would stay at a constant average equatorial distance from the planet. In reality, radiation belt

207 particles are constantly moving radially, towards or away from the planet, due to electric and

208 magnetic field fluctuations. The individual path of a particle is similar to that of a random walk,

209 and the net movement of the radiation belt population can be described by a diffusion equation.

210 Thus, radial diffusion itself is not an actual physical mechanism. It is instead a mathematical

211 formalism that describes the average outcome of various physical processes during which time-

212 varying fields transfer energy to and from charged particles. Radial diffusion therefore plays not

213 only a role in explaining the observed spatial distribution of radiation belt particles in space but

214 also in explaining their acceleration to high energies.

215

216 The concept of radial diffusion was introduced during the year following the discovery of the

217 Earth's radiation belts (Van Allen and Frank 1959) in order to explain their existence. It was then

218 transposed to the radiation belts of other magnetized planets, partly even before in-situ

219 measurements became available (Mead and Hess 1973; Van Allen et al. 1980a).

220

221 *Why a review on radial diffusion?*

222 Once viewed as the most important acceleration mechanism for the Earth's radiation belts, radial

223 diffusion remains an elusive process despite many years of research. Doubts upon the efficacy of

224 the radial diffusion process remain. Various definitions exist. There is a variety of analytic

225 expressions to quantify radial diffusion present in the literature. The role played by the different

226 possible drivers of radial diffusion remains uncertain. For all these reasons, advancing radial

227 diffusion research constitutes a major scientific challenge to tackle in order to guarantee further

228 progress in our abilities to understand and to model radiation belt dynamics.

229

230 In this review, we present the motives underlying the developments of different radial diffusion

231 models. We describe the methods developed over the years to quantify radial diffusion. We also

232 provide the necessary theoretical tools to better navigate radial diffusion research; the interested

233 reader may want to refer to this special section (**Section 5**) when necessary.

234

235 *Outline of the review*

236 1. **Section 1** is the "MOTIVATION" Section. In the remainder of this section, the importance

237   of radial diffusion research is detailed.

238 2. **Section 2** is the "FOUNDATION" Section. It deals with early works on radial diffusion.

239   After a brief introduction of adiabatic invariant theory, the section presents the variety of

240   observations that led to the introduction of the concept of radial diffusion. The early

241   theoretical picture of the radial diffusion process at Earth is discussed, together with the

242   seminal work of Fälthammar (1965). This includes a derivation of the radial diffusion
243   equation (equation 2-30). Pioneering methods for quantifying radial diffusion coefficients are
244   also presented.
245   3.   **Section 3** is the "EXPANSION" Section. It deals with radial diffusion at the Outer Planets.
246   While some of the concrete diffusion drivers may be different to Earth, the general physics is
247   the same and can be studied well because the different configuration of Outer Planet
248   radiation belts allows the formation and observation of diffusion signatures that are not
249   obvious at Earth.
250   4.   **Section 4** is the "EVOLUTION" Section. It deals with the latest developments in radial
251   diffusion research at Earth. In particular, the new sets of formulas proposed by Fei et al.
252   (2006) to describe similar drivers as in **Section 2.3** are introduced and discussed.
253   5.   **Section 5** is the "NAVIGATION" Section. It provides the necessary theoretical toolkit to
254   address radial diffusion research. It introduces the third adiabatic invariant and discusses
255   mechanisms leading to its violation (that is, physical processes at the heart of radial
256   diffusion). This section also discusses when radial diffusion can be viewed as a pragmatic
257   approximation and when it offers an acceptable description of planetary environments.
258   6.   **Section 6** is the "CONCLUSION" Section. A summary of the key points of this review is
259   provided, together with a discussion of some of the challenges associated with modern radial
260   diffusion research.

261

262   *Scope of the review*
263 This review deals with the statistical description of cross drift shell motion for trapped radiation
264 belt populations that conserve the first two adiabatic invariants (a definition of the concepts of
265 adiabatic invariants and drift shell is provided **Section 2.1** and **Section 5.1**). While there exist
266 some "anomalous" and "neoclassical" radial diffusion processes, they require violation of one or
267 two of the first two adiabatic invariants (because they are driven by a combination of pitch angle
268 scattering and shell splitting – e.g., Roederer and Schulz 1969; O'Brien 2014; Cunningham et al.
269 2018). These processes are out of the scope of the review.

270

271   1.2.   Why radial diffusion research?

272

273   1.2.1.   Scientific challenge

274

275 Radiation belt dynamics is governed by a variety of concurrent source and loss processes whose
276 individual contributions are difficult to evaluate (e.g., Walt 1996). Radial diffusion acts both as a
277 source and a loss mechanism as it redistributes trapped particles throughout a magnetosphere
278 depending on the overall radial distribution (see also **Section 2.3.2**). Thus, uncertainty in the
279 amplitude of radial diffusion leads to uncertainty in the relative contribution of other processes to
280 the observed particle distribution.

281

282 Take for example the formation of a narrow third Earth's radiation belt at ultra-relativistic
283 energies in 2012, which led to scientific controversy. The creation of this third radiation belt was

284 first explained in terms of losses to the magnetopause by radial diffusion, combined with
285 scattering into the Earth's atmosphere by electromagnetic ion cyclotron waves (Shprits et al.
286 2013). A competing explanation later claimed that losses to the magnetopause by radial diffusion
287 were the only necessary mechanism to create the third radiation belt (Mann et al. 2016), and led
288 to a series of rebuttals (Shprits et al. 2018; Mann et al. 2018).
289
290 More importantly, radial diffusion toward the Earth from an external source was originally
291 thought to be the dominant acceleration mechanism for the radiation belts. Subsequent
292 observations of local peaks in the radial profiles of electron phase space density brought about a
293 paradigm shift (see also **Section 2.3.2**). As a result, most recent works now consider that internal
294 local acceleration prevails in the Earth's radiation belts (e.g. Thorne 2010). Local acceleration
295 was also suggested to apply to the Giant Planets (Woodfield et al. 2014, 2018). Yet,
296 observational evidence demonstrated the importance of radial diffusion for accelerating particles
297 at Jupiter and Saturn (Kollmann et al. 2018). Also at Earth, the debate continues (e.g., Su et al.
298 2015). Radial diffusion and local acceleration are in a "battle royale" (Jaynes et al. 2018a) for the
299 title of dominant acceleration mechanism.
300
301 In order to reach a careful understanding about the physics of a magnetosphere, evaluation of all
302 the different mechanisms at play is required and this includes radial diffusion. Without
303 considering all processes, it is impossible to resolve the different controversies surrounding
304 radiation belt dynamics.
305

306 1.2.2. Space weather challenge
307
308 Radial diffusion plays a central role in a complex set of physical processes that determine the
309 structure, intensity and variability of the radiation environment through which satellites must
310 operate. Inability to accurately specify and forecast energetic radiation belt particles hampers our
311 ability to use technological systems in space.
312
313 Indeed, the Earth's radiation belts with their "killer" electrons at relativistic energies pose serious
314 threats to spacecraft, such as internal charging hazards (e.g., Horne et al. 2013). Energetic ions
315 cause displacement damage in semiconductor devices. All radiation pose total dose hazards over
316 the lifetime of a spacecraft. Yet, as our society relies more and more on space systems (for
317 crucial purposes such as communication, navigation, Earth observation, defense, timing signals,
318 etc.), the number of satellites flying within or through the Earth's radiation belts is constantly
319 increasing. In addition, the increased use of electric propulsion means that spacecraft spend more
320 time in the heart of the belts – they need a few months after launch to reach geostationary orbit,
321 compared to a few days in the traditional case of chemical propulsion (e.g., Horne and Pitchford
322 2015).
323
324 Reliable and cost-effective spacecraft design requires good knowledge of the radiation
325 environment (e.g., Xapsos et al. 2013). Radiation drives the requirements for spacecraft and
326 scientific instruments orbiting Earth as well as the Outer Planets. In particular, the spacecraft

327   design community needs a specification of the mean and worst-case radiation environments in
328   which the satellites will operate (O'Brien et al. 2013). These requirements can be determined by
329   empirical models based on a compilation of data from prior missions (e.g., Sawyer and Vette
330   1976; Vette 1991; O'Brien et al. 2018) and physics-based numerical simulations (e.g., Maget et
331   al. 2007; Maget et al. 2008; Glauert et al. 2018; Horne et al. 2018). However, empirical models
332   rely on samples with limited accuracy and limited coverage (in space, time, energy, etc.). A
333   common way to alleviate this difficulty is to combine data analysis with physical models. One of
334   the benefits of theoretical modeling is that it can reconstruct a complete picture of the space
335   environment based on sparse experimental information. In addition, physics-based models can
336   reproduce realistic dynamics for the radiation belts, including the effects of geomagnetic storms.
337   This feature is particularly helpful for post-event analysis, when spacecraft that are not
338   necessarily equipped with sensors to monitor their local environment report anomalies during the
339   course of a mission (e.g., Green et al. 2017).
340
341   *Diffusion-driven models as a solution*
342   In order to minimize the computational resources required and the execution time of the codes,
343   many physics-based models rely on the adiabatic theory of magnetically trapped particles
344   (introduced **Section 2.1**) in order to reduce the number of variables to handle. Rather than
345   focusing on the dynamics of individual particles, they solve a diffusion equation to describe the
346   average variations of distribution functions – quantities that relate directly to particle flux
347   measurements (e.g., Beutier and Boscher 1995; Subbotin and Shprits 2009; Su et al. 2010; Tu et
348   al. 2013; Glauert et al. 2014). The same models, appropriately modified, have also been used to
349   study the radiation belts of Jupiter (e.g., Santos-Costa and Bourdarie 2001; Woodfield et al.
350   2014; Nénon et al. 2017, 2018) and Saturn (Santos-Costa et al. 2003; Lorenzato et al. 2012;
351   Clark et al. 2014; Woodfield et al. 2018). Simpler but still diffusion-driven models have also
352   been applied to Uranus and Neptune (Selesnick and Stone 1991, 1994; Richardson 1993).
353
354   One of the objectives of radial diffusion research is to generate the radial diffusion coefficients
355   that appear in the corresponding diffusion equation. These coefficients are core inputs required
356   by the physics-based models to develop realistic radiation belt dynamics. Therefore, an accurate
357   evaluation of these coefficients is paramount.
358
359   The most commonly used radial diffusion coefficients for the Earth's radiation belts are the ones
360   proposed by Brautigam and Albert (2000) and by Ozeke et al. (2014). Because both formulations
361   are simple functions of location and magnetic activity, their use is straightforward. (See also
362   **Sections 2.4.2** and **4.3** for information about the formulas by Brautigam and Albert (2000) and
363   by Ozeke et al. (2014), respectively). For the Giant Planets, the diffusion coefficient is
364   commonly parameterized as a power law in distance with exponents based either on the theory
365   by Brice and McDonough (1973) or on fits to observations (**Section 3.2**). In all cases, doubts
366   remain as to the validity of these parameterizations.
367
368   In effect, different works have yielded different values for the radial diffusion coefficients and
369   still today the scattering among all possible values spans several orders of magnitude (e.g., Walt

370   1971a, Fig. 6; Tomassian et al. 1972, Fig. 7; Mogro-Campero 1976; Van Allen 1984, Tab. III;
371   Roussos et al. 2007, Fig. 9; Huang 2010, Fig. 6). While physical arguments can help explain part
372   of this radial diffusion coefficient variability (**Section 2.4.2**), determining the most suitable
373   coefficients to use in diffusion-driven models remains a challenge.
374
375

376   **2.   FOUNDATION: What are the origins of radial diffusion research?**
377
378   Before presenting experimental evidence of radiation belt radial diffusion at Earth and at the
379   Giant Planets, we briefly introduce the adiabatic theory of magnetically trapped particles in the
380   first part of this Section. Additional information is provided **Section 5.1.1**.
381

382   2.1.   Brief introduction to the adiabatic theory of magnetically trapped particles
383
384   Planetary radiation belts are formed of energetic charged particles with energies on the order of
385   MeV. These particles are trapped in the planetary magnetic field, where they undergo three
386   forms of quasi-periodic motion on three very distinct timescales: (1) a fast gyration about a field
387   line, (2) a slower bounce motion along the field line, and (3) a slow drift motion around the
388   planet (e.g., Schulz and Lanzerotti 1974; Walt 1994; Roederer and Zhang 2014; see also the
389   illustration **Fig. 11a Section 5.1**). The magnitude of each of these three periodicities is
390   characterized by an adiabatic coordinate (e.g. Northrop 1963; Roederer 1967). The fundamental
391   temporal condition for conservation of an adiabatic coordinate is that the time variations of the
392   fields are negligible on the timescale of the corresponding quasi-periodic motion.
393
394   The first adiabatic coordinate M is associated with gyro-motion. It is equal to
395

$$M = \frac{p_\perp^2}{2m_o B} \tag{2-1}$$

396

397   where m_o is the particle rest mass, B is the local magnetic field, $p = \sqrt{T^2 + 2Tm_o c^2}/c$ is the
398   relativistic momentum, T is the kinetic energy, $p_\perp = p \sin \alpha$ and $p_\parallel = p \cos \alpha$ are the
399   components of the momentum $\boldsymbol{p}$ perpendicular and parallel to the magnetic field vector,
400   respectively, and α is the local pitch angle between the particle velocity and the local magnetic
401   field. The first adiabatic coordinate M is sometimes called magnetic moment but it is only equal
402   to the magnetic moment resulting from the gyro-motion in the non-relativistic case.
403
404   The second adiabatic coordinate J is associated with bounce motion. It is equal to
405

$$J = \oint p_\parallel ds \tag{2-2}$$

406

407   The integral goes over the full bounce motion along the magnetic field line, and ds is an element
408   of arc of the field line.

409

410   Because all particles bounce through the equatorial plane while only particles with small pitch
411   angles between their velocity and the magnetic field reach to high latitudes of the planet,
412   radiation belt intensities are highest in roughly toroidal regions around a planet, the radiation
413   belts.

414

415   When the relativistic momentum p is conserved, it is easier to calculate numerically other
416   quantities that are equivalent to the adiabatic invariants M and J. These adiabatic constants are
417   the magnetic field at the mirror point $B_m = p^2/(2m_o M)$, the geometric integral $I = J/(2p)$
418   and/or the quantity $K = I\sqrt{B_m}$ (e.g., Roederer 1970, p.50).

419

420   In the case of strong pitch angle scattering, under which neither M nor J are conserved, it can be
421   useful to consider that the quantity $\Lambda = p^3 \oint ds/B$ is approximately conserved (Schulz 1998).
422   Strong pitch angle scattering is common for electrons in high intensity regions at most
423   magnetized planets (Mauk 2014).

424

425   The third adiabatic coordinate is associated with drift motion. The drift velocity $\boldsymbol{V_D}$ of a radiation
426   belt particle (q, M, J) is a function of both electric and magnetic fields. For instance in the case of
427   equatorial particles $\left(\alpha_{eq} = 90°\right)$ the drift velocity of the guiding center $(q, M, J = 0)$ is equal to

428

$$\boldsymbol{V_D} = \frac{-M\boldsymbol{\nabla} B \times \boldsymbol{B}}{\gamma q B^2} + \frac{\boldsymbol{E} \times \boldsymbol{B}}{B^2} \qquad (2\text{-}3)$$

429

430   In the Earth's radiation belts, the electric drift velocity is typically very small in comparison with
431   the magnetic drift velocity

432

$$\left|\frac{\boldsymbol{E} \times \boldsymbol{B}}{B^2}\right| \ll \left|\frac{M\boldsymbol{\nabla} B \times \boldsymbol{B}}{\gamma q B^2}\right| \qquad (2\text{-}4)$$

433

434   Thus, the total guiding-center drift velocity is often approximated by the value of the magnetic
435   drift velocity. This zeroth-order approximation is not valid anymore in the radiation belts of the
436   Giant Planets (because the corotation electric drift is larger at the Giant Planets – see also
437   **Section 3.1.3**).

438

439   The third adiabatic invariant J_3 is inversely proportional to the parameter L^*, as will be discussed
440   in **Section 5.1.1**. L^* is often approximated by the coordinate L, which corresponds to the radial
441   distance of a dipole magnetic field line at the magnetic equator. The pitfalls of such
442   approximation will be highlighted **Section 2.3** and **Section 5.1**.

443

444   If the magnetic and electric field around a planet were stationary, the particles would follow a
445   deterministic motion. The guiding centers would maintain the same average radial distance to the

446 planet and they would evolve along unchanging closed surfaces called *drift shells* with constant
447 energy (see also the illustration **Fig. 11 Section 5.1**). Random fluctuations in the field on the
448 timescale of the radiation belt particle drift period around the planet add a random velocity
449 component and their average effects can be described through radial diffusion.
450
451 *Adiabatic vs non-adiabatic*
452 In this review, we call "adiabatic" the conditions that conserve all three adiabatic invariants,
453 while "non-adiabatic" refers to conditions that violate at least one of the three adiabatic
454 invariants. Because the third adiabatic invariant is associated with the slowest of the three forms
455 of quasi-periodic motion (the drift motion), it is most likely to be violated (much faster variations
456 are required to violate the first or the second invariants).
457
458 It is useful to notice that in order to conserve M, $p_\perp$ will have to change when the local magnetic
459 field experienced by the particle is changed. It is important to understand that changes in B are
460 not equivalent to changes in L^* or the third invariant. The magnetic field (at any point on the field
461 line) can change along a drift shell and the drift shell can change shape over time, even while all
462 invariants are conserved, see discussion in **Section 5.1.2**.
463 For scientific analysis it is often useful to study if measurements are consistent with conservation
464 of invariants, which requires to convert between the native coordinates of the measurement,
465 energy T and pitch angle α, to the more physically meaningful adiabatic coordinates (e.g.
466 Roederer and Lejosne 2018). The calculation of invariants from T, α, and spacecraft location
467 requires an assumed global electromagnetic field model but is otherwise straightforward through
468 the explicit equations provided above and in **Section 5.1.2**. More difficult is the other direction,
469 where we select adiabatic coordinates and want to calculate the equivalent T, α, and location.
470 There is usually no explicit analytic expression for this but the solution can be done numerically
471 or through a lookup table. What is usually found is that particles with pitch angles mirroring
472 close to the magnetic equator change their energy faster for the same B-change at the magnetic
473 equator than particles bouncing to high latitudes, assuming that they conserve at least the first
474 two invariants. The energy change is weaker for relativistic particles. There is also a change in
475 pitch angle for non-equatorial particles when B is changing. α becomes more equatorial in higher
476 B, but this effect is minor in comparison to near equatorially mirroring particles. Thus, it is
477 primarily the difference in the energy change that will modify an initial pitch angle distribution
478 at constant energy (as is the native measurement) when the magnetic field is changing.
479
480 2.2.   First experimental evidence of radiation belt radial diffusion
481
482 2.2.1. Existence of the Earth's outer belt
483
484 Radial diffusion was first introduced to account for the existence of the Earth's outer radiation
485 belt, and characteristic signatures of a process slow enough to conserve the first two adiabatic
486 invariants (equations (2-1) and (2-2)) were found in energetic particle measurements.
487

488   MeV neutrons resulting from the disintegration of atmospheric nuclei struck by GeV cosmic rays
489   can decay in flight while still within the Earth's (or any other planet's) magnetic field, producing
490   energetic electrons and protons. This mechanism, known as cosmic ray albedo neutron decay
491   (CRAND), was first proposed to account for the existence of the Earth's radiation belts (Singer
492   1958; Vernov 1959; Kellogg 1959a). CRAND is still thought to be the major source of Saturn's
493   proton belts (Kollmann et al. 2017; Roussos et al. 2018; Cooper and Sturner 2018). Yet, it was
494   soon realized that CRAND could not sustain the high intensity of Earth's outer belt. Radial
495   diffusion was introduced as another possible source process for the outer belt (Kellogg 1959b).
496
497   A few years later, Explorer 14 measurements reported systematic inward motion of the inner side
498   of the peak of equatorial electron intensities ($E \geq 1.6$ MeV) for several weeks of geomagnetic
499   quiet time following the magnetic storm of December 17-18, 1962 (**Fig. 1**). These data provided
500   the first experimental evidence of radial diffusion in the Earth's outer belt (Frank et al. 1964;
501   Frank 1965; Newkirk and Walt 1968a).
502
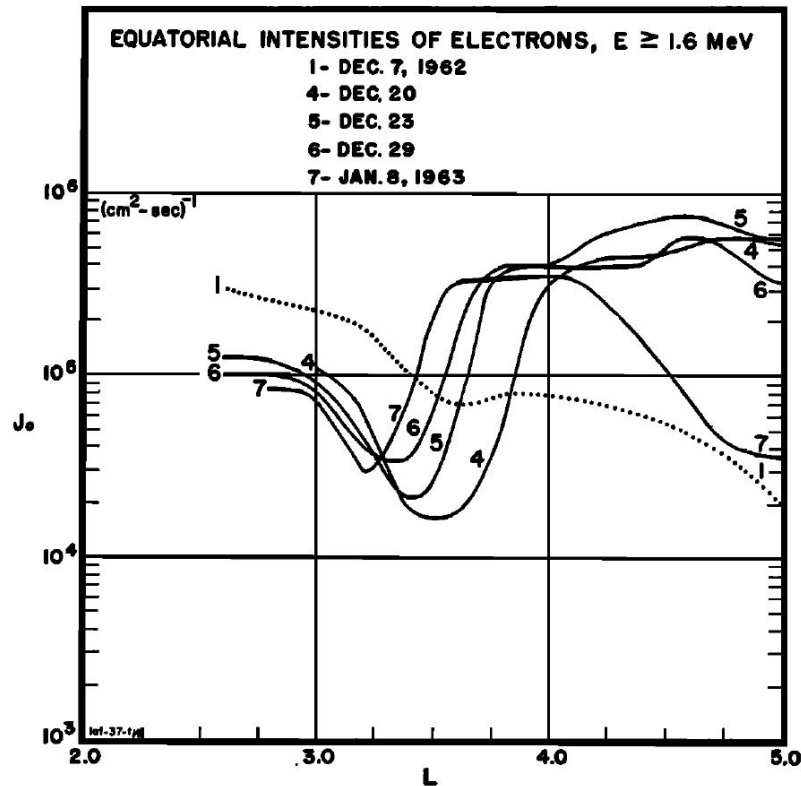
503
504
505   **Fig. 1** The apparent inward motion of energetic electrons ($E \geq 1.6$ MeV) measured by Explorer
506   14 during a geomagnetically quiet time following the magnetic storm of December 17-18, 1962.
507   Newkirk and Walt (1968a) showed that this apparent radial motion was similar to that expected
508   from diffusion by violation of the third adiabatic invariant (Frank et al. 1964)
509

510 A model-observation comparison for the average proton fluxes of the outer belt further supported
511 the idea that radial diffusion is a primary source process for the Earth's outer belt (**Fig. 2;**
512 Nakada et al. 1965; Nakada and Mead 1965).
513
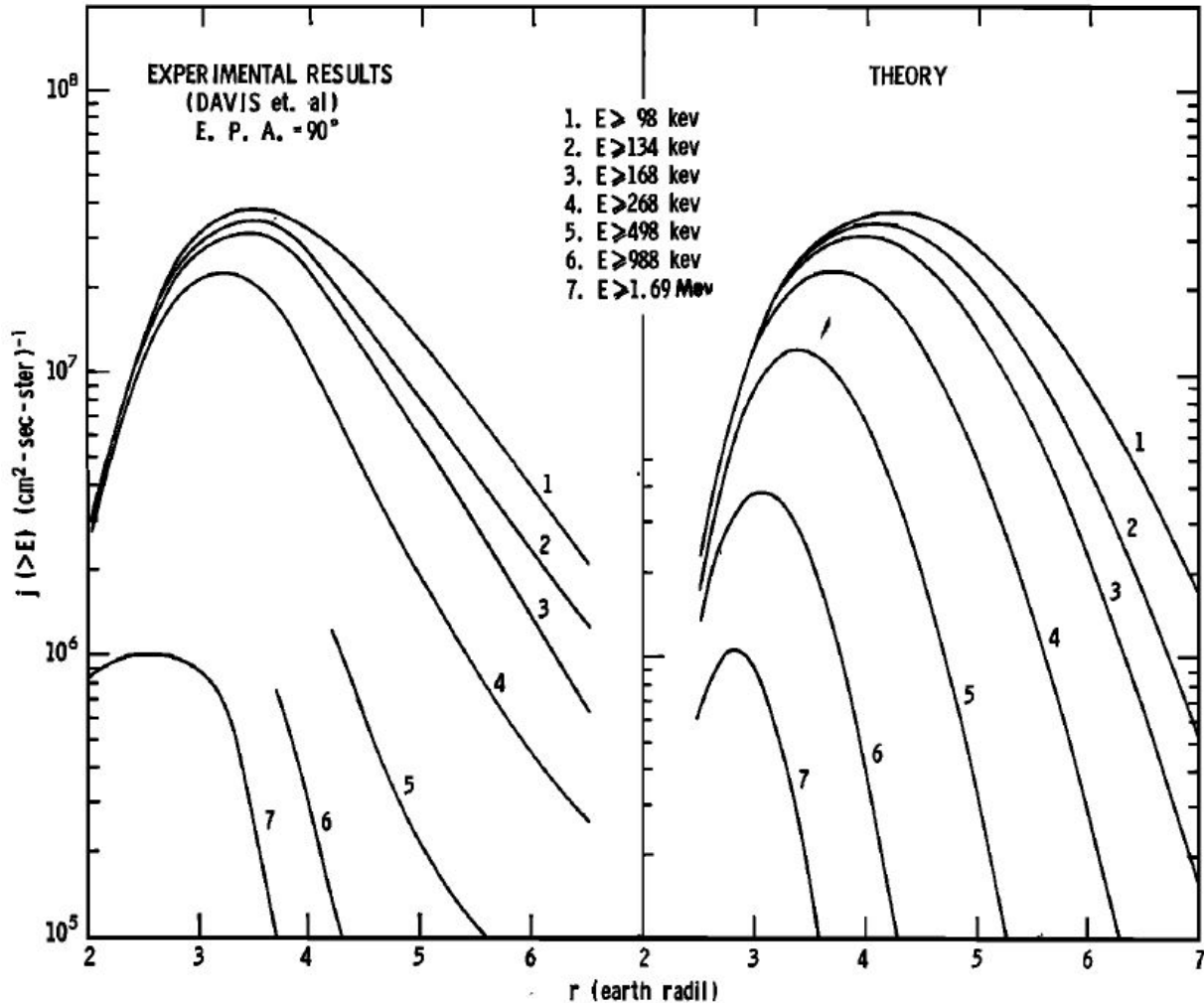
514
515
516 **Fig. 2** Comparison of (left) the observed trapped proton integral fluxes with (right) the
517 distribution expected for radial diffusion from an external proton source located at the outer
518 boundary (Nakada and Mead 1965)
519

520 2.2.2. Artificial radiation belt dynamics
521
522 Studies of artificial belts produced by high altitude nuclear explosions during the Cold War
523 yielded some of the earliest evaluations of the radial diffusion coefficients (Newkirk and Walt
524 1968b; Farley 1969a, 1969b).
525
526 High altitude nuclear explosions carried out by the United States and the Soviet Union (1958-
527 1962) created artificial belts in the inner zone that persisted for years (e.g., Gombosi et al. 2017).

528   Measurements of those energetic electron fluxes indicated that the initially localized peak
529   progressively broadened in radial width (e.g., Brown 1966), providing evidence of radial
530   diffusion in the inner belt (**Fig. 3**). The peak in electron intensity observed **Fig. 3** at L=1.77 is an
531   artificial radiation belt that resulted from a high-altitude nuclear explosion on 1 November 1962.
532   The progressive radial broadening of the peak with time is a clear indication of radial diffusion in
533   the Earth's inner belt.

534
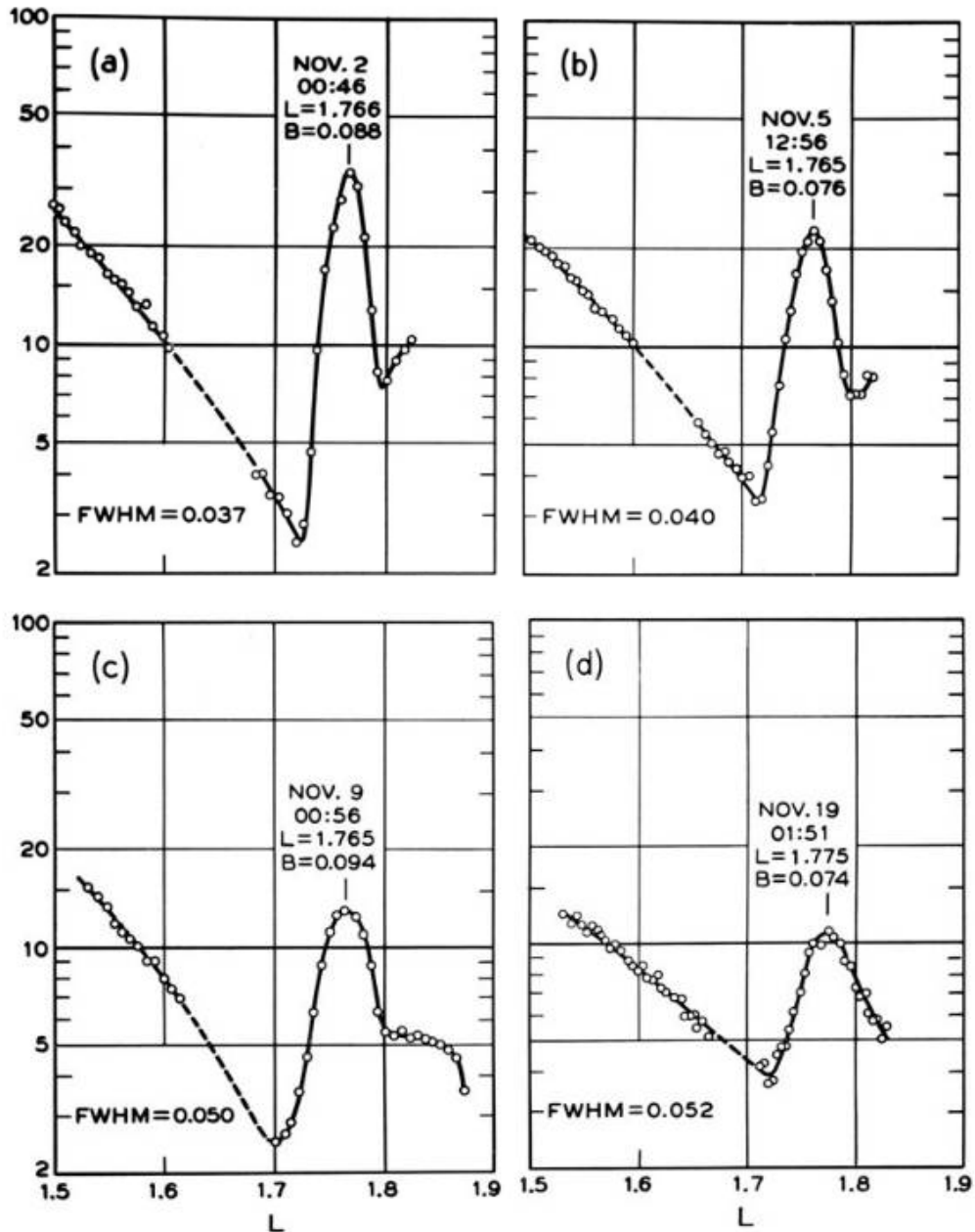
535
536   **Fig. 3** Broadening of the narrow peak in the inner zone electron flux profile (> 1.9 MeV,
537   omnidirectional flux) produced by the third U.S.S.R. nuclear test on November 1, 1962. The
538   intensities displayed are relative. The date, time, and value of the magnetic field of each peak
539   center are noted, together with the full width at half maximum (FWHM) of a Gaussian fitted to

16

540 the peak. This figure was adapted to illustrate the cover of Schulz and Lanzerotti's (1974) book
541 entitled "Particle Diffusion in the Radiation Belts". The data displays the simultaneous effects of
542 radial diffusion and pitch-angle scattering (Brown 1966)
543

544 2.2.3. Diffusion signatures from Giant Planet moons
545

546 *Microsignatures*
547 The most direct observations of radial diffusion can be made after the introduction of a distinct
548 disturbance into the radial intensity profile of a magnetosphere. In the case of Earth, such
549 features usually arise from intensity enhancements following geomagnetic storms (e.g., **Fig. 1**).
550 They can also be caused by high-altitude nuclear explosions (e.g., **Fig. 3**). At the Giant Planets,
551 intensity depletions are common. Different to the Earth, the Giant Planets in our solar system
552 have moons orbiting close enough to the planet that some of them are embedded in the radiation
553 belts. The moons absorb particles that encounter them during their drift around the planet
554 (Thomsen and Van Allen 1980; Hood 1983). The moons are then causing a "drift shadow" where
555 the intensities are depleted. Such features are referred to as "microsignatures" (Van Allen et al.
556 1980b; Roussos et al. 2007). With increasing azimuthal distance to the moon, the microsignature
557 is observed to refill in the case of energetic electrons. This filling can be quantitatively described
558 through radial diffusion (**Fig. 4**). Different to the evolution of intensity enhancements at Earth
559 that evolve at least through a mix of radial, pitch angle and energy diffusion, at the Giant Planets
560 there is little ambiguity in identifying the role played by radial diffusion in controlling the
561 evolution of a microsignature: Local source or loss processes will affect both the microsignature
562 and its environment. Pitch angle diffusion is thought to affect the microsignature and its
563 environment the same way. (An exception might be when the pitch angle diffusion is resulting
564 from waves driven by the particle distribution that is modified in the microsignature. However,
565 the role of pitch angle diffusion on the intensities in regions of microsignatures has not been
566 extensively studied.) Convective transport processes acting coherently on the plasma (through
567 interchange or large scale non-radial electric fields) will displace the microsignature (Roussos et
568 al. 2010), not refill it. Thus, any such process will not be included in a diffusion coefficient
569 derived from microsignatures, even though for example interchange may be also describable
570 through diffusion (**Section 3.1.2**) but on scales larger than the microsignature. This is why
571 microsignature-derived coefficients are sometimes referred to as describing "microdiffusion".
572 Overall, the analysis of microsignature refilling is a relatively robust, though purely
573 phenomenological method to describe radial diffusion, at least on small scales.
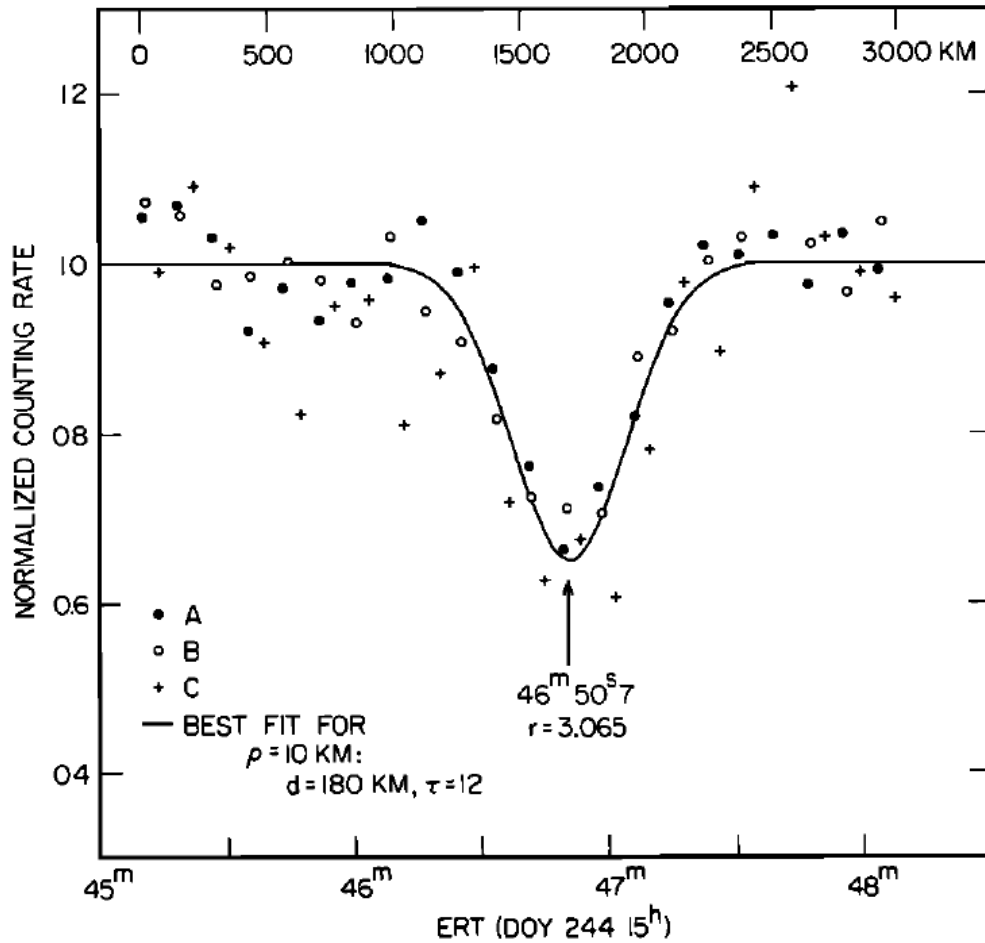
Fig. 4 The 2 MeV electrons downstream of Saturn's moon Mimas. Points: measurements. It can be seen that Mimas has depleted the electron intensities. Line: fit to the data assuming refilling by radial diffusion as a function of time and azimuthal distance to the moon (Van Allen 1980b)

Macrosignatures

If radial diffusion is slow and/or the moon absorption very efficient, the microsignature does not refill after one particle drift around the planet. This will lead to a deeper microsignature over time, until a steady state is reached (Mogro-Campero 1976; Kollmann et al. 2013). Such a feature is called "macrosignature". Macrosignatures are mostly found for ions (**Fig. 5**) because their net drift around Jupiter and Saturn is faster than that of electrons of similar kinetic energy so that ions have less time to refill the drift shadow before the next moon encounter (see also Sec. 3.1 in Roussos et al. 2016). Electrons over a wide energy range at Jupiter and Saturn drift relatively slowly near the relevant moons because, unlike in the Earth's radiation belts, their magnetic drift is competing with the corotation drift that is directed in the opposite direction. Only at very high energies (>10MeV close to Saturn), electrons drift fast enough to also show macrosignatures (Kollmann et al., 2011). Macrosignatures show clearly the presence of radial diffusion: The extent of depleted intensities is found to be much broader in L-shell than what can

18

593   be explained by the size and eccentricity of the moon, the gyroradius effect, and non-circular
594   drift paths. The extended depletion arises from the fact that radial diffusion continuously acts to
595   enhance the intensity in the macrosignature at the price of depleting the intensities outside of the
596   macrosignature.
597
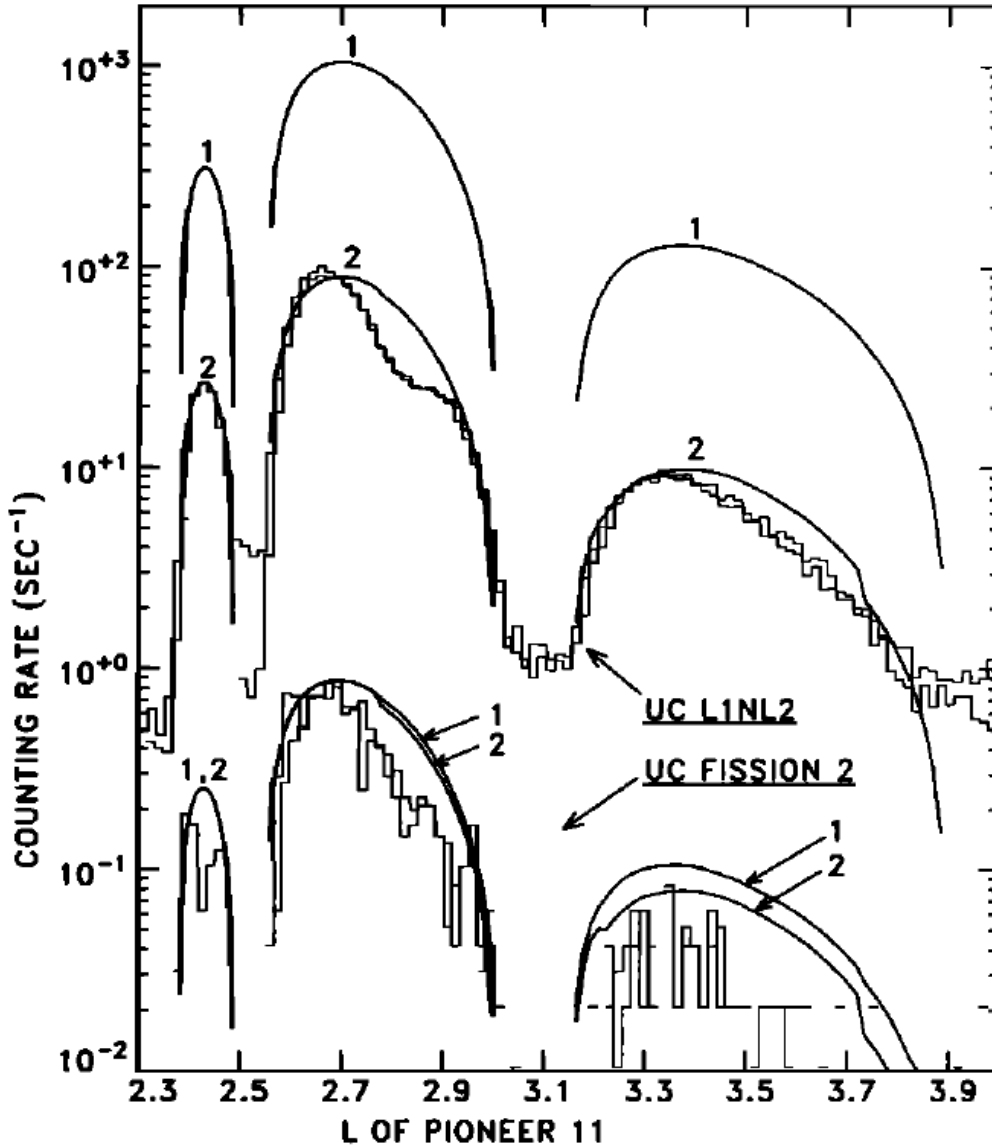
598
599
600   **Fig. 5** Intensity of (1) 15 MeV and (2) 250 MeV protons at Saturn. The broad intensity minima
601   around L=2.3, 2.5, 3.1, and 3.9 are macrosignatures caused by the absorption by various moons
602   of Saturn as well as its main rings. Jagged lines: measurement. Smooth lines: Fit to the data
603   assuming steady state radial diffusion (Cooper 1983)
604
605

606   2.3.   Early theoretical work

607

608   2.3.1. Parker's core mechanism for radial diffusion in the Earth's outer belt

609

610   It was Parker (1960) who first described a physical mechanism by which particles on the same
611   drift shell could be transported to neighboring shells in the Earth's outer belt, with a scenario as
612   follows (**Fig. 6**).

613
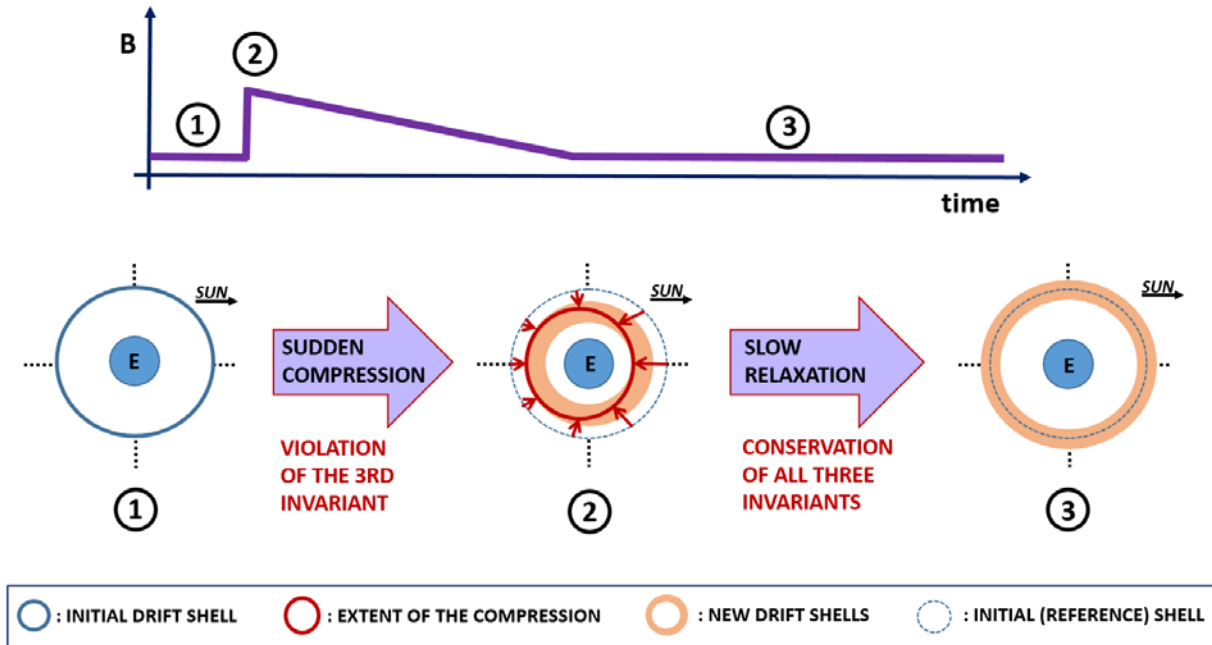
614
615   **Fig. 6** (Top panel) Schematic drawing of a sudden compression of the magnetosphere, indicated
616   by an increase of the magnetic field in the magnetosphere. (Bottom panel) Schematic drawing of
617   the displacement and broadening of a ring of equatorial particles. The particles are initially
618   drifting in a dipole field (blue circle at step 1), and their motions are suddenly modified by the
619   induced electric fields during magnetic field compression (red arrows in step 2). The particles
620   slowly return close to their initial location during the slow relaxation even though the ring of
621   particles has ultimately broadened (light brown band in step 3). See text for details

622

623   The initially dipole magnetic field (1) is suddenly compressed (2), and then slowly returns to its
624   initial configuration (3).

625   (1) Guiding-centers of equatorially trapped energetic particles drift around the Earth, following
626   paths of constant equatorial magnetic field intensity in stationary conditions (see also **Section
627   5.1**). Consider a ring of particles in a dipole field, all drifting along a circle of constant radius
628   **Fig. 6-1**.
629   (2) When the field is suddenly compressed, the particles follow the field lines (Parker, 1960).
630   Their motions depend on the longitude at the time of the compression. Because the
631   compression is stronger on the dayside than on the nightside, particles are transported closer

632 to Earth on the dayside. Particle radial motions are represented by red arrows in **Fig. 6-2**. As
633 a result, different portions of the initial ring of particles now populate different shells as the
634 particles drift around the Earth – the different drift shells are represented in light red-brown
635 area in **Fig. 6-2**. This mechanism is at the heart of the radial diffusion process: Particles are
636 moved inward and outward in a way that is well defined when distinguishing local times (see
637 for example equation (2-37) below). When considering a drift shell average and many such
638 events, particle motion turns into a random, diffusive motion.

639 (3) Then, as the field returns slowly to its initial configuration, no additional motion across drift
640 shells occurs. Yet, because of the sudden compression, the initially narrow ring of particles
641 has broadened around its initial position – the blue ring **Fig. 6-1** has become the light red-
642 brown area **Fig. 6-3**.

643 It is worth noting that cross drift shell motion is zero on average over all local times (see also
644 **Section 5.2.2**), even though there is general inward radial motion during the compression (all the
645 red arrows are pointing inward **Fig. 6-2**). Also, all invariants are conserved during the relaxation,
646 even though the radial distance is changing. This apparent inconsistency comes from the fact that
647 the parameter of interest for radial diffusion is the third adiabatic invariant, or equivalently the L^*
648 coordinate, not radial distance (see also **Section 5.1**). Even though the red arrows indicate
649 $dr/dt < 0$ **Fig. 6-2**, some correspond to $dL^*/dt > 0$ while others correspond to $dL^*/dt < 0$,
650 depending on magnetic local time, and it results that the average displacement in L^* is zero.

651

652 Key points:

653 - *Timescale:* The timescales of this scenario are always longer than the population bounce
654 period; hence the first two adiabatic invariants are conserved. Therefore, "suddenly" means
655 "with a characteristic time that is extremely rapid compared to the population drift period". It
656 indicates that the third invariant alone can be violated (e.g., Northrop and Teller 1960).
657 "Slowly" means "with a characteristic time that is extremely slow compared to the
658 population drift period", so that all three adiabatic invariants are conserved. (The typical
659 timescales invoked in the Earth's radiation belts are of the order of a few minutes for the
660 sudden magnetic compression and a few hours for the relaxation.)

661 - *Particle motion and frozen-field condition:* During the violation of the third invariant, it is
662 implicitly assumed that the plasma obeys the so-called "frozen-field condition", where
663 particles can be visualized as if following the field lines. When the field is suddenly
664 compressed, an induced rotational electric field E_{ind} is set up according to Faraday's law.
665 Provided that there is no component of the electric field parallel to the magnetic field
666 direction, and that the Earth's surface is a perfect conductor, the local magnetic field line
667 velocity coincides with the electric drift $(E_{ind} \times B)/B^2$ (Birmingham and Jones 1968;
668 Fälthammar and Mozer 2007). That "the particles follow the field lines" means that the drift
669 velocity is $(E_{ind} \times B)/B^2$ during that time.

670 - *Asymmetry:* That particles populate different drift shells originate from the fact that the
671 magnetic field compression depends on local time (it is stronger on the dayside than on the
672 nightside). If the magnetic field compression did not dependent on local time, the
673 configuration would stay symmetric: all particles would be transported radially inward by the

674   same amount, and they would stay on a common ring. Thus, no broadening of the ring of
675   particles would occur. In other words, it is essential that the variations of the electromagnetic
676   field depend on local time in order to drive radial diffusion.

677   In summary, sudden field variations that depend on local time cause motion across drift shells. A
678   more comprehensive description for this mechanism is provided **Section 5.2.1**.

679

680   Although an event such as the one described in this **Section** only constitutes a small perturbation
681   for the radiation belts, the cumulative effect of a large number of such events can be significant.
682   In the presence of a continuum of events similar to the one presented **Fig. 6**, the initially narrow
683   ring of particles keeps broadening. A radial diffusion coefficient is a characterization of the
684   average rate at which the broadening occurs. (See for instance Equation (2-44).)

685

686   In summary, radial diffusion was introduced to describe the average rate at which a trapped
687   population changes drift shells in the presence of a large number of small uncorrelated
688   perturbations. This formalism is germane to the Fokker-Planck equation, which describes the
689   evolution of a distribution function as a result of small random changes in the variables (e.g.,
690   Davis and Chang 1962). In the following, we review step by step the derivation of the Fokker-
691   Planck equation, together with its reformulation in terms of a diffusion equation.

692

693   2.3.2.   From the Fokker-Planck equation to the diffusion equation

694

695   *Radial diffusion equation in action variables*
696   If the electromagnetic fields were completely specified all the time, Liouville's equation could be
697   used to determine the exact effects of field perturbations on particle distributions by following
698   particle trajectories through phase space (e.g., Dungey 1965). However, it is experimentally
699   impossible to characterize the electromagnetic fields at every location and at every time.
700   Instruments only provide local, instantaneous measurements that can be converted into global
701   but only statistical information on the fields. Alternatively, one can use numerical models (such
702   as magnetohydrodynamics – MHD – codes) to fully specify the electromagnetic fields and inject
703   test particle to simulate the resulting radiation belt dynamics. Yet, test particle simulations are
704   usually not the preferred approach (because, for instance, they are still computationally very
705   expensive). Due to these limitations, the Fokker-Planck formalism, which aims to calculate the
706   time evolution $\partial f / \partial t$ of a distribution function f, is usually the preferred method. This approach
707   reduces the number of variables to specify by relating average properties of the electromagnetic
708   fields to average characteristics of the radiation belt dynamics.

709

710   Let us consider $(J_i, \varphi_i)_{i=1,2,3}$ the set of action-angle variables associated with a radiation belt
711   population. J_3 is the third adiabatic coordinate, and φ_3 is proportional to the drift period. The
712   objective of this paragraph is to describe the evolution of the number of particles $d\mathcal{N}$ with a set
713   of action variables comprised between J_1 and $J_1 + dJ_1, J_2$ and $J_2 + dJ_2$, and J_3 and $J_3 + dJ_3$,
714   from a time t to a time $t + \Delta t$ – where Δt is a time interval that is long in comparison with the
715   population drift period. To do so, we introduce the drift-averaged distribution f so that

$$d\mathcal{N}(t) = f(J_1, J_2, J_3, t) dJ_1 dJ_2 dJ_3 \tag{2-5}$$

716 In this description, we neglect all phase dependencies (φ_i) – assuming phase mixing (e.g.,
717 Schulz and Lanzerotti 1974, p.47), and we consider that the first two adiabatic invariants of the
718 radiation belt population remain constant.
719
720 The evolution of the distribution function is described in terms of a Markov process in J_3 (e.g.
721 Chandrasekhar 1943; Lichtenberg and Lieberman 1992, p.321 et seq.; Walt 1994, p.97 et seq;
722 Roederer and Zhang 2014, p.116 et seq.):

$$f(J_1, J_2, J_3, t + \Delta t) = \int f(J_1, J_2, J_3 - \Delta J_3, t) \, P(J_1, J_2, J_3 - \Delta J_3; \Delta J_3, \Delta t) d(\Delta J_3) \tag{2-6}$$

723 where $P(J_1, J_2, J_3 - \Delta J_3; \Delta J_3, \Delta t)d(\Delta J_3)$ indicates the probability that an ensemble of phase points
724 that have a set of action variables equal to $(J_1, J_2, J_3 - \Delta J_3)$ experiences an increment equal to ΔJ_3
725 after a time interval Δt. Thus, the transition probability P represents the physical mechanisms
726 responsible for the violation of the third adiabatic invariant. By definition of the transition
727 probability:

$$\int P(J_1, J_2, J_3; \Delta J_3, \Delta t)d(\Delta J_3) = 1 \tag{2-7}$$

728 It is assumed that the increment ΔJ_3 after Δt is small $(\Delta J_3 / J_3 \ll 1)$, that is, it is assumed that the
729 transition probability P is large only for small ΔJ_3. A Taylor expansion for the integrand
730 equation (2-6) yields

$$
f(J_1, J_2, J_3 - \Delta J_3, t) P(J_1, J_2, J_3 - \Delta J_3)
$$
$$
= f(J_1, J_2, J_3, t) P(J_3) - \Delta J_3 \frac{\partial}{\partial J_3}(fP) + \frac{\Delta J_3^2}{2} \frac{\partial^2}{\partial J_3^2}(fP) \tag{2-8}
$$

731 We want to find an expression for $\partial f / \partial t = (f(J_1, J_2, J_3, t + \Delta t) - f(J_1, J_2, J_3, t))/\Delta t$. Inserting
732 the Taylor expansion (2-8) into equation (2-6) leads to

$$\frac{\partial f}{\partial t} = -\frac{\partial}{\partial J_3}(D_1 f) + \frac{1}{2}\frac{\partial^2}{\partial J_3^2}(D_2 f) \tag{2-9}$$

733 where D_1 is the average change in J_3 per unit time:

$$D_1 = \frac{1}{\Delta t} \int \Delta J_3 \, P(J_1, J_2, J_3; \Delta J_3, \Delta t) d(\Delta J_3) \tag{2-10}$$

734 And D_2 is the average square change in J_3 per unit time:

$$D_2 = \frac{1}{\Delta t} \int (\Delta J_3)^2 \, P(J_1, J_2, J_3; \Delta J_3, \Delta t) d(\Delta J_3) \tag{2-11}$$

735   One can use Hamilton's equations to show that

$$D_1 = \frac{1}{2} \frac{\partial D_2}{\partial J_3} \tag{2-12}$$

736   With $D_{J_3 J_3} = D_2/2$ the diffusion coefficient associated with the third invariant, it results that the
737   evolution of the drift-averaged distribution function is described by:

$$\frac{\partial f}{\partial t} = \frac{\partial}{\partial J_3} \left(D_{J_3 J_3} \frac{\partial f}{\partial J_3} \right) \tag{2-13}$$

738   A change of variables provides the diffusion equation in terms of magnetic flux ($\propto J_3$), or
739   L^* ($\propto 1 / J_3$) coordinate (see for instance Roederer and Zhang 2014, p. 120, see also equations
740   (2-28) and (2-30) below).
741
742   *Derivation of the relation between the advection (D_1) and the diffusion (D_2) coefficients*
743   To understand the result provided equation (2-12), we follow the derivation presented by
744   Lichtenberg and Lieberman (1992, p.322 and seq.). For a time interval Δt that is small in
745   comparison with the characteristic time for the variation in J_3:

$$\Delta J_3 = J_3(t + \Delta t) - J_3(t) = \frac{dJ_3}{dt} \Delta t + \frac{d^2 J_3}{dt^2} \frac{(\Delta t)^2}{2} \tag{2-14}$$

746   with φ_3 the angle variable associated to drift motion, and H the Hamiltonian:
747

$$\begin{cases} \dfrac{dJ_3}{dt} = -\dfrac{\partial H}{\partial \varphi_3} \\ \dfrac{d\varphi_3}{dt} = \dfrac{\partial H}{\partial J_3} \end{cases} \tag{2-15}$$

748
749   Combining equations (2-14), and (2-15), it results that:
750

$$\Delta J_3 = -\frac{\partial H}{\partial \varphi_3} \Delta t + \frac{(\Delta t)^2}{2} \left(\frac{\partial}{\partial J_3} \left(\frac{\partial H}{\partial \varphi_3} \right)^2 - \frac{\partial}{\partial \varphi_3} \left(\frac{\partial H}{\partial \varphi_3} \frac{\partial H}{\partial J_3} + \frac{\partial H}{\partial t} \right) \right) \tag{2-16}$$

751
752   The first term on the right side of equation (2-16) is zero on average over φ_3 provided that the
753   distribution is uniform in φ_3. Indeed:

754

$$\left[\frac{\partial H}{\partial \varphi_3}\right] = \frac{1}{\int \Pi(\varphi_3)d\varphi_3} \int \frac{\partial H}{\partial \varphi_3}(\varphi_3)\Pi(\varphi_3)d\varphi_3 \tag{2-17}$$

755

756   where $\Pi(\varphi_3)d\varphi_3$ is the probability that particles are between φ_3 and $\varphi_3 + d\varphi_3$ with
757    $\int \Pi(\varphi_3)d\varphi_3 = 1$. When the distribution is uniform in φ_3, $\Pi(\varphi_3) = cst.$, and we obtain that

$$\left[\frac{\partial H}{\partial \varphi_3}\right] = \frac{1}{2\pi} \int_0^{2\pi} \frac{\partial H}{\partial \varphi_3}(\varphi_3)d\varphi_3 \tag{2-18}$$

758   Because H is periodic in φ_3, it follows that

$$\left[\frac{\partial H}{\partial \varphi_3}\right] = \frac{1}{2\pi}(H(2\pi) - H(0)) = 0 \tag{2-19}$$

759   For similar reasons, the third and fourth terms in equation (2-16) are also zero when averaging
760   over φ_3. Thus averaging (2-16) over φ_3 and inserting it into (2-10) yields:

$$D_1 = \langle \Delta J_3 \rangle = \frac{\Delta t}{2} \frac{\partial}{\partial J_3}\left[\left(\frac{\partial H}{\partial \varphi_3}\right)^2\right] \tag{2-20}$$

761   where [ ] denotes the average of the bracketed quantity and $\langle\ \rangle$ denotes the average change per
762   unit time Δt of the bracketed quantity.
763   To describe D_2 (2-11), we take the square of equation (2-16) and we only keep the terms up to
764   second order in Δt:
765

$$(\Delta J_3)^2 = \left(\frac{\partial H}{\partial \varphi_3}\right)^2 (\Delta t)^2 \tag{2-21}$$

766   Thus,

$$D_2 = \langle (\Delta J_3)^2 \rangle = \Delta t \left[\left(\frac{\partial H}{\partial \varphi_3}\right)^2\right] \tag{2-22}$$

767   As a result:

$$\langle \Delta J_3 \rangle = \frac{1}{2}\frac{\partial}{\partial J_3}\langle (\Delta J_3)^2 \rangle \tag{2-23}$$

768   and we obtain the equation (2-12).

769

770   *General diffusion equation*

771   It should be noted that the diffusion concept is very general and in principle not limited to the

772   third invariant. A more general expression is

773

$$\frac{\partial f}{\partial t} = \sum_{i,j} \frac{\partial}{\partial J_i}\left(D_{i,j}\frac{\partial f}{\partial J_j}\right) + Sources - Losses \tag{2-24}$$

774

775   where $D_{i,j}$ are the diffusion coefficients and J_i are the action variables. The violation of the first

776   and second adiabatic invariants can be rewritten in terms of diffusion in kinetic energy D_{EE} and

777   equatorial pitch angle $D_{\alpha\alpha}$, as well as cross terms $D_{\alpha E}$, $D_{E\alpha}$ (e.g. Schulz and Lanzerotti, 1974,

778   p.55). Diffusion in the first and second adiabatic invariants is mathematically equivalent, it is

779   less intuitive, but it can allow for more stable or more accurate numeric solutions of equation (2-

780   24) (Subbotin and Shprits 2012).

781

782   The "Sources" and "Losses" terms account for changes in $\partial f / \partial t$ that are not due to diffusion.

783   These processes can be sorted into three categories:

784   1) Processes that are independent on the distribution function f. An example is the CRAND

785   source process that provides particles irrespective of the already existing population (Selesnick et

786   al. 2007).

787   2) Processes that scale with the distribution function f. An example is charge exchange that

788   effectively converts ions into neutrals that are not magnetically trapped anymore and are

789   therefore lost from the considered region. The loss rate for this process is proportional to the

790   distribution function (Kollmann et al. 2011).

791   3) Processes that steadily change a variable of the distribution function f. An example is gradual

792   energy loss due to synchrotron emission (Santos-Costa and Bourdarie 2001) or while passing

793   through a plasma, or planetary atmosphere or ring (Nénon et al. 2018).

794

795   *Radial diffusion equation*

796   Historically, the derivation of the diffusion equation has been done in a dipole field, by tracking

797   the number of particles whose adiabatic invariants are comprised between M and $M + dM$, J and

798    $J + dJ$, and L and $L + dL$ at time t, introducing the distribution function $f_0(M,J,L,t)$ such that

$$d\mathcal{N}(t) = f_0(M,J,L,t)dMdJdL \tag{2-25}$$

799   Let us point out that the definition of the L coordinate in equations (2-25) and seq. can be a

800   source of ambiguity. Strictly speaking, the L coordinate of these equations refers to the third

801   adiabatic invariant. Thus, it corresponds to the Roederer's L^* coordinate (1970). Yet, for

802   radiation belt particles in a dipole field, L^* merges with the normalized equatorial radial distance

803   (thus $L = L^*$ in this special case).

804
805 A reformulation of the equation (2-9) is
806

$$\frac{\partial f_0}{\partial t} = -\frac{\partial}{\partial L}(\langle \Delta L \rangle f_0) + \frac{1}{2}\frac{\partial^2}{\partial L^2}(\langle (\Delta L)^2 \rangle f_0)$$
(2-26)

807
808 where $\langle \Delta L \rangle$ and $\langle (\Delta L)^2 \rangle$ represent the average displacement in L per unit time, and the mean
809 square displacement in L per unit time, respectively. These two coefficients are related in a
810 dipole field (Dungey 1965; Fälthammar 1966):
811

$$\langle \Delta L \rangle = \frac{L^2}{2}\frac{\partial}{\partial L}\left(\frac{\langle (\Delta L)^2 \rangle}{L^2}\right)$$
(2-27)

812
813 This result is equivalent to the equation (2-12) – when assuming a dipole field, or appropriately
814 substituting L by L^* in the most general case.
815 Consequently, the equation (2-26) reduces to
816

$$\frac{\partial f_0}{\partial t} = \frac{\partial}{\partial L}\left(\frac{D_{LL}}{L^2}\frac{\partial}{\partial L}(L^2 f_0)\right)$$
(2-28)

817
818 where
819

$$D_{LL} = \frac{\langle (\Delta L)^2 \rangle}{2} = \frac{[(\Delta L)^2]}{2\,\Delta t}$$
(2-29)

820
821 The operator [ ] indicates an average and the bracket operator $\langle \ \rangle$ indicates an average per
822 time interval Δt. It is important to recognize that generally $\langle (\Delta L)^2 \rangle \neq \langle (\Delta L) \rangle^2$. Assuming
823 otherwise leads to wrong derivations of diffusion coefficients. If the diffusion driver is known, it
824 may be possible to express D_{LL} through the power spectrum of the underlying field fluctuations
825 under certain assumptions, see for example equations (2-43) and (2-51) derived in this section.
826
827 When comparing diffusion coefficients, it is important to note that while D_{LL} has the unit of
828 1/time its meaning is similar to a (normalized) distance^2 per time in a dipole field. This means
829 that D_{LL} cannot be directly compared with pitch angle diffusion $D_{\alpha\alpha}$ or energy diffusion D_{EE}/E^2,
830 which have the same units but the dimensions of angle^2 per time and normalized energy^2 per
831 time. Diffusion coefficients represent the potential of the respective diffusion to act. In the
832 absence of gradients, however, there will be no net diffusive transport, irrespective of the
833 diffusion coefficient. Another way of comparing the importance of different diffusion modes is
834 therefore to compare the respective $\partial f_0/\partial t$ terms.
835
836 Sometimes, the distribution function is associated with the third adiabatic invariant J_3, rather
837 than with the actual L coordinate. The third invariant J_3 is proportional to the magnetic flux Φ

838 encompassed by the population drift shell. In that case, with $F(M, J, \Phi, t)$ the new distribution
839 function, given that $F d\Phi = f_0 dL$ and $d\Phi \propto dL/L^2$ in a dipole field, we obtain that

$$\frac{\partial F}{\partial t} = L^2 \frac{\partial}{\partial L}\left(\frac{D_{LL}}{L^2}\frac{\partial F}{\partial L}\right) \tag{2-30}$$

840 The value and functional dependence of the radial diffusion coefficient characterize the overall
841 influence of cross drift shell motion on radiation belt dynamics.
842
843 When using diffusion theory to analyze data it is instructive to express equation (2-30) as
844

$$\frac{\partial F}{\partial t} = L^2 \frac{\partial(D_{LL}/L^2)}{\partial L}\frac{\partial F}{\partial L} + D_{LL}\frac{\partial^2 F}{\partial L^2} \tag{2-31}$$

845
846 It can be seen that the diffusion rate scales with the first two derivatives of F. Measured data can
847 be noisy, in which case the data needs to be fit to a smooth curve before determining these
848 derivatives. While it is straightforward to fit noisy data with a function that describes F and
849 $\partial F/\partial L$ well, there is usually ambiguity in determining $\partial^2 F/\partial L^2$, making it sometimes difficult
850 in practice to determine the precise value of $\partial F/\partial t$ from radial diffusion.
851
852 In summary, the radial diffusion equation provides a description for the evolution of the
853 distribution function that is valid on average over the drift phase. Working with a time resolution
854 that is greater than the drift period is advantageous when it comes to describing radiation belts
855 dynamics over long time scales (for instance, over many years) as this minimizes the
856 computational resources required (e.g., Glauert et al. 2018, see also **Section 1.2.2**). On the other
857 hand, the radial diffusion equation assumes that fluctuations in action variables are small
858 $(\Delta J_3/J_3 \ll 1)$. It also relies on the assumption that the transition probability P as well as the
859 distribution function f only depend on J_3 and are independent of the phase φ_3.
860
861 When the radial diffusion equation (2-30) applies, the distribution function evolves so as to
862 smooth its radial gradient $(\partial F/\partial L = 0 \implies \partial F/\partial t = 0)$. The distribution function F at the peaks
863 decreases and F in the valleys increases. That is why the formation of a local peak in the radial
864 profile of a population phase space density is usually viewed as the result of local processes (for
865 instance: a local acceleration breaking either one or two of the first two adiabatic invariants, or a
866 local loss).
867
868 *Solving the radial diffusion equation in a simple analytic case*
869 The most basic approach to study energetic particle measurements is to compare it to the
870 assumptions that (1) no other processes occur besides radial diffusion, (2) radial diffusion scales
871 with $D_{LL} = D_0 L^n$, and (3) a steady state with $\partial F/\partial t = 0$ is reached. Then, equation (2-30) is
872 solved by
873

$$F = AL^{3-n} + B \qquad \text{For } n \neq 3 \tag{2-32}$$
$$F = A \ln(L) + B \qquad \text{For } n = 3$$

874
875 Phase space density profiles usually fall toward a magnetized planet (e.g.,Paonessa 1985; Cheng
876 et al. 1987, 1992; Schulz 1991, p.216; Kollmann et al. 2011). While this feature is indicative of
877 additional sources or losses, it is important to point out that equation (2-32) illustrates that a
878 falling profile alone does not mean that there are increasingly strong losses distributed along a
879 path toward the planet.
880 The solution (2-32) requires two boundary conditions to determine its parameters A and B.
881 These boundary conditions are able to implicitly impose non-diffusive processes that act outside
882 of the considered region. A boundary condition with a straightforward physical interpretation is
883 one that forces F to zero at a location of strong losses, like the planetary atmosphere. This
884 boundary condition alone is able to explain generally falling phase space density profiles without
885 the presence of distributed losses (like from an extended atmosphere or planetary ring) across the
886 considered region.
887 The second boundary condition is often chosen at the outer boundary of the considered range. It
888 represents an external reservoir of particles that diffuse into the considered region but there is no
889 direct relation to a physically meaningful source rate.
890 A signature for the onset of losses within the considered region, or any other process not
891 described well by radial diffusion, is if the slope of a phase space density profile changes
892 abruptly, which interestingly is also found at all magnetized planets with radiation belts.
893
894 *More realistic numerical solutions to the diffusion equation*
895 Equation (2-32) is a solution to the diffusion equation in its simplest form and usually does not
896 represent actual conditions in space realistically. Non-radial diffusion as well as various sources
897 and losses need to be included (2-24). After compiling such a generalized diffusion equation,
898 there is usually no analytic solution for it anymore (except for still very simple cases like in
899 Thomsen et al. 1977) and the equation needs to be solved numerically. One detail that makes
900 such a numerical calculation challenging is that different processes are assumed to conserve
901 different variables that are used to parameterize the distribution function F: radial diffusion is
902 assumed to conserve M and J, energy diffusion and gradual energy loss are assumed to conserve
903 α_{eq} and L and are usually expressed as a function of E, not the associated invariants. Similarly,
904 pitch angle diffusion is usually defined in a way to conserve E and L. In such cases, it is common
905 to use two different grids to describe F. One is regularly spaced in M, J, and L and it is used to
906 describe radial diffusion. The results are then interpolated on a regularly spaced grid in E, α_{eq},
907 and L to compute the other diffusion modes (Varotsou et al. 2008; Subbotin and Shprits 2009).
908
909 2.3.3. Fälthammar's analytic expressions for radial diffusion through magnetic and electric
910 potential disturbances
911
912 The objective of the very first theoretical works on radial diffusion in the Earth's radiation belts
913 was to study the cumulative effect of many sudden impulses ("si") or storm sudden
914 commencements ("ssc") with a time evolution similar to the one presented **Section 2.3.1** (that is,
915 a sudden variation with a very short rise time, followed by a slow return to the initial
916 configuration) (e.g. Parker 1960, Davis and Chang 1962). Fälthammar (1965, 1968) made less

917 assumptions on the time variations of the fields. He described radial diffusion analytically, in a
918 more general – yet still simplified – way. Because these works have been central to radial
919 diffusion research, they are the object of this section.
920
921 In Fälthammar's works, two different drivers for radial diffusion are discussed separately: (1)
922 magnetic disturbances and (2) electric potential disturbances. In both cases, the assumption is
923 that the background field is a magnetic dipole field. Idealized electric and magnetic field
924 fluctuations are introduced to describe small drift motion perturbations. In the following, as well
925 as in **Section 4.2.1**, we will calculate the diffusion coefficients resulting from magnetic and
926 electric disturbances using two different approaches that we then compare in **Section 4.2.2**. It
927 will be shown how the statistical properties of these field fluctuations determine the radial
928 diffusion coefficient.
929
930 *Radial diffusion through magnetic disturbances*
931 Magnetic field distortions in the Earth's outer magnetosphere are due to currents flowing on the
932 magnetopause, on the neutral sheet, and within the magnetosphere (Schulz and Lanzerotti 1974,
933 p.23 and seq.). The Mead magnetic field model accounts for the permanent compression of the
934 magnetosphere by the solar wind (Mead, 1964). In Fälthammar's works, the magnetic field
935 considered is a simplified Mead geomagnetic field model, with a disturbance field b
936 superimposed to the background dipole field. This disturbance consists of a symmetric part (S) –
937 which is independent of magnetic local time –, and an asymmetric part (A) – which depends on
938 local time. In spherical coordinates (r, θ, φ), with r the geocentric distance, θ the colatitude
939 measured from the pole, and φ the azimuthal angle measured from the midnight meridian and
940 counted positive eastward, the field perturbation vector expressed in the spherical base
941 $(e_r, e_\theta, e_\varphi)$ is:
942

$$b = \begin{pmatrix} S(t) \cos\theta + A(t)\, r \sin 2\theta \cos\varphi \\ -S(t) \sin\theta + A(t)\, r \cos 2\theta \cos\varphi \\ -A(t)\, r \cos\theta \, \sin\varphi \end{pmatrix} \tag{2-33}$$

943 This vector describes magnetic field distortions. This field model is curl free by design – which
944 is a limit to its use (currents within the magnetosphere are omitted).
945 In the equatorial plane, it is:
946

$$b\left(r, \theta = \frac{\pi}{2}, \varphi\right) = -(S(t) + A(t)\, r \cos\varphi)\, e_\theta \tag{2-34}$$

947
948 (e.g., Fälthammar 1965, 1968). Assuming frozen-in flux conditions, the induced electric field
949 E_{ind} associated with the magnetic disturbance b is
950

$$
\boldsymbol{E}_{ind} = \begin{pmatrix} -\dfrac{r^2}{7}\dfrac{dA}{dt}(t)\sin\theta\sin\varphi \\[2mm] \dfrac{2r^2}{7}\dfrac{dA}{dt}(t)\cos\theta\sin\varphi \\[2mm] -\dfrac{r}{2}\dfrac{dS}{dt}(t)\sin\theta + \dfrac{2r^2}{21}\dfrac{dA}{dt}(t)(3-7\sin^2\theta)\cos\varphi \end{pmatrix} \tag{2-35}
$$

951

952   With these expressions, it is straightforward to derive the radial component of the drift velocity

953   of equatorial particles, to first-order approximation in $|b/B_d|$:

954

$$
\frac{dr}{dt} = \frac{E_{ind,\varphi}}{B_d} - \frac{M}{q\gamma B_d r_o}\frac{\partial b}{\partial \varphi} \tag{2-36}
$$

955

956   where r_o is the initial unperturbed value of the particle radial location, $B_d = B_E R_E^3/r_o^3$ is the

957   amplitude of the magnetic dipole field at the equatorial radial distance r_o, M is the relativistic

958   magnetic moment and γ is the Lorentz factor. In this model, the electric and magnetic

959   perturbations are small in the sense that their contribution to the drift motion is much smaller

960   than the contribution of the magnetic gradient.

961   For an equatorial particle trapped in the Earth's dipole field, the angular drift velocity is the

962   angular magnetic drift velocity, and it is equal to $\Omega = 3M/(\gamma q r_o^2)$. With the drift phase φ

963   reformulated in terms of angular drift velocity ($\varphi(t) = -\Omega t + \varphi_0$), the radial displacement for

964   an equatorial particle initially located at r_o with a phase φ_0 is:

965

$$
\begin{aligned}
r(t) - r_o = -\frac{5}{7}\frac{r_o^2\Omega}{B_d}\int_0^t A(\xi)\sin(\Omega\xi - \varphi_0)\,d\xi - \frac{r_o}{2B_d}\big(S(t) - S(0)\big) \\[2mm]
- \frac{8}{21}\frac{r_o^2}{B_d}\big(A(t)\cos(\Omega t - \varphi_0) - A(0)\cos(\varphi_0)\big)
\end{aligned} \tag{2-37}
$$

966

967   where ξ is another parameter describing time.

968   This expression is only valid in its current form if there are no other contributions to the drift

969   velocity, particularly no significant contribution from corotation drift, as it is important at the fast

970   rotating gas giant magnetospheres where it can cancel out the magnetic drifts (Roussos et al.

971   2018b).

972

973   With the exception of the integral term in (2-37) that we define here as

974

$$
X(t) = -\frac{5}{7}\frac{r_o^2\Omega}{B_d}\int_0^t A(\xi)\sin(\Omega\xi - \varphi_0)\,d\xi \tag{2-38}
$$

975

976   all the other terms on the right hand side of equation (2-37) are bounded, and these terms are of

977   the order of $b/B_d \ll 1$. Thus, only $X(t)$ can potentially lead to large cumulative effects.

978   Therefore, it is important to take a closer look at this integral.

979   -   If the signal A has frequencies close to the angular drift velocity Ω, the amplitude of the
980   integral X can increase with time, and the radial displacement can become significant.
981   -   The integral $X(t)$ only depends on the signal A, i.e., it only depends on the asymmetric
982   perturbations of the magnetic field. This result is understandable given that symmetric
983   variations of the fields cannot broaden drift shells (see also **Sections 2.3.1** and **5.2.1**), thus
984   they cannot contribute to radial diffusion.
985   -   The integral $X(t)$ consists of the partial integration of two nearly equal contributions: (1) the
986   induced electric field (first term in the equation (2-36)) contributes 8/21 of the 5/7 factor in
987   the radial displacement (i.e. about 55%), and (2) the magnetic disturbance (second term in
988   the equation (2-36)) contributes 1/3 of the 5/7 factor in the radial displacement (i.e. about
989   45%). Thus, one cannot arbitrarily omit the induced electric fields when evaluating radial
990   diffusion caused by magnetic disturbances.

991   In theory, equation (2-37) can be used to determine $r(t)$ for each particle, which can then be
992   used to construct the full particle distribution function without the need of involving a diffusion
993   formalism and accepting its approximations. In practice, such an approach is not possible
994   (outside of a numerical model that traces particles) because the real field perturbations are not
995   well known. So Fälthammar assumed that $A(t)$ are realizations of a stationary stochastic process.
996   In other words, A fluctuates randomly and its statistical properties are time-independent. In
997   particular, because the background field is the dipole field, the mean of A is zero.
998   In that context, after a time t that is much longer than the autocorrelation time of the signal A,
999   and much longer than the particle drift period $(2\pi/\Omega)$, the expected value of the square
1000   displacement $(r(t) - r_o)^2$ grows linearly with time t. Thus, over a long period of time t, the
1001   expected value of the square displacement per unit time will be constant and will be identical for
1002   all initial drift phases φ_0:
1003

$$\langle (r(t) - r_o)^2 \rangle = \frac{d}{dt}[(r(t) - r_o)^2] = cst. \tag{2-39}$$

1004
1005   where the symbol $[\ \ ]$ denotes the expectation value and the symbol $\langle\ \ \rangle$ denotes the average
1006   change per unit time. It is this constant rate of change value that determines the radial diffusion
1007   coefficient D_{LL}.
1008

$$D_{LL} = \frac{1}{2}\langle \left(\frac{r(t) - r_o}{R_E}\right)^2 \rangle \tag{2-40}$$

1009
1010   This step is crucial as it turns individual particle motions $r(t)$ that in principle are deterministic
1011   (but in reality not well known) into a stochastic parameter that drives the time evolution of the
1012   distribution of particles (a quantity that can be measured).
1013   With the idealized models chosen, the radial diffusion coefficient for this case is:
1014

$$D_{LL,m,eq} = \frac{1}{2}\left(\frac{5}{7}\right)^2 \left(\frac{r_o^2 \Omega}{R_E B_d}\right)^2 \int_0^\infty [A(t)A(t+\xi)]\cos(\Omega\xi)d\xi \tag{2-41}$$

1015

1016 where the subscript m indicates that radial diffusion is driven by magnetic disturbances, and the
1017 subscript eq refers to equatorial particles. Because A is a stationary signal, $[A(t)A(t + \xi)]$ is
1018 independent of time t. It only depends on the lag ξ. For ξ greater than the autocorrelation time of
1019 A, $[A(t)A(t + \xi)]$ is zero, and the integration over ξ can be extended to infinity.

1020

1021 By introducing $P_A(\Omega)$ the power spectrum of the asymmetric field perturbation A evaluated at
1022 the angular drift velocity Ω:

1023

$$P_A(\Omega) = 4 \int_0^\infty [A(t)A(t + \xi)]\cos(\Omega\xi)d\xi \qquad (2\text{-}42)$$

1024

1025 we obtain that:

1026

$$D_{LL,m,eq} = \frac{1}{8}\left(\frac{5}{7}\right)^2 \frac{R_E^2 L^{10}}{B_E^2} \Omega^2 P_A(\Omega) \qquad (2\text{-}43)$$

1027

1028 In terms of magnetic drift frequency ($\nu = \Omega/2\pi$), the diffusion coefficient is also

1029

$$D_{LL,m,eq} = \frac{\pi^2}{2}\left(\frac{5}{7}\right)^2 \frac{R_E^2 L^{10}}{B_E^2} \nu^2 P_A(\nu) \qquad (2\text{-}44)$$

1030

1031 In the case of randomly occurring events with a very short rise time and a very long recovery
1032 time, the power spectrum of the signal A is proportional to ν^{-2}. In that case, the ν terms cancel
1033 so that the radial diffusion coefficient is proportional to L^{10} ($D_{LL,m,eq} \propto L^{10}$), and it is
1034 independent of energy.
1035 More generally, if the power spectrum of the signal A is proportional to ν^{-n}, the variations of the
1036 radial diffusion coefficient with normalized equatorial radial distance L, first adiabatic invariant
1037 M, or kinetic energy T are the following:

1038

$$D_{LL,m,eq} \propto L^{6+2n}M^{2-n} \propto L^{12-n}T^{2-n} \qquad (2\text{-}45)$$

1039

1040 The expression to the right is only true for non-relativistic equatorial particles and the assumed
1041 dipole field. In other words, the so often assumed L^{10} variation of $D_{LL,m,eq}$ results from: (1) a
1042 specific model for the magnetic field disturbance, where the asymmetric perturbations of the
1043 field are proportional to L, and (2) a specific regime for the time variations of the fields, with a
1044 random succession of events with a very short rise time and a very long recovery time.

1045

1046 For a given kinetic energy, the radial diffusion coefficient $D_{LL,m}$ for off-equatorial particles is
1047 proportional to the diffusion coefficient in the equatorial case $D_{LL,m,eq}$ (Fälthammar 1968; Schulz
1048 and Lanzerotti 1974, p.89)

1049

$$D_{LL,m} = \Gamma(\alpha_{eq})D_{LL,m,eq} \qquad (2\text{-}46)$$

1050

1051 where $\Gamma(\alpha_{eq})$ is a multiplying factor that depends strongly on the pitch angle at magnetic
1052 equator α_{eq}. $\Gamma(\alpha_{eq})$ is obviously equal to 1 in the equatorial case ($\alpha_{eq} = 90°$) and it is close to
1053 0.1 for the most field-aligned particles. A representation of this pitch-angle multiplying factor is
1054 provided **Fig. 7**.
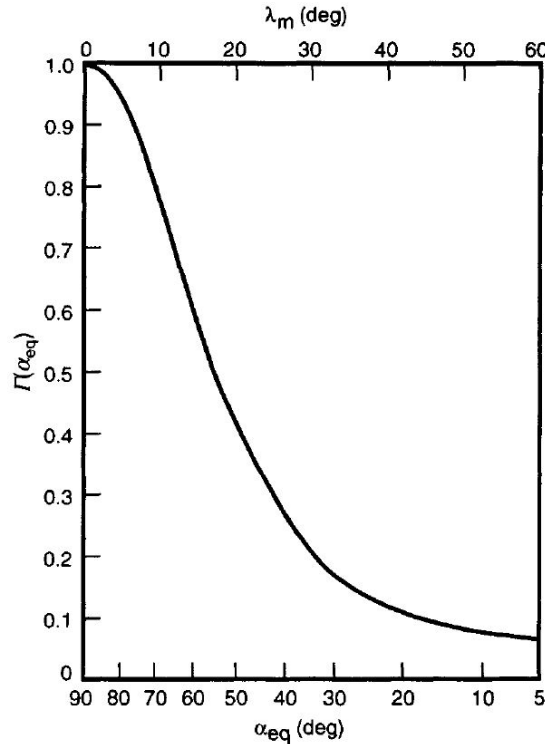
1055

1056 **Fig. 7** Pitch-angle factor $\Gamma(\alpha_{eq})$ for the radial diffusion coefficient driven by magnetic
1057 fluctuations, as a function of the equatorial pitch angle α_{eq} and the mirror latitude λ_m. For a
1058 given energy, the diffusion coefficient decreases up to a factor 10 as the equatorial pitch angle
1059 decreases (Walt 1994)

1060

1061 In comparison, the angular drift velocity does not vary a lot with equatorial pitch angle (less than
1062 a 50% difference between the angular drift velocities of equatorial and field-aligned particles for
1063 a given energy – e.g, Schulz 1991, p.211, eq. (171)). Therefore, the pitch angle dependence of
1064 $D_{LL,m}$ is described by $\Gamma(\alpha_{eq})$. It shows that equatorial particles diffuse more efficiently than off-
1065 equatorial particles in the case of magnetic disturbances.

1066

1067 *Radial diffusion through electric potential disturbances*
1068 Similar calculations can be applied to the case of electric potential disturbances ($\nabla \times \boldsymbol{E} = \boldsymbol{0}$) in
1069 the absence of magnetic field perturbations. The background magnetic field is a dipole. We

1070 specify only the component of the electric field fluctuation that leads to radial motion: the
1071 azimuthal component. It is described by a partial Fourier sum around r_o:
1072

$$E_\varphi(r_o, \varphi, t) = \sum_{n=1}^{N} E_{\varphi n}(t) \cos(n\varphi + \gamma_n) \tag{2-47}$$

1073
1074 where the phases γ_n do not vary with time t. Equation (2-47) can be used to represent a time-
1075 dependent dawn-to-dusk electric field for example.
1076
1077 If there are no other electric fields besides E_φ or if there is a purely radial corotational electric
1078 field (**Section 3**), the radial component of the drift velocity of equatorial particles is:
1079

$$\frac{dr}{dt} = \frac{E_\varphi}{B_d} \tag{2-48}$$

1080
1081 The quantities $E_{\varphi n}(t)$ are assumed to be individually and jointly stationary and ergodic, so that
1082 $[E_{\varphi n}(t)] = [E_{\varphi n}(t + \tau)]$, $[E_{\varphi m}(t - \tau)E_{\varphi n}(t)] = [E_{\varphi m}(t)E_{\varphi n}(t + \tau)]$ and these quantities are
1083 independent of t, both when $m = n$ and $m \neq n$.
1084 The fluctuating part of the electric field is:
1085

$$\tilde{E}_{\varphi n}(t) = E_{\varphi n}(t) - [E_{\varphi n}] \tag{2-49}$$

1086
1087 From these fluctuations, the diffusion coefficient is:
1088

$$D_{LL,e} = \frac{1}{2}\left(\frac{1}{R_E B_d}\right)^2 \sum_{n=1}^{N} \int_0^\infty [\tilde{E}_{\varphi n}(t)\tilde{E}_{\varphi n}(t + \xi)] \cos(n\Omega\xi)\, d\xi \tag{2-50}$$

1089
1090 where the subscript e in $D_{LL,e}$ stands for electric potential disturbances and Ω stands for the
1091 angular drift velocity. The equation (2-50) accounts for radial diffusion driven by electric field
1092 fluctuations. With $P_E(n\nu)$ the power spectrum of the nth harmonic of the electric field
1093 fluctuations evaluated at the nth harmonic of the drift frequency ν, the diffusion coefficient is
1094

$$D_{LL,e} = \frac{L^6}{8R_E^2 B_E^2} \sum_{n=1}^{N} P_E(n\nu) \tag{2-51}$$

1095
1096 This expression is valid for all equatorial pitch angles.
1097
1098 The radial diffusion coefficient driven by electric field fluctuations varies with L^6 provided that
1099 $\sum_{n=1}^{N} P_E(n\nu)$ is independent of L. The drift frequency ν does not vary much with equatorial pitch
1100 angle. Therefore, unless $P_E(n\nu)$ varies strongly with frequency, radial diffusion driven by

1101   electric field fluctuations is nearly independent of equatorial pitch angle for particles of given
1102   kinetic energy.
1103
1104   *Radial diffusion as an aggregate*
1105   In Fälthammar's work, electric potential disturbances and magnetic disturbances are discussed
1106   separately because they are thought to originate from different sources. In practice, when both
1107   diffusion mechanisms are concurrent, it is assumed that they are uncorrelated. Therefore, it is
1108   usually assumed that the total radial diffusion coefficient D_{LL} can be written as the sum of the
1109   two different diffusion coefficients:
1110

$$D_{LL} = D_{LL,m} + D_{LL,e} \qquad\qquad (2\text{-}52)$$

1111
1112   This representation requires an artificial division of the electric field perturbation into two parts:
1113   an induced component, which is accounted for in $D_{LL,m}$, and an electric potential component,
1114   whose statistical properties define $D_{LL,e}$. This can pose a limit to the implementation of these
1115   formulas. Indeed, an electric field measurement is always the sum of induced and electrostatic
1116   components, and their individual contributions can be difficult to evaluate.
1117
1118   2.4.   Methods to quantify radial diffusion
1119
1120   2.4.1.   Solving the Fokker-Planck equation to quantify radial diffusion
1121
1122   Early works relied on particle flux measurements to solve the Fokker-Planck equation, assuming
1123   that radial distribution of the radiation belts was determined exclusively by radial diffusion and
1124   loss processes. The radial diffusion coefficient was adjusted so that the modelled distribution
1125   would fit observations.
1126
1127   Assuming a time-stationary distribution, the objective was to fit the average radial distribution of
1128   the trapped particles. This technique was first applied by Nakada and Mead (1965) in the case of
1129   trapped protons in the outer belt (**Fig. 2**). In the presence of time-varying radial structures in the
1130   belts, the objective was to reproduce the observed time evolution of the radial distribution. This
1131   was done to investigate the inward motion of electrons with E $\geq$ 1.6 MeV during a
1132   geomagnetically quiet time interval of ten days following the magnetic storm of December 17-
1133   18, 1962 (Newkirk and Walt 1968a, **Fig. 1**). This technique was also applied in the years
1134   following the Starfish injection in the inner belt to account for the fact that the observed decay
1135   rate was 20 times smaller than the decay rate deduced from atmospheric scattering theory
1136   (Newkirk and Walt 1968b; Farley 1969a, 1969b). In all cases, the resulting radial diffusion
1137   coefficients were no more than tentative estimates. Early determinations of the radial diffusion
1138   coefficient would generally discuss the ambiguity of the approach.
1139

1140   Indeed, the soundness of the method relies on the validity of a multitude of criteria and
1141   assumptions. In practice, the validity of these criteria and assumptions remains uncertain. Below
1142   are a few examples of the intrinsic difficulties in determining radial diffusion coefficients
1143   directly from particle flux measurements.

1144   - Conditions must be such that the Fokker-Planck equation is likely to apply. In particular, the
1145   assumption that field disturbances cause small drift motion perturbations must be valid
1146   (**Section 2.3.2**). Therefore, large injection events must be excluded from the analysis.
1147   - There must be strong radial gradients in the particle population distribution so that the radial
1148   diffusion coefficient can be determined.
1149   - It is usually necessary to assume that the radial diffusion coefficient is time-independent
1150   during the time interval considered.
1151   - The radial diffusion coefficient must be the only unknown. Uncertainty in the importance of
1152   other processes leads to uncertainty in the value of the radial diffusion coefficient.
1153   - Solving the Fokker-Planck equation requires setting boundary conditions or arbitrary
1154   constants of integration (see for instance equation (2-32)).
1155   - The drift-averaged distribution function f must be determined accurately. This can be a
1156   major difficulty when particle measurements are scarce, or when the magnetic field geometry
1157   is uncertain, such as in the outer belt for instance (e.g. Green and Kivelson 2004).

1158   Even though methods were designed to circumvent some of these difficulties (Lanzerotti et al.
1159   1970), limitations remained (Walt and Newkirk 1971; Lanzerotti et al. 1971).
1160
1161   Additional information on early methods for determining radial diffusion coefficients from
1162   particle data is provided in Walt's review of radial diffusion (1971b). Technical details are
1163   discussed thoroughly in Schulz and Lanzerotti's book, in particular Chapter 5 (1974).
1164

1165   2.4.2. Analyzing magnetic and electric field disturbances to quantify radial diffusion in the
1166   Earth's radiation belts
1167

1168   *Magnetic field disturbances*
1169   Early quantifications of radial diffusion driven by magnetic field fluctuations were based on a
1170   restrictive version of the simplified Mead geomagnetic field introduced **Section 2.3.3** (equation
1171   (2-33)). In this model, $S(t)$ and $A(t)$ are not independent parameters. Instead, they are both
1172   constrained to be directly related to the geocentric stand-off distance to the subsolar point on the
1173   magnetopause $b(t)$:
1174

$$S = B_1 \frac{R_E^3}{b^3} \tag{2-53}$$

1175
1176   with $B_1 = 0.25\ G$, and
1177

$$A = -B_2 \frac{R_E^3}{b^4} \tag{2-54}$$

1178

1179 with $B_2 = 0.21\ G$. For typical solar wind conditions, $b \sim 10\ \mathrm{R_E}$ (e.g., Mead 1964; Nakada and

1180 Mead 1965; Schulz and Eviatar 1969). The asymmetric part of the fluctuation is proportional to

1181 the symmetric part of the fluctuation ($\Delta A = -4B_2 \Delta S/(3B_1 b)$), and so are the power spectra:

1182

$$P_A = \frac{16}{9}\left(\frac{B_2}{B_1}\right)^2 \frac{1}{b^2} P_S \qquad (2\text{-}55)$$

1183

1184 where P_A is the power spectrum of the asymmetric field perturbation and P_S is the power

1185 spectrum of the symmetric part of the fluctuation. In that context, the radial diffusion coefficient

1186 equation (2-43) is also

1187

$$D_{LL,m,eq} = 2\Omega^2\left(\frac{5B_2}{21B_E B_1}\right)^2 L^{10}\left(\frac{R_E}{b}\right)^2 P_S(\Omega) \qquad (2\text{-}56)$$

1188

1189 (e.g. Lanzerotti and Morgan 1973). It is worth noticing that $4B_2/3B_1 b \sim 0.1 R_E^{-1}$. In other words,

1190 a fluctuation of the stand-off distance of the magnetopause Δb is more noticeable in the

1191 symmetric fluctuation of the magnetic field ΔS than in the asymmetric fluctuation of the

1192 magnetic field ΔA. This indicates that the symmetric part of the fluctuation is more readily

1193 measured. Consequently, the equation (2-56) is preferred to the equation (2-43) when it comes to

1194 quantifying radial diffusion driven by magnetic disturbances.

1195

1196 The power spectrum of the symmetric part of the fluctuation P_S can be estimated using satellite

1197 measurements. This was done for instance by Lanzerotti et al. (1978), who analyzed magnetic

1198 field variations measured by the ATS 6 satellite at geostationary orbit during the month of

1199 August 1974. Noticing a dependence of magnetic power with the *Kp* index, they provided radial

1200 diffusion coefficients at $L = 6.6$ as a function of geomagnetic activity.

1201

1202 At orbits other than the geostationary orbit, spacecraft cross different L shells in a short time.

1203 This complicates the power spectrum analysis. Thus, efforts have been made to derive the

1204 symmetric fluctuation power spectrum P_S from ground observations. For instance, Nakada and

1205 Mead (1965), and later Lanzerotti and Morgan (1973) considered that the disturbance in the

1206 horizontal (H) component of the magnetic field measured on the ground is about 50% larger than

1207 the symmetric fluctuation at the magnetic equator. Therefore, they assumed that the symmetric

1208 fluctuation power spectrum P_S is proportional to the power spectrum of the horizontal

1209 component of the magnetic field fluctuations measured on the ground. Nakada and Mead (1965)

1210 analyzed ground-based measurements of the frequency and amplitude of both sudden impulses

1211 and sudden commencements to quantify radial diffusion. Lanzerotti and Morgan (1973) analyzed

1212 power spectra of geomagnetic field fluctuations measured by conjugate stations near $L=4$, for

1213 approximately 6 days in December 1971 and 12 days in January 1972. Once again, their analysis

1214 revealed a strong dependence of magnetic power with geomagnetic activity.

1215

1216 *Brautigam and Albert's formulation of radial diffusion driven by magnetic disturbances*

1217 From the discrete values determined at $L = 4$ by Lanzerotti and Morgan (1973), and at $L = 6.6$ by
1218 Lanzerotti et al (1978), Brautigam and Albert (2000) determined a parameterization of the radial
1219 diffusion coefficient as a function of L and Kp index – an index chosen to quantify geomagnetic
1220 activity. A L^{10} dependence of the radial diffusion coefficient was assumed, even though the
1221 experimental data points at $L=4$ and $L = 6.6$ did not display such dependence. A least squares
1222 fitting technique was implemented to determine $D_0^M(Kp) = D_{LL,m,eq}L^{-10}$. It resulted that
1223

$$D_{LL,m,eq}^{B\&A}(L, Kp) = 10^{(0.506Kp-9.325)}L^{10} \qquad (2\text{-}57)$$

1224
1225 where "*B&A*" stands for Brautigam and Albert's empirical law for radial diffusion.
1226 Discrepancies between the modelled values and the experimental values are within a factor of 6.
1227 Despite this apparent lack of representativeness, modern radiation belt simulations that use
1228 Brautigam and Albert's empirical law for radial diffusion equation (2-57) yield plausible results
1229 when solving the Fokker-Planck equation (e.g. Kim et al. 2011). That is why this empirical law
1230 became a well-accepted reference quantification for radial diffusion in the Earth's radiation belts.
1231
1232 *Electric potential disturbances*
1233 Estimates of radial diffusion driven by electric potential disturbances (equation (2-51) **Section**
1234 **2.3.3**) suffered from a lack of in-situ measurements. Early works by Cornwall (1968) and
1235 Birmingham (1969) quantified radial diffusion driven by electric potential disturbances by
1236 postulating functional forms for the autocorrelation function. They considered that the most
1237 important mode for electric field fluctuations was the fundamental mode of a uniform dawn-to-
1238 dusk electric field (n=1 equation (2-47) **Section 2.3.3**), and they provided estimates for the
1239 average amplitude of the fluctuations (a few tenths of mV/m) and for the correlation time (an
1240 hour).
1241 Hours of DC electric field fluctuations measured by an array of balloons located near $L = 6$ at
1242 approximately 30 km altitude were analyzed and mapped to the magnetic equator to provide an
1243 estimate of the radial diffusion coefficient at that location (Holzworth and Mozer 1979). Electric
1244 field measurements obtained by balloons indicated that the magnetospheric electric field power
1245 spectrum depends on geomagnetic activity (Kp index), but not L nor local time (Mozer 1971).
1246 Direct evaluation of electric field power spectral densities was first provided by the Combined
1247 Release and Radiation Effects Satellite (Brautigam et al. 2005). Yet, unrealistic outputs were
1248 obtained when the coefficient for radial diffusion driven by electric potential disturbances was
1249 included in modern radiation belt simulations (e.g. Kim et al. 2011). Therefore, it became
1250 common practice to omit this process and to consider that radial diffusion is mainly driven by
1251 magnetic disturbances, as described by Brautigam and Albert (2000). In other words, it is now
1252 common practice to assume that $D_{LL} = D_{LL,m}^{B\&A}$ when modeling the Earth's radiation belt
1253 dynamics.
1254
1255 There are many published compilations of the radial diffusion coefficients determined during
1256 that era (see for instance Fig. 20 in the article by West et al. (1981)). They show a clear
1257 scattering among all possible values at any given L shell. Consistency among the various

1258 theoretical and experimental radial diffusion coefficient estimates suggests that the underlying
1259 theory is valid.
1260
1261

3.   EXPANSION: Radial diffusion beyond Earth

1263

1264 3.1.   Radial diffusion drivers most relevant for the Giant Planets
1265

1266 The mathematical formalism of radial diffusion (equation (2-30)) is a universal concept that can
1267 arise at any magnetized planet, not just Earth. Because planets and their magnetospheres differ,
1268 the drivers of radial diffusion can be different and we discuss several mechanisms below
1269 (namely, the ionospheric winds, the interchange process, and the corotation cancellation). Our
1270 focus will be on Jupiter and Saturn because these are the best studied Giant magnetized Planets.
1271

1272 3.1.1.   Ionospheric fields and thermospheric winds
1273

1274 A difference between Earth and the Giant Planets is that corotation plays a much larger role
1275 because the Giant Planets have larger magnetospheres coupled to ionospheres rotating with the
1276 planets at faster speeds. Jupiter is the most extreme case: It enforces azimuthal plasma speeds of
1277 at least half of rigid corotation up to distances as large as 50 planetary radii (which is outside its
1278 intense radiation belts) and yields speeds up to 500 km/s (Waldrop et al. 2015) (therefore
1279 comparable to nominal solar wind speeds). Different to Earth, a theoretical plasmapause of
1280 Jupiter and Saturn would be beyond the dayside magnetopause, meaning that the entire
1281 magnetosphere is rotation dominated (Mauk et al. 2009). The magnetospheric plasma
1282 approximately corotates with the ionospheric plasma because it is roughly frozen-in (Hill 1979).
1283 The ionosphere is forced to corotation due to friction with the dense atmosphere and therefore
1284 the planet itself. Thus, ionospheric plasmas roughly corotate with Jupiter and Saturn (Cowley et
1285 al., 2003, 2004), which is very different from the two cell convection pattern of the Earth's high
1286 latitude ionosphere (Cowley 1982).
1287

1288 Corotation yields a radial electric field that results in electric drifts ($\boldsymbol{E} \times \boldsymbol{B}/B^2$) of charged
1289 particles. Corotation, as well as any other electric field, does not yield diffusion as long as the
1290 fields are constant (see for instance equation (2-50) **Section 2.3.3**). However, if the ionospheric
1291 electric field changes for whatever reason over time, this affects the particle drifts in a way that
1292 can be described with radial diffusion. Mechanisms to explain how the ionospheric electric field
1293 can change are time variable winds or turbulence directly in the ionosphere (Brice and
1294 McDonough 1973) or reconnection affecting the polar caps (Coroniti 1974).
1295

1296 *Theory*
1297 Several authors have studied the effect of varying ionospheric fields in a magnetic dipole field
1298 under different assumptions (Jacques and Davis 1972; Brice and McDonough 1973; Coroniti

1299   1974). All of them yield radial diffusion coefficients with a L-shell dependence that ranges from

1300 $L^2(L-1)$ to L^5, which is weak compared to what was discussed in **Section 2.3**.

1301   Here we follow Jacques and Davis (1972) to present an illustration of the concept in a time-

1302   stationary dipole field.

1303

1304   Let us assume that the footpoint of a dipole field line in the ionosphere is shifted over N steps

1305   due to an arbitrary process. Each step takes the time t_1 and changes the location by $\Delta\theta$ in co-

1306   latitude. In a dipole field, with θ the magnetic colatitude of the field line footpoint, we have that

1307

$$L = 1/sin^2\theta \tag{3-1}$$

1308

1309   This is because the ionosphere is at radial distance $r = 1R_P$ with the planetary radius R_P and

1310   because L is normalized to the planet radius R_P and therefore dimensionless. Differentiating the

1311   equation (3-1), it follows that

1312

$$\Delta L/\Delta\theta = -2L(L-1)^{1/2} \tag{3-2}$$

1313

1314   As $\Delta\theta$ describes a stochastic process that can move θ in any direction, we can then calculate the

1315   radial diffusion coefficient according to equation (2-29).

1316

$$D_{LL} = \frac{2L^2(L-1)[\Delta\theta^2]}{Nt_1} \tag{3-3}$$

1317

1318   It can be seen that radial diffusion under these assumptions scales with $L^2(L-1)$ and the

1319   properties of the fluctuation $[\Delta\theta^2]$ that are not known and therefore usually pragmatically

1320   assumed to be independent of L.

1321

1322   Coroniti (1974) calculates radial diffusion in a different way, by considering fluctuating dawn-

1323   dusk electric fields following dayside reconnection. The result is $D_{LL} \propto L^3$ and scales therefore

1324   similar as equation (3-3). The absolute value of D_{LL} can in principle be calculated from the

1325   reconnection period and duration but these values are difficult to measure.

1326

1327   Brice and McDonough (1973) calculate a radial diffusion coefficient from electric potential

1328   fluctuations that arise from turbulence in the ionosphere. They find $D_{LL} \propto L^3$ for corotating

1329   particles with small magnetic drifts, $D_{LL} \propto L^{3.5}$ for non-relativistic particles with large magnetic

1330   drifts, and $D_{LL} \propto L^5$ for relativistic particles with large magnetic drifts. Again, there are no

1331   absolute values available from theory as the electric potential changes cannot be directly

1332   measured.

1333

1334   *Experimental evidence*

1335 The mechanism suggested by Brice and McDonough (1973) is time dependent winds in the
1336 ionosphere. Wind patterns can be affected by changes in solar extreme ultraviolet (EUV)
1337 heating. Signatures of changes in the radial diffusion coefficient have been observed following
1338 enhanced (Tsuchiya et al. 2011) or variable (Kollmann et al. 2017) EUV irradiance at Jupiter and
1339 Saturn. These observations indicate that radial diffusion may indeed be somehow related to
1340 ionospheric winds. Note that this does not mean that all intensity changes need to result from
1341 changes in the intensity of radial diffusion and/or EUV as there are other reasons for that (de
1342 Pater et al., 1995; Roussos et al., 2018b).
1343
1344 A more literal test of the theory above is to calculate radial diffusion coefficients and compare
1345 their *L*-dependence with theory. Small exponents, between 2 and 4, are able to reproduce
1346 measurements of MeV electrons and protons at Jupiter (Birmingham et al. 1974; Mogro-
1347 Campero 1976; de Pater et al. 1994; Nénon et al. 2017; 2018) and MeV electrons at Saturn
1348 (Lorenzato et al. 2012), consistent with radial diffusion resulting from ionospheric winds as
1349 discussed above. keV electrons (Roussos et al. 2007) and MeV protons (Kollmann et al. 2017) at
1350 Saturn do behave differently and show exponents in the range of 6 to 10, which is more
1351 consistent with the mechanisms discussed in **Section 2** that had been initially developed for
1352 Earth but should be applicable to some degree at all magnetized planets. The differences in
1353 exponents suggest that the diffusion coefficient may have additional dependencies on energy, *L*-
1354 shell, particle mass, or time and that the ionospheric winds mechanism described above is only
1355 dominating in a limited range of these parameters. Han et al. (2018) for example find evidence
1356 that diffusion from ionospheric winds needs to be combined with diffusion from dawn-dusk
1357 magnetospheric electric field perturbations driven by the solar wind (equation (2-51)) in order to
1358 explain the long-term dependence of Jupiter's electron belts.
1359
1360 There is no consistent picture on the actual parameter range yet. When considering model-data
1361 comparisons it is important to keep in mind that several other processes besides radial diffusion
1362 (diffusion in other modes, interaction with neutral material, etc.) have to be incorporated in the
1363 models. Not all parameters are well known and only a few studies made an effort to test how
1364 sensitive their result is on the diffusion exponent.
1365

1366 3.1.2. Interchange
1367
1368 Another difference of Jupiter and Saturn to Earth is that these Gas Giants are orbited by moons
1369 that release material that is ionized and fills the magnetosphere. The mass of this plasma cannot
1370 accumulate forever but needs to be shed from the system. This can be done through interchange.
1371
1372 *The interchange process*
1373 Interchange is the plasma equivalent of the Rayleigh Taylor instability: a dense liquid on top of a
1374 lighter liquid is not a stable configuration and both liquids will eventually interchange their
1375 positions. In the case of a fast rotating magnetosphere as that of the giant planets, the driving
1376 force is the sum of gravity and centrifugal force. Parcels of plasma interchange their location if
1377

$$\frac{\partial \eta}{\partial L} < 0 \qquad (3\text{-}4)$$

1378

1379   where η is the flux tube content (number of particles on a magnetic flux tube) per magnetic flux
1380   (Southwood and Kivelson 1987; Ma et al., 2019).

1381

$$\eta = \int n \, \frac{ds}{B} = \frac{NL^2}{2\pi B_P R_P^2} \qquad (3\text{-}5)$$

1382

1383 n is the particle number density, B the space dependent magnetic field, and ds an infinitesimal
1384   length along the field line. The expression to the right is the flux shell content per magnetic flux
1385   within L to $L + \Delta L$ (Siscoe et al. 1981a, b), and the equality is true for a dipole field (Sittler et al.,
1386   2008). N is the number of particles on a flux shell with "unit" extent $\Delta L = 1$, B_P is the magnetic
1387   field on the equatorial planetary surface, and R_P is the planetary radius. Flux tube, flux shell
1388   content, and this content normalized by magnetic flux are not always carefully distinguished.

1389

1390   For a weak centrifugal force but large pressure gradients in the magnetosphere, interchange can
1391   also occur for

1392

$$\frac{\partial (pV^\gamma)}{\partial L} > 0 \qquad (3\text{-}6)$$

1393

1394   where p is the thermal plasma pressure, V the flux shell volume, and γ the specific heat ratio
1395   (Southwood and Kivelson 1987). Such interchange may be one of the drivers (Pontius and Wolf
1396   1990; Sergeev et al. 1996) of bursty bulk flows at the Earth (Baumjohann et al. 1990).

1397

1398   Note that interchange only occurs in certain regions in L and only up to certain energies. It is
1399   only observed outward of the moons Io and Enceladus (Dumont et al. 2014; Azari et al. 2018),
1400   which is expected based on $\partial \eta / \partial L$ (Sittler et al. 2008; Bagenal et al. 2016). It is only observed
1401   up to energies of hundreds of keV, which is expected because high energy particles have fast
1402   magnetic drifts out of the corotating and inwardly moving flux tube (Paranicas et al. 2016).

1403

1404   The interchange process is radially asymmetric (Hill et al., 2005; Chen et al., 2010): Inward
1405   transport occurs relatively quickly through narrow channels or small bubbles. Outward transport
1406   is slow and occurs over wide longitude ranges. Most studies on interchange are on its inward
1407   component as it leaves obvious "injection" signatures in plasma, radiation, energetic neutrals,
1408   fields, and waves measurements (Mitchell et al., 2015). The net outflow on the other hand is less
1409   studied (Waldrop et al., 2015) and is even below detection limit in the regions where Saturn's
1410   interchange injections are observed (Wilson et al., 2013).

1411

1412   It has been suggested to describe interchanges as a diffusive process. Indeed the inward transport
1413   resulting from interchange is roughly consistent with phenomenological diffusion coefficients at

1414   Jupiter (Krupp et al. 2005, their equation 7). Below we first summarize the justification of
1415   describing interchange through diffusion and then discuss the issues of this approach.
1416
1417   *Diffusion from interchange*
1418   According to equation (2-29), the diffusion coefficient scales with $[(\Delta L)^2]$ – the expected value
1419   of $(\Delta L)^2$ – and Δt – a characteristic time for the interchange process. We will not be able to
1420   constrain $(\Delta L)^2$ from theory here but we will calculate the timescale Δt, which will then
1421   immediately scale a diffusion coefficient that is used to describe the net effect of interchange.
1422
1423   Let us assume that a plasma parcel of size ΔL interchanges with another parcel and in the process
1424   moves by ΔL. Recent studies show that injections transport particles inward over $\Delta L/L \leq 0.2$
1425   (Krupp et al. 2005; Paranicas et al. 2016), while the outward portion is difficult to observe (Chen
1426   et al. 2010). A small $\Delta L/L$ is required because the derivation of the diffusion formalism uses a
1427   Taylor expansion that only is a good approximation for $\Delta L/L \ll 1$ (see also equation (2-14)).
1428
1429   During the interchange process, the net centrifugal energy U is released over the time Δt of the
1430   interchange process. The energy released is dissipated in the ionosphere due to the currents that
1431   are set between the magnetosphere and the ionosphere during interchange. It can be calculated as
1432   (Summers and Siscoe 1985)
1433

$$\frac{U}{\Delta t} = 2 \int_0^\rho J_r \, E_r \, dA \tag{3-7}$$

1434
1435   where $J_r = E_r \Sigma$ is the radial current density that scales with the height-integrated Pedersen
1436   conductivity Σ. $E_r = B_{pol} v$ is the radial electric field that scales with the polar magnetic field
1437 $B_{pol} \approx 2B_P$ and the interchange bulk flow speed $v = 2\pi r/\Delta t$. $dA = 2\pi r \, dr$ is an infinitesimal
1438   area that is integrated over the injection flux tube of radius ρ. The factor 2 equation (3-7) is
1439   included to take account of both hemispheres. Inserting everything in equation (3-7) yields
1440   (Summers and Siscoe 1985)
1441

$$\frac{1}{\Delta t} = \frac{U}{(2B_P \pi \rho^2)^2 \, 4\pi\Sigma} \tag{3-8}$$

1442
1443   We identify $2B_P \pi \rho^2$ in (3-8) as the magnetic flux Φ in the equatorial interchange cell that equal
1444   to flux $2B_P R_P^2 \Delta\theta^2$ on the planetary surface. This can be related to the step size in L if we
1445   approximate equation (3-2) with $\Delta\theta \sim -\Delta L/(2L^{3/2})$ (Siscoe and Summers 1981).
1446
1447   Let us now determine U in order to provide an absolute value of the radial diffusion coefficient.
1448   The centrifugal energy of a shell with ΔL per enclosed magnetic flux in the initial configuration
1449   shall be $E_1 = \tilde{M}_1 \Omega^2 R_1^2/2 + \tilde{M}_2 \Omega^2 R_2^2/2$ and the equivalent quantity of the final configuration
1450 $E_2 = \tilde{M}_1 \Omega^2 R_2^2/2 + \tilde{M}_2 \Omega^2 R_1^2/2$, where $\tilde{M} = m\eta$ is the mass of particles on a flux shell with
1451   extent $\Delta L = 1$ per magnetic flux, with m being the single particle mass. Ω is the angular rotation

1452   frequency of the planet. The released energy per magnetic flux $U_c^* = U/\Phi$ is (Siscoe et al.
1453   1981b)
1454

$$U_c^* = E_2 - E_1 = -\frac{\Omega^2 m}{2\pi B_P}\frac{d(NL^2)}{dL}\Delta L^2 \, L \tag{3-9}$$

1455

1456   To calculate the second equality, we were using $R_2^2 - R_1^2 = (R_1 + \Delta R)^2 - R_1^2 \sim 2R_1 \, \Delta R$ to
1457   approximate the difference in distance and $R_1 \sim LR_p$. We also expressed the difference in masses
1458   through $\widetilde{M}_2 - \widetilde{M}_1 = (d\widetilde{M}/dL)\Delta L$.
1459

1460   Combining equations (2-29), (3-8), (3-9) yields (Summers and Siscoe 1985)
1461

$$D_{LL,i} = \frac{-m\Omega^2 L^4}{8\pi^2 B_P^2 R_P^2 \Sigma}\frac{d(NL^2)}{dL}[(\Delta L)^2] \; = D_i \frac{d(NL^2)}{dL} \quad \text{for } \frac{d(NL^2)}{dL} < 0 \tag{3-10a}$$

$$D_{LL,i} = 0 \quad\quad\quad\quad\quad\quad\quad\quad\quad\quad\quad\quad \text{for } \frac{d(NL^2)}{dL} \geq 0 \tag{3-10b}$$

1462

1463   The second equality in equation (3-10a) is a definition for the proportionality constant D_i. We
1464   distinguish between (3-10a) and (3-10b) because interchange only occurs for $d(NL^2)/dL < 0$.
1465

1466   Interchange acts on the bulk plasma. A diffusion equation for interchange therefore does not use
1467   the phase space density at fixed 1st and 2nd adiabatic invariant but uses instead η or NL^2. Like the
1468   phase space density, η is a conserved quantity during transport. This is because n does not
1469   change (in the absence of sources or losses removing particles) and because interchange
1470   conserves magnetic flux.
1471   In equation (2-30), the diffusion coefficient is independent on the particle distribution, meaning
1472   that the efficiency of the physical drivers of radial diffusion is independent of particle
1473   distribution. The drivers provide each single particle with the same chance of moving inward or
1474   outward. Yet if there are more particles at one J_3 than at another (i.e. if the distribution function
1475   radial gradient is nonzero), it will look as if the particles were behaving so as to smooth the
1476   radial gradient of the distribution function. Therefore $\partial f/\partial t$ depends on f even though usually
1477 D_{LL} does not depend on it. Interchange driven diffusion is different. Its diffusion equation is
1478   nonlinear in the sense that the diffusion coefficient itself depends on the particle distribution
1479   (equation (3-10)) so that already the efficiency of the physical drivers of radial diffusion is a
1480   function of particle distribution.
1481

$$\frac{\partial(NL^2)}{\partial t} = L^2 \frac{\partial}{\partial L}\left(\frac{D_i}{L^2}\left(\frac{d(NL^2)}{dL}\right)^2\right) \tag{3-11}$$

1482

1483   Equations (2-30) and (3-11) yield a different overall behavior: Equation (2-30) smoothes out any
1484 L-gradient in the distribution function F, Equation (3-11) only smoothes out $d(NL^2)/dL < 0 \, L$-
1485   gradients.
1486

1487   For a steady state with $\partial(NL^2)/\partial t = 0$, no additional sources or losses, and assuming $D_i \propto L^m$,
1488   equation (3-11) is solved by a power law
1489

$$NL^2 = \frac{A}{L^{\frac{m}{2}-2}} + B \tag{3-12}$$

1490
1491   which is coincidently formally the same as the equivalent solution of the diffusion equation (2-
1492   30) given in equation (2-32). This similarity between the solutions disappears when sources or
1493   losses are added to equation (3-11).
1494
1495   *Challenges*
1496   There has been a discussion if and to what extent the diffusion formalism is applicable to
1497   interchange (Hill 1983; Southwood and Kivelson 1989; Pontius and Hill 1989), for example
1498   because interchange may be better described through a systematic convection flow pattern
1499   instead of random motions.
1500
1501 NL^2 used in equation (3-11) is a quantity that describes the bulk plasma, summing over all
1502   energies and species. This is why equation (3-11) is used to model plasma distributions (Sittler et
1503   al. 2008; Jurac and Richardson 2005). Radiation belt studies are interested in the high energy
1504   population that does not contribute significantly to NL^2. In case of interchange, generalizing (3-
1505   11) to distinguish invariants is not that straightforward. Higher energy particles can be included
1506   in the above formalism as a second population with flux shell content N^*L^2 (Siscoe et al. 1981b).
1507   This population contributes to the interchange energy U not through its mass and centrifugal
1508   energy U_c. Instead, the radiation component U_R to the interchange energy U contributes through
1509   the change in internal energy density u due to adiabatic heating and the change in flux tube
1510   volume V when interchanging parcels 1 and 2 between the initial state (index i) and final state
1511   (index f).
1512

$$U_R = \left(u_{1f}V_{1f} + u_{2f}V_{2f}\right) - \left(u_{1i}V_{1i} + u_{2i}V_{2i}\right) \tag{3-13}$$

1513
1514   The *L*-dependence of this expression can be evaluated through $V \propto L^4$ for a dipole field, $u =$
1515 $3p/2$ when treating the energetic particles as an ideal gas, and $pV^\gamma = cst.$ for adiabatic
1516   compression of that gas (Gold 1959). Repeating the same derivation for the diffusion coefficient
1517   as above but now combining $U=U_c+U_R$ leads to a diffusion coefficient of the form (Summers
1518   and Siscoe 1985)
1519

$$D_{LL,i2} = D_i \frac{d(NL^2)}{dL} + D_{i2} \frac{d(N^*L^2)}{dL} \tag{3-14}$$

1520
1521   This new diffusion coefficient couples NL^2 and N^*L^2, each of which needs to described by two
1522   separate diffusion equations sharing the same $D_{LL,i2}$ that need to be solved self-consistently.
1523

1524 Even N^*L^2 is not sufficient for radiation belt studies that are interested in the phase space density
1525 at specific values of the 1st and 2nd adiabatic invariants or their equivalent quantities. There is no
1526 readily available diffusion coefficient for these cases. The diffusion coefficients in equations (3-
1527 10) and (3-14) do not account for the energy dependence of the interchange. The latter occurs
1528 because the actual transport does not involve the whole flux shell but occurs in narrow flux
1529 tubes. High energy particles quickly leave the flux tube due to their magnetically drift (different
1530 to the low energy, corotating plasma) meaning that increasingly energetic particles will have
1531 smaller $[(\Delta L)^2]$ and are not efficiently transported through interchange (Paranicas et al. 2016).
1532 Such particles with fast magnetic drifts will relatively frequently pass through interchange flow
1533 channels. The magnetic field in these channels is enhanced compared to the background
1534 magnetospheric field within the plasma sheet and depleted above it (Lai et al., 2016). As the
1535 magnetic gradients are steep, they may change L^* of the passing particles depending on the
1536 bounce phase.

1538 In summary: it is under debate if interchange can be described with the diffusion formalism in
1539 the first place. In either case, there is no sufficient theoretical basis to describe energy or
1540 invariant resolved distribution functions, as it is needed for many practical applications. It
1541 remains an open question how to implement interchange injections into magnetosphere models
1542 that use radial diffusion.

1544 3.1.3. Corotation cancellation

1546 Another difference between Earth and Jupiter and Saturn is that the orientation of the magnetic
1547 field relative to the direction of the planetary rotation is opposite. While this at first appears like
1548 an unimportant detail, it may in fact be a game changer for the transport of radiation belt
1549 electrons.

1551 *Theory*
1552 The total drift of a charged particle around a planet is the sum of a magnetic drift, due to the
1553 gradient and the curvature of the magnetic field, plus an electric drift, due mainly to the
1554 corotation electric field that arises when the planet is conducting and rotating (see for instance
1555 equation (2-3) in the equatorial case). The corotation electric drift only depends on the planetary
1556 rotation period and distance to the planet and is the same for all particle species. The direction
1557 and value of the magnetic drifts depend on the orientation of the planetary's magnetic field and
1558 the particle energy and charge. It is therefore possible that corotation and magnetic drifts cancel
1559 each other out so that particles become stationary in their azimuthal location if they have the
1560 right energy. This energy condition is sometimes referred to with the generic term "resonance".
1561 If the electrons are close to this resonance, where these drifts cancel out, they follow banana
1562 orbits that are not centered around the planet but orbit around a point away from the planet
1563 (Cooper et al. 1998).
1564 In the case of Earth, corotation cancellation occurs for keV protons and therefore does not play a
1565 role for radiation belt energies (e.g. Korth et al. 1999). Jupiter and Saturn both have their
1566 magnetic dipole moment oriented opposite to how it is at Earth. This means that corotation

1567 cancellation occurs for electrons, not protons. The corotation cancellation energy is *L*-shell
1568 dependent and is < 10 MeV at Saturn and < 200 MeV at Jupiter (Roussos et al. 2018).
1569
1570 Local time stationary electrons are sensitive to any local time fixed electric field component
1571 beyond the steady, radial corotation field. Perturbations in the total electric field will change the
1572 *L*-shell of the electrons depending on their initial azimuthal location (Selesnick et al. 2016;
1573 Roussos et al. 2018). The change in *L*-shell is significant for corotation resonant electrons and
1574 vanishes away from the corotation cancellation energy (**Fig. 8**). When the electric field stops
1575 changing, also the changes in *L*-shell stop. This behavior is equivalent to the scenario described
1576 in **Fig. 6** following a compression of the magnetosphere. It can therefore be described through
1577 radial diffusion using a generalized version of equation (2-50) that accounts for the corotation
1578 drift (Han et al., 2018) instead of only using the magnetic gradient drift that is sufficient at Earth.
1579
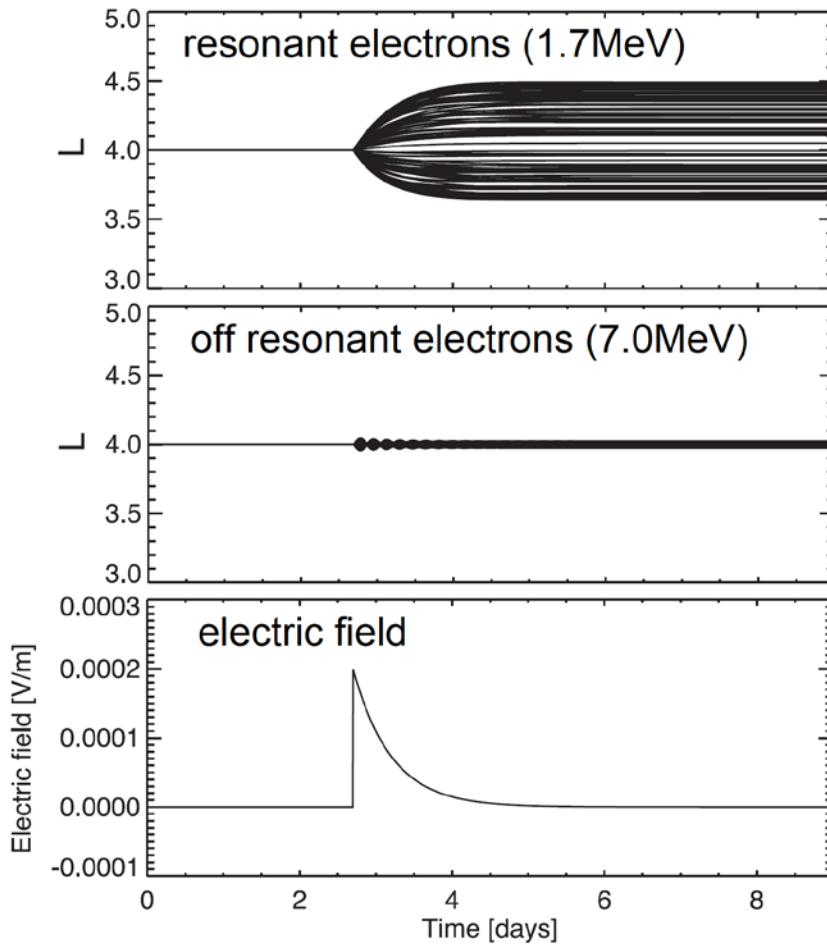
1580
1581
1582 **Fig. 8** Guiding center traces of electrons starting at different local times under the action of a
1583 time dependent electric field (lower panel). It can be seen that resonant electrons with energies
1584 where corotation and magnetic drifts cancel out strongly change their *L*-shell (upper panel) while
1585 electrons of other energies (example shown in the middle panel) are less affected. The change in

1586 location as a response to field changes is similar to what was sketched in **Fig. 6**. Figure adapted
1587 from (Roussos et al. 2018)
1588
1589
1590 *Experimental evidence*
1591 Saturn's electron radiation belt is highly dynamic. It shows abrupt enhancements following
1592 corotating interaction regions, coronal mass ejections, and tail reconnection (Roussos et al. 2014,
1593 2018). These enhancements decay over several weeks (Roussos et al. 2018). This behavior can
1594 be qualitatively reproduced by tracing particles under changes in the electric field (see **Fig. 8**)
1595 that are consistent with what has been observed (Andriopoulou et al. 2014). So far there has been
1596 no attempt made to reproduce this through a diffusion coefficient calculated through equation (2-
1597 50).
1598 Also Jupiter's electron belt shows dynamics on the timescale of days (de Pater et al., 1995;
1599 Tsuchiya et al. 2011). There has been a case study discussing in-situ observations where the
1600 enhancement was only near energies where corotation cancelled out (Roussos et al. 2018),
1601 supporting a highly energy dependent radial transport resulting from corotation cancellation.
1602
1603 3.2.   Phenomenological radial diffusion coefficients
1604
1605 *Methods*
1606 Radial diffusion coefficients at the Giant Planets can be determined phenomenologically from
1607 fitting measured moon absorption signatures under the assumption that the absorption occurs
1608 solely due to collisions with the insulating body of a moon, which is then refilled by radial
1609 diffusion (Van Allen et al. 1980b, **Section 2.2.3**). These assumptions are valid for Saturn's inner
1610 moons like Tethys and Mimas (Roussos et al. 2007) and some of Jupiter's moons like Amalthea
1611 (Fillius et al. 1974) or Callisto. It might still be approximately valid for moons with ionospheres
1612 like Enceladus or Europa (Mogro-Campero 1976). It obviously breaks down at Ganymede,
1613 which has an internal magnetic field, and Io, where absorption at the moon body is insufficient
1614 and additional losses like pitch angle diffusion are needed (Nénon et al. 2017). The signatures
1615 that these latter moons leave in the particle measurements may still be used to constrain radial
1616 diffusion but this requires to first properly describe the particle loss/deflection that occurs in their
1617 direct vicinity.
1618
1619 If theoretical radial diffusion profiles are fit to measured radial phase space density curves, the
1620 moon macrosignatures must be deep, as it is the case for Saturn's proton belts (Kollmann et al.
1621 2013; **Fig. 5 Section 2.2.3**), in order to robustly estimate the radial diffusion coefficient. There
1622 have been attempts to fit more subtle moon signatures (Hood 1983). However, even fitting
1623 extended regions where supposedly only radial diffusion is acting is challenging. The solution to
1624 a radial diffusion equation (2-28) without further sources or losses requires two boundary
1625 conditions (**Section 2.3.2.**; Thomsen et al. 1977). In the absence of a strong moon absorption
1626 there is no physically preferred location where to choose the boundary conditions. One may
1627 select them in a region where one expects radial diffusion to happen and then calculate the
1628 solution for a larger *L* range. Comparison between this solution and the measurements may

1629 reveal regions where non-diffusive processes, like moon losses, occur that can then be further
1630 analyzed, for example to determine the diffusion coefficient. However, the diffusion solution is
1631 very sensitive to the boundary conditions: A small change in the phase space density at one
1632 location used as a boundary condition can cause strong changes at another location, as calculated
1633 from the radial diffusion equation. Robust solutions therefore require phase space density
1634 gradients that are steeper than the variability in the solutions due to the different boundary
1635 conditions.
1636
1637 When fitting radial phase space density profiles with diffusion models it is important that
1638 transport in the fit region is indeed occurring dominantly through radial diffusion and that all
1639 other source and loss processes, like energy loss in dense plasma and neutral tori, are properly
1640 accounted for. Large parts of the magnetospheres of Jupiter and Saturn show signatures of radial
1641 transport through injection events (Clark et al. 2016; Azari et al. 2018) and it is still questionable
1642 to model injection transport with diffusion (**Section 3.1.2**).
1643
1644 *Results*
1645 Diffusion coefficients are usually fit well with power laws $D_{LL} \propto L^n$. At Jupiter, there is evidence
1646 for $2 < n < 4$, and at Saturn for $6 < n < 10$ (**Section 3.1.1**).
1647 Absolute values for diffusion coefficients can be found for example in Mogro-Campero 1976;
1648 Van Allen 1984; Roussos et al. 2007; Kollmann et al. 2013; Nenon et al. 2017, 2018. Values for
1649 ions and electrons do not seem to differ significantly. There is a scatter in the calculated values
1650 by an order of magnitude or more, even when comparing results using the same method. This
1651 suggests that diffusion is time dependent. It has not been studied if this apparent time
1652 dependence can be organized through another quantity, like the magnetic activity index Kp at
1653 Earth for instance (e.g., Lanzerotti and Morgan 1973; Lejosne et al. 2013; Ali et al. 2016).
1654
1655

1656 **4. EVOLUTION: Why and how did radial diffusion research evolve in the Earth's**
1657 **radiation belts?**
1658

1659 4.1. Motivation
1660

1661 4.1.1. Improved spatial and temporal resolutions for radiation belt observations
1662
1663 In the 1990s, the spatial and temporal resolutions of radiation belt observations improved
1664 significantly. Complex structures and rapid dynamics were revealed thanks to a growing network
1665 of satellites and ground stations providing multipoint measurements (with data from the Polar
1666 spacecraft, the Global Positioning System GPS satellites, the Solar Anomalous and
1667 Magnetospheric Particle Explorer SAMPEX, the Combined Release and Radiation Effects
1668 Satellite CRRES, the Geostationary Operational Environmental Satellite System GOES, the
1669 Wind spacecraft close to the L1 Lagrange point, the Canadian array of ground instruments

1670 CANOPUS, etc.). These new sets of observations led to a reassessment of the traditional
1671 description of the Earth's radiation belts provided by the Fokker-Planck equation.
1672
1673 In particular, it was noticed that relativistic electron fluxes near geostationary orbit could
1674 increase significantly (by a couple orders of magnitude), much faster than expected (on a
1675 timescale ranging from a couple of hours to a couple of days). Given the strategic importance of
1676 geostationary orbit, understanding the dynamics of these "killer" electrons became a priority
1677 (e.g., Baker 1994). A good correlation between ultra-low frequency (ULF) wave power and
1678 enhanced relativistic electron fluxes was found near geostationary orbit (Rostoker 1998, Mathie
1679 and Mann 2000). Thus, mechanisms involving ULF waves were proposed to explain large and
1680 rapid enhancements of outer belt relativistic electron fluxes during geomagnetic storms. While
1681 some of the proposed processes required pitch angle scattering (e.g., Liu et al. 1999; Summers
1682 and Ma 2000), the ULF wave drift resonance theory proposed an explanation consistent with the
1683 conservation of the first two adiabatic invariants.
1684
1685 4.1.2. Drift resonance to account for outer belt relativistic electron flux enhancements
1686
1687 The ULF wave drift resonance theory provides a mechanism by which electrons can be
1688 continuously accelerated and transported towards the Earth by the work of a time varying electric
1689 field. The process was first proposed by Hudson et al. (1999). It was then developed by
1690 Elkington et al. (1999, 2003).
1691
1692 In this model, equatorial electrons are drifting in an asymmetric time-stationary magnetic field,
1693 similar to the magnetic field model introduced **Section 2.3.3** (**Fig. 9, Left**). Because the magnetic
1694 field depends on local time, the time-stationary drift contour of an electron population is not
1695 circular as it would be in a dipole. The electrons drift away from the Earth from midnight to
1696 noon, and they drift towards the Earth from noon to midnight. Thus, the radial electric field
1697 oscillation of a toroidal ULF wave (E_r **Fig. 9, Left**) do work on the particles ($q\boldsymbol{E} \cdot \boldsymbol{V_D} \neq 0$). This
1698 leads to a variation of the particle kinetic energy. Indeed, the energy equation is:
1699

$$\frac{dW}{dt} = M \frac{\partial B}{\partial t} + q\boldsymbol{E} \cdot \boldsymbol{V_D} \tag{4-1}$$

1700
1701 where W is the notation for the kinetic energy of the equatorial electron guiding center chosen by
1702 Elkington et al. (1999, 2003), M is the first invariant, $\boldsymbol{E}$ is the electric field and $\boldsymbol{V_D}$ is the drift
1703 velocity.
1704 In the studies, the effect of the associated magnetic field oscillations is neglected. Thus,
1705

$$\frac{dW}{dt} = q\boldsymbol{E} \cdot \boldsymbol{V_D} \tag{4-2}$$

1706
1707 If the electric field variations are such that $q\boldsymbol{E} \cdot \boldsymbol{V_D}$ is always positive, the electrons interacting
1708 with the ULF wave will experience a net energy gain. The magnitude of this energy gain

1709   depends on the power delivered along the drift trajectory. Thus, it is a function of the angle
1710   between the radial electric field E and the drift velocity V_D. In the presence of a radial electric
1711   field of constant amplitude, the angle between the electric fields E and the drift velocity V_D
1712   depends on the radial component of the magnetic drift velocity $(-M\nabla B \times B/\gamma q B^2)$. Thus, it
1713   depends on the magnetic field distortion $(\partial B/\partial\varphi)$. The more asymmetric the magnetic field is,
1714   the more distorted the drift shell is, and thus, the more power is delivered. Similarly, the
1715   azimuthal electric field oscillation of a poloidal mode ULF wave also does work on the particles.
1716   Thus, a resonant interaction between an electron and a poloidal mode wave can exist under
1717   certain special conditions (Elkington et al. 2003; Perry et al. 2005, 2006).
1718
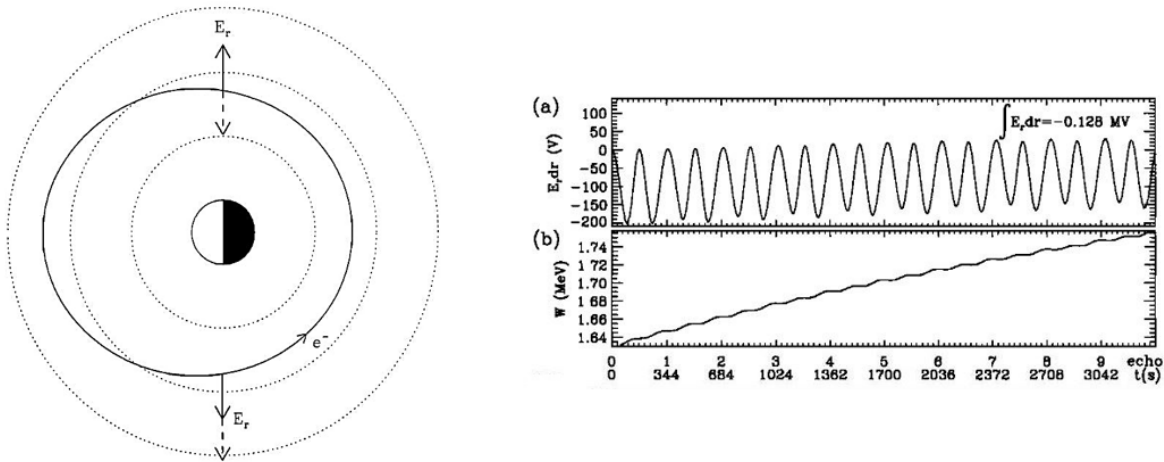
1719
1720
1721   **Fig. 9** (Left) Drift contour of an equatorial electron trapped in an asymmetric time-stationary
1722   magnetic field and orientation of the radial electric field oscillation of a toroidal ULF wave. The
1723   solid arrows shows the orientation of the electric field at t = 0 for an electron starting at dusk, and
1724   the dashed arrows indicate the electric field direction half a drift period later. (Right) (a)
1725   Numerical evaluation of a quantity proportional to the work of the electric field $(E \cdot V_D)dt$ and
1726   (b) Evolution of the particle kinetic energy (W) as a function of time. The electric field is always
1727   pointing outward when the electron is drifting radially inward and it is inward when the electron
1728   is drifting outward. Thus, $qE \cdot V_D$ is always positive and the electron is continuously gaining
1729   energy as it drifts around Earth. Left: (Hudson et al. 1999). Right: (Elkington et al 1999)
1730
1731   In all cases, the drift resonance mechanism characterizes the action of a monochromatic
1732   oscillation in one single global mode. It is important to remember that the drift resonance theory
1733   was proposed to suggest a process by which radiation belt particles would rapidly gain
1734   significant energy, while conserving their first two adiabatic invariants. Drift resonance requires
1735   a monochromatic oscillation in a single mode. This mechanism differs from the core mechanism
1736   for radial diffusion.
1737
1738   The connection between drift resonance and radial diffusion comes from the theoretical
1739   considerations that (re-)emerged at the time from the analysis of drift resonance: namely that the

1740   most asymmetric background field would lead to the most efficient energization mechanism.
1741   Indeed, from the analysis of drift resonance processes, Elkington et al. (2003) suggested that the
1742   asymmetric nature of the background magnetic field could lead to a form of enhanced radial
1743   diffusion in the presence of multiple ULF frequencies (i.e., in the presence of a broadband ULF
1744   wave). It is this suggestion that motivated the derivation of a new set of analytic expressions for
1745   radial diffusion: the analytic expressions by Fei et al (2006).
1746
1747   It is interesting to note that Schulz and Eviatar (1969) had already analyzed radial diffusion
1748   driven by magnetic disturbances in the case of a slightly asymmetric background magnetic field.
1749   They found that in the case of a slightly asymmetric background field, the value of the radial
1750   diffusion coefficient is proportional to the power spectrum of the field fluctuations at all
1751   harmonics of the drift frequency, although the first harmonic remains the main contributor. In a
1752   background dipole field, only the first harmonic of the power spectrum of the magnetic
1753   fluctuations contributes to radial diffusion. Thus, experimental works following Schulz and
1754   Eviatar's study assumed a background magnetic dipole field. As shown in the following, Fei et
1755   al.'s study had similar consequences: subsequent works relying on Fei et al's formulas assumed a
1756   background magnetic field too.
1757

1758   4.2.   New analytic expressions for radial diffusion
1759

1760   4.2.1. Fei et al.'s analytic expressions for radial diffusion
1761

1762   New expressions for the radial diffusion coefficients were proposed by Elkington et al. (2003),
1763   and further developed by Fei et al. (2006) to include the effect of an asymmetric background
1764   magnetic field. Because of the popularity of these formulas, the assumptions underlying the
1765   various resulting expressions for radial diffusion are highlighted in the following paragraph.
1766   However, the magnetic and electric contributions to diffusion in Fei formalism are not self-
1767   consistent, leading to problems discussed in **Section 4.2.2**.
1768

1769   *Time-stationary asymmetric magnetic field model*
1770   The background magnetic field model considered is the superposition of a dipole field and a
1771   time-stationary asymmetric disturbance. In the equatorial plane, the magnitude of the magnetic
1772   field B_0 at a location (r, φ) is:
1773

$$B_0 = \frac{B_E R_E^3}{r^3} + (\Delta B) \cos \varphi \qquad (4\text{-}3)$$

1774

1775   where ΔB is a small perturbation: $(\Delta B) r^3 / B_E R_E^3 \ll 1$.
1776   The unperturbed drift contour for equatorial radiation belt particles at Earth is characterized by
1777 $B_0 = $ cst. (see also **Section 5.1.1**). With the magnetic field model chosen equation (4-3), the
1778   equation of the drift contour is:
1779

$$r(\varphi) = r_o \left(1 + \frac{\Delta B}{3 B_E R_E^3} r_o^3 \cos \varphi \right) \tag{4-4}$$

1780

1781   where r_o is the average radius of the drift contour.

1782

1783   *L* as the normalized average radius of the time-stationary drift contour*

1784   Because the magnetic field is assumed to be time-stationary, the third adiabatic coordinate L^* is

1785   regarded as a spatial coordinate (see also **Section 5.1.1** for more info about L^*). For a radiation

1786   belt population of equatorial particles with an average radius of the drift contour equal to r_o, it is

1787   considered that L^* becomes the normalized average radius of the contour:

1788

$$L^* = r_o / R_E \tag{4-5}$$

1789

1790   Differentiating the equation (4-4), the authors obtained that:

1791

$$\frac{dL^*}{dr} = \frac{1}{R_E} \left(1 - \frac{4}{3} \frac{\Delta B}{B_E} L^{*3} \cos \varphi \right) \tag{4-6}$$

1792

1793   Thus, with Fei et al's model, a displacement of an equatorial particle away from the initial drift

1794   contour leads to a time variation of the L^* parameter:

1795

$$\frac{dL^*}{dt} = \frac{dL^*}{dr} \frac{dr}{dt} \tag{4-7}$$

1796

1797   where dr/dt corresponds to the radial motion away from the drift contour driven by field

1798   fluctuations. In Fei et al.'s model, two different drivers for radial diffusion are discussed

1799   separately: (1) the magnetic field disturbances and (2) the electric field disturbances.

1800

1801   *Magnetic disturbances*

1802   The magnetic field fluctuations are in the direction of the background magnetic field

1803   (compressional perturbations). They are described by a Fourier sum around r_o:

1804

$$\delta B(r, \varphi, t) = \sum_{n=1} \delta B_n(t) \cos(n\varphi) \tag{4-8}$$

1805

1806   The radial drift motion driven by the magnetic field disturbances is equal to

1807

$$\frac{dr}{dt} = -\frac{M}{q\gamma B_d r_o} \frac{\partial(\delta B)}{\partial \varphi} \tag{4-9}$$

1808

1809   where $B_d = B_E R_E^3 / r_o^3$ is the amplitude of the magnetic dipole field at the equatorial radial
1810   distance r_o. Combining equations (4-6), (4-7), (4-8) and (4-9), it results that
1811

$$
\begin{aligned}
\frac{dL^*}{dt}(r, \varphi, t) = {} & \frac{ML^{*2}}{q\gamma B_E R_E^2} \sum_{n=1} n\delta B_n(t) \sin(n\varphi) \\
& - \frac{2}{3} \frac{ML^{*5}}{q\gamma B_E R_E^2} \frac{\Delta B}{B_E} \sum_{n=1} n\, \delta B_n(t) \sin\big((n+1)\varphi\big) \\
& - \frac{2}{3} \frac{ML^{*5}}{q\gamma B_E R_E^2} \frac{\Delta B}{B_E} \sum_{n=1} n\, \delta B_n(t) \sin\big((n-1)\varphi\big)
\end{aligned}
\tag{4-10}
$$

1812
1813   The resulting diffusion coefficient is obtained with an approach similar to the one proposed by
1814   Fälthammar (1965) (see also **Section 2.3.3**). The equation (4-10) is integrated between a time
1815 $t = 0$ and a time t to obtain the variation of L^*. Then, the variation of L^* is squared.
1816

$$
\big(L^*(t) - L^*(0)\big)^2 = (a + b + c)^2
\tag{4-11}
$$

1817
1818   where a, b and c are the integrals of the 3 terms on the right hand of the equation (4-10).
1819   It is then considered that the different integrals are uncorrelated, so that:
1820

$$
\big\langle \big(L^*(t) - L^*(0)\big)^2 \big\rangle = \frac{d}{dt}\Big[\big(L^*(t) - L^*(0)\big)^2\Big] = \frac{d}{dt}[a^2] + \frac{d}{dt}[b^2] + \frac{d}{dt}[c^2]
\tag{4-12}
$$

1821
1822   where the symbol $\langle\ \rangle$ denotes the expected rate of change of the bracketed quantity, the symbol
1823 $[\ ]$ denotes the expectation value, and d/dt denotes the rate of change.
1824   As a result, Fei et al. (2006) obtained a diffusion coefficient driven by compressional magnetic
1825   disturbances equal to:
1826

$$
\begin{aligned}
D_{LL,b,eq} = {} & \frac{M^2}{8q^2\gamma^2 B_E^2 R_E^4} L^{*4} \sum_{n=1} n^2 P_n^B(n\Omega) \\
& + \frac{2}{9} \frac{M^2}{q^2\gamma^2 B_E^2 R_E^4} \left(\frac{\Delta B}{B_E}\right)^2 L^{*10} \sum_{n=1} n^2 P_n^B((n+1)\Omega) \\
& + \frac{2}{9} \frac{M^2}{q^2\gamma^2 B_E^2 R_E^4} \left(\frac{\Delta B}{B_E}\right)^2 L^{*10} \sum_{n=1} n^2 P_n^B((n-1)\Omega)
\end{aligned}
\tag{4-13}
$$

1827   where Ω is the angular drift velocity of the population considered, and P_n^B is the power spectrum
1828   of the nth harmonic of the magnetic field fluctuation δB:

$$P_n^B(\omega) = 4 \int_0^\infty [\delta B_n(t)\delta B_n(t+\xi)]\cos(\omega\xi)d\xi \qquad (4\text{-}14)$$

1829

1830 The subscript b in $D_{LL,b,eq}$ indicates that the coefficient quantifies radial diffusion driven by

1831 magnetic disturbances according to Fei et al's model.

1832 The first term on the right hand of equation (4-13) does not depend on the asymmetry of the

1833 *background* magnetic field ΔB. It characterizes radial diffusion in the case of a background

1834 dipole field, to which small, local time dependent, magnetic disturbances are superimposed

1835 (equation (4-8)). The second and third terms on the right hand of equation (4-13) characterize

1836 radial diffusion enabled by the asymmetry of the background field. Because they are proportional

1837 to $(\Delta B/B_E)^2$, they are small in comparison with the first term (Fei et al. 2006).

1838

1839 *Electric disturbances*

1840 The electric field disturbance is assumed to be in the azimuthal direction. It is described by a

1841 Fourier sum around r_o:

1842

$$\delta E_\varphi(r,\varphi,t) = \sum_{n=1} \delta E_{\varphi n}(t)\cos(n\varphi) \qquad (4\text{-}15)$$

1843

1844 The motion driven by electric field fluctuations is:

1845

$$\frac{dr}{dt} = \frac{\delta E_\varphi}{B_d} \qquad (4\text{-}16)$$

1846

1847 And it results that

1848

$$\begin{aligned}
\frac{dL^*}{dt}(r,\varphi,t) &= \frac{1}{B_d}\sum_{n=1}\delta E_{\varphi n}(t)\cos(n\varphi) \\
&\quad -\frac{2}{3}\frac{\Delta B}{B_d^2}\sum_{n=1}\delta E_{\varphi n}(t)\cos((n+1)\varphi) \\
&\quad -\frac{2}{3}\frac{\Delta B}{B_d^2}\sum_{n=1}\delta E_{\varphi n}(t)\cos((n-1)\varphi)
\end{aligned} \qquad (4\text{-}17)$$

1849

1850 Following an approach similar to the one presented in the case of magnetic disturbances, the

1851 authors obtained that:

1852

$$D_{LL,\epsilon.eq} = \frac{L^{*6}}{8B_E^2 R_E^2}\sum_{n=1} P_n^E(n\Omega) \qquad (4\text{-}18)$$

$$+\frac{2}{9B_E^2 R_E^2}\left(\frac{\Delta B}{B_E}\right)^2 L^{*12} \sum_{n=1} n^2 P_n^E((n+1)\Omega)$$

$$+\frac{2}{9B_E^2 R_E^2}\left(\frac{\Delta B}{B_E}\right)^2 L^{*12} \sum_{n=1} n^2 P_n^E((n-1)\Omega)$$

1853

1854   where P_n^E is the power spectrum of the nth harmonic of the electric field fluctuation δE_φ. The

1855   subscript ϵ in $D_{LL,\epsilon.eq}$ indicates that the coefficient quantifies radial diffusion driven by azimuthal

1856   electric disturbances according to Fei et al's model. The first term on the right hand of equation

1857   (4-18) does not depend on the asymmetry of the magnetic field ΔB. The second and third terms

1858   on the right hand of equation (4-18) characterize radial diffusion enabled by the asymmetry of

1859   the field. Because they are proportional to $(\Delta B/B_E)^2$, they are small in comparison with the first

1860   term.

1861

1862   *Radial diffusion as an aggregate*

1863   When both electric and magnetic diffusion mechanisms are concurrent, it is assumed that their

1864   actions are uncorrelated. Therefore, Fei et al. (2006) assumed that the radial diffusion coefficient

1865 D_{LL} can be written as the sum of the two diffusion coefficients:

1866

$$D_{LL,eq} = D_{LL,b,eq} + D_{LL,\epsilon,eq} \tag{4-19}$$

1867

1868   The subscript eq indicates that the coefficients have been computed in the case of equatorial

1869   particles. No theoretical description was proposed for non-equatorial particles.

1870

1871   4.2.2.   A comparison between Fei et al.'s expressions and Fälthammar's formulas

1872

1873   Despite apparent similarities, none of the electric and magnetic diffusion coefficients derived by

1874   Fei et al (2006) (**Section 4.2.1**) is identical to the electric and magnetic diffusion coefficients

1875   derived by Fälthammar (1965) (**Section 2.3.3**) (**Fig. 10**). By discussing the action of the

1876   magnetic field perturbations and the action of the induced electric fields in separate ways, the

1877   underlying assumption of Fei et al.'s approach is that electric and magnetic perturbations are

1878   uncorrelated. The validity of this assumption is often wrongly attributed to Brizard and Chan

1879   (2001). Yet, it is inconsistent with Faraday's law ($\mathbf{\nabla} \times \mathbf{E} = -\partial \mathbf{B}/\partial t$).

1880

1881   Fei et al.'s formulas for radial diffusion are incorrect. They provide an underestimation of the

1882   total radial diffusion coefficient by a factor 2 in the case of magnetic disturbances described by

1883   the simplified Mead model introduced **Section 2.3.3** (equation (2-33), in the absence of

1884   electrostatic potential fields – and forcing $S(t) = 0$ (Lejosne 2019). Given the uncertainties in

1885   measuring actual field fluctuations, this factor 2 may not seem extremely important in its own

1886   right. Yet, it is enough to demonstrate the difference between the two coexisting formalisms.

1887

1888   Although Fei et al's formalism is inadequate from a theoretical standpoint, it is very convenient
1889   from a practical standpoint. It is indeed difficult to differentiate the induced and electrostatic
1890   components of an electric field measurement. This poses a serious problem when it comes to
1891   applying Falthammar's formalism to quantify radial diffusion. The same problem is
1892   circumvented when applying Fei et al's erroneous formalism.
1893
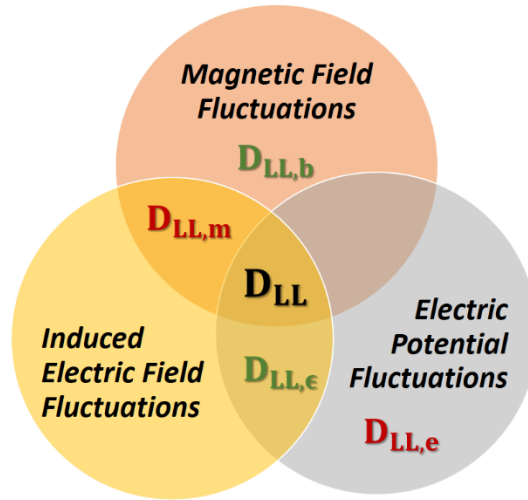
Fälthammar (1965): $D_{LL} = D_{LL,m} + D_{LL,e}$
Fei et al. (2006): $D_{LL} = D_{LL,b} + D_{LL,\epsilon}$

1894
1895   **Fig. 10** Separating the field perturbations according to the nature of the source: different models
1896   of D_{LL} count and combine different types of electromagnetic fluctuations (Lejosne 2019)
1897
1898   In all cases, the Fokker-Planck equation (equation (2-28) **Section 2.3.2**) calls for only one global
1899   radial diffusion coefficient to characterize the statistical properties of cross drift shell motion. It
1900   is represented in the center of **Fig. 9**. The cross drift shell motion is generated by all
1901   perturbations, regardless of their nature. Thus, the validity of the approach which consists of
1902   dividing of the radial diffusion coefficient into a sum of distinct contributions is worth
1903   questioning.
1904   The artificial separation between electric potential disturbances and magnetic disturbances in
1905   Fälthammar's study was justified by the fact that these disturbances originate from different
1906   sources. In practice, the correlation between electric potential disturbances and magnetic
1907   disturbances is unknown. A potential correlation between these fluctuations would result in a
1908   global radial diffusion coefficient distinct from the sum of the different contributions.
1909

1910   4.3.   Modern methods to quantify radial diffusion
1911
1912   Many modern studies rely on Fei et al's analytic expressions to quantify radial diffusion.
1913   Magnetohydrodynamics (MHD) simulations, ground-based data and/or satellite measurements

1914   are analyzed to determine the power spectrum of the compressional component of the magnetic
1915   field, and the power spectrum of the azimuthal component of the electric field. These power
1916   spectra are then used as to compute a magnetic diffusion coefficient, and an electric diffusion
1917   coefficient, following equations (4-13) and (4-18) respectively. It is usually considered that the
1918   background magnetic field is a dipole field ($\Delta B = 0$). Thus, only the first terms of the equations
1919   (4-13) and (4-18) are computed (e.g. Tu et al. 2012; Ozeke et al. 2012, 2014; Ali et al. 2015,
1920   2016; Liu et al. 2016; Li et al. 2017; Jaynes et al. 2018b). The resulting electric diffusion
1921   coefficients $D_{LL,\epsilon,eq}$ are usually one or two orders of magnitude greater than the magnetic
1922   diffusion coefficients $D_{LL,b,eq}$, even though this result has been the object of discussion (e.g.
1923   Olifer et al. 2019).
1924   Ozeke et al. (2014) analyzed many years of ground and space based measurements to derive new
1925   analytic expressions for the radial diffusion coefficients. The power spectrum of the azimuthal
1926   component of the electric field was derived from ground measurements of the D component
1927   (geomagnetic east-west) of the magnetic field, following a mapping method developed by Ozeke
1928   et al. (2009). The power spectrum of the magnetic field compressional component was derived
1929   from in situ measurements by the Active Magnetospheric Particle Tracer Explorers (AMPTE),
1930   GOES and the Time History of Events and Macroscale Interactions during Substorms (THEMIS)
1931   spacecraft. In-situ field measurements were used because according to Ozeke et al. (2012), it is
1932   difficult to estimate compressional fields using ground data. Mapping approaches such as the one
1933   assumed by Lanzerotti and Morgan (1973) – discussed **Section 2.4.2** – yield "results which are
1934   not a good representation of the in-situ data". Yet, the final radial diffusion parameterization
1935   obtained by Ozeke et al. (2014) is similar to Brautigam and Albert's formulation for radial
1936   diffusion driven by magnetic disturbances $D_{LL,m,eq}^{B\&A}$ (see also **Section 2.4.2**). In fact, the
1937   difference between radiation belt simulations with either of the two parameterizations for radial
1938   diffusion has been found to be negligible (Drozdov et al. 2017). The parameterization for radial
1939   diffusion according to Ozeke et al. (2014) is:
1940

$$\begin{cases} D_{LL,b,eq}^{Oz}(L,Kp) = 6.62 \times 10^{-13}L^8 10^{-0.0327L^2+0.625L-0.0108Kp^2+0.499Kp} \\ \qquad D_{LL,\epsilon,eq}^{Oz}(L,Kp) = 2.16 \times 10^{-8}L^6 10^{0.217L+0.461Kp} \end{cases} \qquad (4\text{-}20)$$

1941
1942   where "OZ" stands for Ozeke et al.'s empirical law for radial diffusion.
1943
1944

1945   **5.   NAVIGATION: What are radial diffusion key concepts?**
1946
1947   The objective of this section is to provide the essential toolkit to navigate radial diffusion
1948   research. It includes three principles:
1949   (1)   The appropriate coordinate to study radial diffusion is L^*;
1950   (2)   Radial diffusion requires violation of L^*;
1951   (3)   Radial diffusion is a formalism that trades accuracy for expediency.
1952

1953 In the following, we detail each of these different aspects, and we highlight the caveats and the
1954 challenges associated with each one of them.
1955

1956 5.1. L^* is the appropriate coordinate to study radial diffusion
1957

1958 The terminology of "radial" diffusion is confusing because it seems to imply that the variable of
1959 reference is the equatorial radial distance. However, this is inaccurate. The variable of reference
1960 is L^*. "Radial" is a misnomer that is used to date for historical reasons: there was a decade worth
1961 of major works (e.g., Kellogg 1959b; Fälthammar 1965) before the adiabatic coordinate L^* was
1962 even introduced (Roederer 1970). L^* accounts for adjustments in particle drift motions that result
1963 from the difference between the real magnetic field and a magnetic dipole field under stationary
1964 conditions. In contrast, early works on radial diffusion were carried out assuming a background
1965 magnetic dipole field! The Fokker-Planck diffusion equation, whose inputs includes the radial
1966 diffusion coefficient, is set in adiabatic reference space. Thus, the appropriate coordinate to study
1967 radial diffusion is not radial distance, it is the third adiabatic invariant - or equivalently L^*.
1968 In this section, we introduce the L^* coordinate, we describe the characteristic features resulting
1969 from the distinction between L^* and normalized equatorial radial distance, and we discuss the
1970 associated challenges.
1971

1972 5.1.1.   Adiabatic theory of magnetically trapped particles and definition of the L^* coordinate
1973

1974 The analysis of radiation belt dynamics requires mapping measured particle fluxes into a three-
1975 dimensional adiabatic reference space (e.g. Roederer and Lejosne 2018 and references therein).
1976 The three adiabatic coordinates of this reference space (M, J, L^*) characterize the magnitudes of
1977 the three distinct pseudo-periodic motions of the trapped radiation belt population: (1) gyration
1978 perpendicular to the magnetic field direction (M), (2) bounce along equipotential magnetic field
1979 lines between mirror points (J) and (3) drift around the Earth (L^*). M and J are defined in
1980 **Section 2.1**.
1981

1982 Under stationary conditions, radiation belt particles are represented by guiding centers bouncing
1983 and drifting along closed surfaces called drift shells. The intersection of a drift shell with the
1984 minimum-B surface defines a closed curve called a drift contour (Γ). These notions are
1985 illustrated **Fig. 11**.
1986
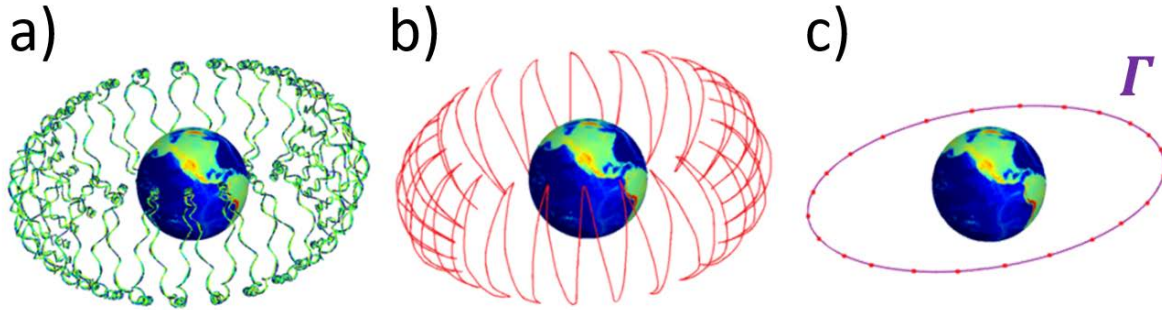
1987
1988
1989   **Fig. 11** An illustration of the path of a radiation belt particle trapped in the Earth's stationary
1990   magnetic field, with different levels of accuracy: a) Exact path of a radiation belt particle trapped
1991   in the Earth's magnetic field; b) Guiding center approximation: the guiding center bounces and
1992   drifts along its drift shell; c) Bounce-averaged description of the guiding center drift path: the
1993   intersection of the drift shell with the minimum-B surface is called the drift contour (Γ). The 3D
1994   diffusion-driven radiation belt models (equation (2-24) **Section 2.3.2**) are even more compact:
1995   they provide a description of the radiation belt dynamics that is averaged over the drift phase
1996
1997   An adiabatic coordinate can vary if the forces acting on a particle vary on a timescale shorter
1998   than the corresponding period.
1999
2000   *Definition of L^*:*
2001   The adiabatic invariants are calculated by an integral over the periodic motion. The third
2002   adiabatic invariant is
2003

$$J_3 = \oint_{shell} (\boldsymbol{p} + q\boldsymbol{A}) \cdot \boldsymbol{dl} \qquad (5\text{-}1)$$

2004
2005   where $\boldsymbol{p}$ is the particle's momentum, $\boldsymbol{A}$ is the local magnetic vector potential, and $\boldsymbol{dl}$ is the path
2006   length. The integral goes over the entire drift around the planet. If the particles do not surround
2007   the planet, J_3 cannot be computed and L^* is not defined.
2008   Because the contribution from the particle's momentum $\boldsymbol{p}$ is negligible, the third adiabatic
2009   invariant is proportional to the magnetic flux Φ encompassed by the drift contour Γ:
2010

$$\Phi = \oint_{\Gamma} \boldsymbol{A} \cdot \boldsymbol{dl} \qquad (5\text{-}2)$$

2011
2012   where $\boldsymbol{A}$ is the local magnetic vector potential and $\boldsymbol{dl}$ is the path length along the drift contour Γ.
2013   Because the notion of magnetic flux is not very intuitive, Roederer (1970) introduced the
2014   adiabatic coordinate L^*, defined by the equation:
2015

$$L^* = \frac{2\pi B_E R_E^2}{|\Phi|} \tag{5-3}$$

2016

2017 where $B_E = 30,000\ nT$ is the magnitude of the equatorial magnetic field at one Earth radius

2018 $R_E = 6,372\ km$. Note that also other values have been used throughout the years since the value

2019 of the Earth's dipole moment slowly varies with time.

2020 Thus, L^* is a normalized quantity related to the magnetic flux encompassed by the drift contour

2021 of a given particle. Therefore, to determine L^*, it is necessary to determine the drift contour Γ.

2022

2023 *Characterization of the drift contour Γ in the general case:*

2024 In a steady state, the total energy of the guiding center ε is constant along the drift contour Γ

2025 (e.g. Schulz and Lanzerotti 1974, p.40, eq. (1.63)). In other words, for all bounce-averaged

2026 guiding center locations r which are elements of Γ:

2027

$$\varepsilon(r) = T(r) + qU(r) = cst. \tag{5-4}$$

2028

2029 where U is the electrostatic potential (measured either at the mirror point or equivalently at the

2030 magnetic equator – U is constant along equipotential magnetic field lines), and T is the guiding

2031 center kinetic energy:

2032

$$T = E_o \sqrt{1 + \frac{2MB_m}{E_o}} - E_o \tag{5-5}$$

2033

2034 where $E_o = m_o c^2$ is the rest mass energy (511 keV for an electron, 938 MeV for a proton), M is

2035 the relativistic magnetic moment, and B_m is the mirror point magnetic field intensity. Therefore,

2036 the definition of the drift contour depends on (1) the characteristics of the population considered

2037 (energy, charge, mass, pitch angle), and (2) the characteristics of the fields (magnetic and electric

2038 field geometry).

2039

2040 *Characterization of the drift contour Γ for energetic particles:*

2041 For Earth's radiation belt populations, it is commonly assumed that the kinetic energy is so high

2042 that the effect of electrostatic potentials on trapped particle drift motion can be omitted ($T \geq$

2043 $100\ keV \gg |qU|$, thus $\varepsilon \approx T$). As a result, the drift shell and the corresponding drift contour

2044 are characterized by the relation:

2045

$$B_m(r) = cst. \tag{5-6}$$

2046

2047 Therefore, the tracing of a drift contour related to a radiation belt population does not depend on

2048 the population charge, mass, or energy. It only depends on the magnetic field geometry and the

2049 population equatorial pitch angle.

2050

2051   It is important to keep in mind that this approximation can break down, even at Earth (e.g.
2052   Selesnick et al. 2016). At Saturn, the magnetic field close to the planet is very symmetric and yet
2053   a non-radial electric field component forces energetic and plasma particles to deviate from
2054 $B_m(\mathbf{r}) = cst.$ contours (Andriopoulou et al. 2012; Thomsen et al. 2012).
2055

2056   *Characterization of the drift contour Γ for energetic particles in a dipole field:*
2057   In the special case of radiation belt particles trapped in a magnetic dipole field, the drift contour
2058 Γ is a circle ($r = cst. = r_0$) and the magnetic flux encompassed by the drift contour Γ is equal
2059   to $|\Phi| = 2\pi B_E R_E^3 / r_0$. Thus, for radiation belt particles in a dipole field, L^* merges with the
2060   normalized equatorial radial distance ($L^* = r_0/R_E$). That is why the L^* coordinate is often
2061   associated with the equatorial radial distance of a particle's drift shell.
2062

2063   *Physical meaning of L*:*
2064   The association between the L^* coordinate and the normalized equatorial radial distance of a
2065   particle's drift shell is not possible in magnetic topologies other than the magnetic dipole field.
2066   However, since L^* is an adiabatic invariant, L^* remains constant when all non-dipolar
2067   contributions to the magnetic field are turned off adiabatically (that is, with a characteristic time
2068   that is extremely slow compared to the population drift period).

2069   The coordinate L^* corresponds to the normalized radius of the circular guiding contour on which
2070   particles are found after non-dipolar contributions to the magnetic field and all electric field
2071   components have been turned off adiabatically.

2072   An illustration of this concept is provided **Fig. 12**.
2073
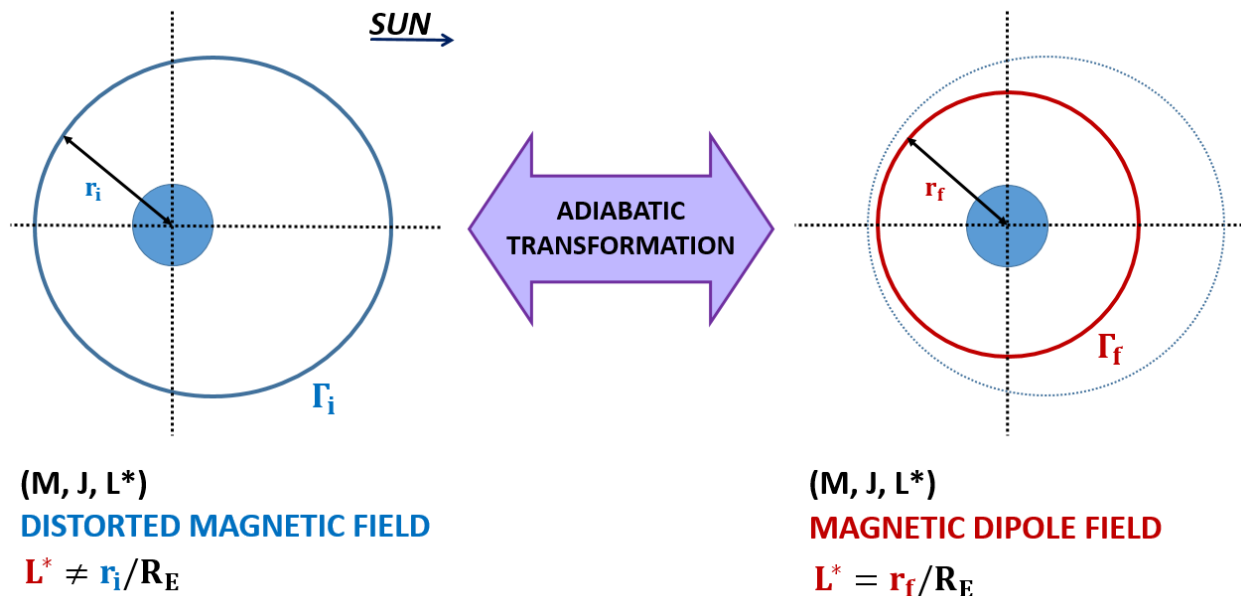
Fig. 12 Representation of the physical meaning of the L* coordinate. (Left) A population with
adiabatic invariants (M, J, L^*) is trapped in a distorted magnetic field. The initial drift contour Γ_i
is represented in blue. When the magnetic field is adiabatically transformed into a dipole field,
the population conserves all three invariants. (Right) In the resulting dipole field, the drift

2079 contour for the population with the same adiabatic invariants (M, J, L^*) is a circle of radius $R_E L^*$
2080 The final drift contour Γ_f is represented in red.

2081

2082 ### 5.1.2. Misconceptions about L^*

2083

2084 *L^* is not a spatial coordinate, it is the electromagnetic coordinate of a geomagnetically trapped*
2085 *particle:*
2086 Azimuthal asymmetries in the electric and/or magnetic fields lead to drift shell distortions that
2087 are pitch angle dependent. Particles with different pitch angles that are observed on a common
2088 field line at a given local time have different L^* coordinates and they populate different drift
2089 shells. This effect is called shell splitting (e.g., Stone 1963; Roederer and Schulz 1971; Roederer
2090 1972; Schulz 1972; Roederer et al. 1973; Selesnick et al. 2016). Therefore, the point at which a
2091 field line crosses the equatorial plane does not uniquely define the drift contour.

2092

2093 *"Energization by radial transport" is not equivalent to "violation of the third adiabatic*
2094 *invariant":*
2095 Too often, the L^* coordinate is hastily introduced as "roughly the normalized equatorial distance
2096 of particle drift shells". A side effect of the routine association between L^* and normalized
2097 equatorial radial distance is the incorrect belief that energization by radial transport requires
2098 violation of the third adiabatic invariant. In fact, it is possible to energize particles while
2099 conserving all three adiabatic invariants. In **Fig. 12** for instance, the distorted magnetic field
2100 (left) is slowly transformed into a dipole field (right). The conservation of the third invariant
2101 means that the magnetic flux encompassed by the initial drift contour Γ_i (left) is equal to
2102 magnetic flux encompassed by the final drift contour Γ_f (right). Because the area within the
2103 initial drift contour Γ_i is larger than the area within the final drift contour Γ_f, we deduce that the
2104 initial amplitude of the magnetic field at the mirror point along Γ_i is smaller than the final
2105 amplitude of the dipole magnetic field at the mirror point along Γ_f. Therefore, because of the
2106 conservation of the first adiabatic invariant (see equation (2-1)), the kinetic energy of the
2107 population considered is higher in the dipole configuration (right) than in the initially distorted
2108 configuration (left). In other words, there is an energy gain that accompanies the magnetic
2109 dipolarization represented **Fig. 12**.

2110

2111 If the dipole field (right) slowly returns to its initially distorted configuration (left), the
2112 population considered will lose exactly the same amount of kinetic energy as it had gained
2113 during the dipolarization. The kinetic energy of the population considered will return to its initial
2114 value. Therefore, adiabatic energization is a reversible process. Even when so, fully adiabatic
2115 changes in particle fluxes are known to play an important role in the storm time dynamics of the
2116 Earth's radiation belts (e.g., Dessler and Karplus 1961; Kim and Chan 1997).

2117

2118 It is worth emphasizing the key role played by induced electric fields during adiabatic
2119 energization. It is indeed the induced electric fields that make the connection between changing
2120 magnetic fields and particles' acceleration. During changes in the magnetic field configuration,

2121   the energy transfer results from two betatron effects acting simultaneously: a gyro-betatron, in
2122   which the curl of the induced electric field acts around the circle of gyration, and a drift betatron,
2123   in which the curl of the induced electric field acts around the drift circle. If the magnetic field
2124   changes slowly enough, the gyro-betatron acceleration ensures conservation of the first adiabatic
2125   invariant while the drift betraton acceleration ensures conservation of the third adiabatic
2126   invariant (e.g. Fillius and McIlwain 1967; Roederer 1970).

2127

2128   5.1.3. Challenges inherent to the L^* coordinate

2129

2130   The L^* coordinate depends on the topologies of the electric and magnetic fields, and on the
2131   characteristics of the population considered (charge, mass, energy, pitch angle) (equation (5-4)).
2132   This definition becomes somewhat simpler for Earth's radiation belt populations (equation (5-
2133   6)). Even so, L^* is a cumbersome parameter to handle:

2134   -   It requires knowledge of the global electromagnetic field geometry at a given instance – an
2135   information that no measurement can provide. Thus, the quantification of L^* is always
2136   somewhat uncertain.
2137   -   The standard method for determining L^* requires a computationally expensive drift contour
2138   tracing (see for instance the numerical recipe provided by Roederer and Zhang (2014, p. 83)).
2139   Therefore, some approximation of the L^* parameter is often preferred in practice.

2140   Thus, any work on radial diffusion requires setting a magnetic field model, and setting a method
2141   to quantify the L^* coordinate. It is understood that both parameterizations should be as accurate
2142   as possible.
2143   In addition, it is important to keep in mind that L^* is a parameter for stably trapped populations.
2144   This poses a limit to radial diffusion studies. Indeed, the drift contour needs to be a closed curve
2145   for L^* to be determined. Thus, populations located on open field lines and quasi-trapped
2146   populations cannot be parametrized with L^*. For instance, particles located in the nightside of the
2147   geostationary orbit can be in the drift loss cone during active times, drifting towards regions of
2148   open field lines in the dayside where they are lost ("magnetopause shadowing"). In addition,
2149   there exist regions of space close to the dayside magnetopause of the Earth where each field line
2150   has two minima. This particular geometry leads to drift orbit bifurcations (also known as
2151   Shabansky orbits), and it precludes the definition of L^* (e.g. Öztürk and Wolf 2007). Therefore,
2152   if the population considered is not stably trapped, it is strictly speaking impossible to attribute a
2153 L^* coordinate, never mind computing a radial diffusion coefficient!

2154

2155   5.2.   Violation of the third adiabatic invariant

2156

2157   Radial diffusion is a statistical characterization of the violation of the third adiabatic invariant
2158   across a particle population. Thus, this concept has to do variations of the magnetic flux
2159   encompassed by the drift contour of a trapped population. In the following, we discuss the
2160   ingredients required for the violation of the third adiabatic invariant, in the most general way.

2161

2162   5.2.1.   Relation between magnetic field variations and violation of L^*

2163

2164   *The violation of L^* requires field fluctuations that depend on local time*

2165   The broadening of an initially thin drift shell is indicative of the violation of the L^* coordinate for

2166   the population considered. In the following we expand on the mechanism proposed by Parker

2167   (1960), introduced **Section 2.3.1**. We show that the condition for an initially thin drift shell to

2168   broaden is the presence of asymmetric field fluctuations, i.e., field fluctuations that depend on

2169   local time, with a characteristic time comprised between the bounce and the drift periods of the

2170   population considered. The case of equatorial particles trapped in a time varying magnetic field

2171   is discussed for the sake of simplicity. Generalization is straightforward (via an appropriate

2172   redefinition of the drift contour – equation (5-4)).

2173

2174   Let us track the drift motions of two radiation belt equatorial guiding centers with the same three

2175   adiabatic invariants $(M, J = 0, L^*)$, located at r_1 and r_2 along the same drift contour Γ_i (**Fig. 13**).

2176   By definition of a drift contour, the equatorial magnetic field intensity is the same at r_1 and r_2 at

2177   time t: $B(r_1, t) = B(r_2, t) = B_i$.

2178   As the magnetic field starts varying (with a characteristic time that is long enough so as to

2179   conserve the first two invariants, but short in comparison with the drift period of the trapped

2180   population), the drift velocity departs from its value under stationary conditions, and the guiding

2181   centers move away from their initial drift contour Γ_i (the motions are represented by the red and

2182   blue arrows **Fig. 13**, right panel).

2183   At time $t + dt$, the guiding center initially located at r_1 is now at $r_1 + dr_1$, and the guiding

2184   center initially located at r_2 is now at $r_2 + dr_2$. In order for the two guiding centers to share the

2185   same guiding contour at $t + dt$, thus to remain on the same drift shell at $t + dt$, the new

2186   locations should be such that $B(r_1 + dr_1, t + dt) = B(r_2 + dr_2, t + dt)$.

2187   With a first order approximation in dt, one obtains that $B(r_1 + dr_1, t + dt) = B(r_1, t) +$

2188 $(dB(r_1, t)/dt)dt$, and $B(r_2 + dr_2, t + dt) = B(r_2, t) + (dB(r_2, t)/dt)dt$. Since $B(r_1, t) =$

2189 $B(r_2, t) = B_i$, it results that $B(r_1 + dr_1, t + dt) = B(r_2 + dr_2, t + dt) = cst. \Leftrightarrow$

2190 $dB(r_1, t)/dt = dB(r_2, t)/dt$. In other words, if the magnetic field varies in a similar way all

2191   along the initial drift shell ($dB(r, t)/dt = cst.$ along Γ_i), the guiding centers will stay on a

2192   common shell. On the other hand, if the magnetic field variations depend on local time, the

2193   initially thin drift shell will broaden.

2194

SUN

r_2

$\odot$
$B(r,t)$

r_1

$\Gamma_i: B_i = cst$

time t **(M, J, L*)**	$B(r_1) = B_i$ $B(r_2) = B_i$

SUN

$r_2 + dr_2$

$\odot$
$B(r,t+dt)$

$r_1 + dr_1$

SUDDEN VARIATION

time t+dt **(M, J, ?)**	$B(r_1 + dr_1) = B_i + \dfrac{dB}{dt}(r_1)dt$ $B(r_2 + dr_2) = B_i + \dfrac{dB}{dt}(r_2)dt$
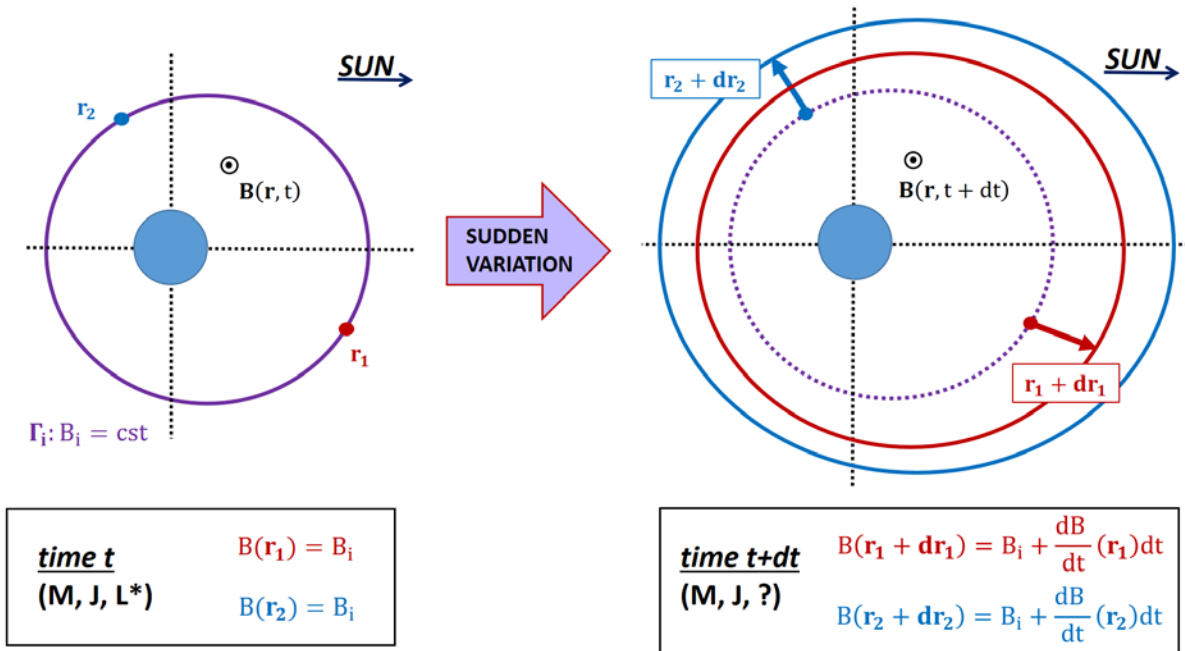
Fig. 13 Schematic drawing of the broadening of the drift shell. (Left) Initially, the guiding centers located at r_1 and r_2 have the same adiabatic invariants. They share the same drift contour Γ_i. The magnetic field varies during dt, a time interval that is long enough so as to conserve the first two invariants, but small enough so that the third invariant can be violated. At $t + dt$, the guiding centers have new locations ($r_1 + dr_1$ and $r_2 + dr_2$, respectively). These new locations determine new drift contours ($B(r_1 + dr_1) = cst.$, in red on the right panel, and $B(r_2 + dr_2) = cst.$, in blue on the right panel). For the drift contours to merge, it is necessary that $(B(r_1 + dr_1) = B(r_2 + dr_2))$. That is, the variation of the magnetic field should be the same at r_1 and r_2

In Parker's scenario (**Section 2.3.1**), the compression of the magnetic field is stronger on the dayside than on the nightside, which commonly happens as a result of enhanced solar wind pressure. Particles are transported closer to Earth on the dayside than on the nightside, and different portions of the initial ring of particles populate different shells as the particles drift around the Earth.
More generally, we find that the condition for a thin drift shell of equatorial radiation belt particles to broaden is that the time variations of the equatorial magnetic field depend on local time. This concept is at the heart of the formulation of the instantaneous rate of change of L^*.

Analytical expressions for the instantaneous rate of change of L^* (dL^*/dt):
The following results have been demonstrated in real space (**r**) by Lejosne et al. 2012 and Lejosne, 2013. Equivalent formulas had already been demonstrated by Northrop (1963) in the ($\alpha, \beta, \varepsilon$) coordinate system, where α and β are coordinates related to the magnetic field topology (Euler potentials) and ε identifies with the total energy of particles in the static case. The

2221   underlying theoretical framework and formula derivations are gathered in the **Appendix**. In the
2222   following, the quantities considered are averages over the bounce period of the population
2223   considered – because it is assumed that the first two adiabatic invariants are conserved.
2224   In the most general case, the instantaneous rate of change of L^* is:

$$\frac{dL^*}{dt}(\boldsymbol{r_o}, t) = \frac{L^{*2}}{2\pi B_E R_E^2} \oint_{\boldsymbol{r}\in\Gamma(r_o)} \frac{B_o(\boldsymbol{r}, t)}{|\nabla_o \varepsilon(\boldsymbol{r}, t)|} \left(\frac{d\varepsilon}{dt}(\boldsymbol{r}, t) - \frac{d\varepsilon}{dt}(\boldsymbol{r_o}, t)\right) dl \tag{5-7}$$

2225   where $\mathbf{r_o}$ is the guiding center location along the drift contour $\Gamma(r_o)$ at time t, B_o is the equatorial
2226   magnetic field intensity, ε is the total (kinetic+potential) energy of the guiding center, and $\nabla_o \varepsilon$ is
2227   the gradient of ε determined with constant mirror point magnetic field intensity. The drift
2228   contour Γ comprises of all equatorial radial distances around the planet that a particle with fixed
2229   adiabatic invariants can have. The integral goes over the full drift contour. dl is an infinitesimal
2230   displacement along Γ. Equation (5-7) is equivalent to (5-9), as shown in the **Appendix**.
2231
2232   <u>Reformulations in terms of deviation from the drift-average:</u>
2233   Let us introduce the drift-average spatial operator $[\ \ ]_D$, such that
2234

$$[f]_D(t) = \frac{1}{\tau_D} \oint_{\boldsymbol{r}\in\Gamma} \frac{f(\boldsymbol{r}, t)}{|\boldsymbol{V_D}(\boldsymbol{r}, t)|} dl = \frac{1}{\tau_D} \int_{\tau=0}^{\tau_D} f(\boldsymbol{r}(\tau), t) d\tau \tag{5-8}$$

2235
2236   where the integral is over the drift contour, $\boldsymbol{V_D}$ is the bounce-averaged drift velocity, τ_D indicates
2237   the drift period of the population considered, and Γ is the associated drift contour at time t.
2238 $[f]_D(t)$ determines the spatial average of an arbitrary quantity f at time t, along the drift contour
2239 Γ. Each drift contour element is weighted by the time spent drifting through that location if the
2240   electromagnetic conditions were time-stationary.
2241
2242   With that operator, the equation (5-7) is also:

$$\frac{dL^*}{dt}(\boldsymbol{r_o}, t) = \frac{L^{*2}}{q\Omega B_E R_E^2} \left(\left[\frac{d\varepsilon}{dt}\right]_D(t) - \frac{d\varepsilon}{dt}(\boldsymbol{r_o}, t)\right) \tag{5-9}$$

2243   where $\Omega = 2\pi/\tau_D$ is the population angular drift velocity. This is the same formula as the one
2244   derived by Northrop (1963, eq. (3.80), p.64), reviewed by Cary and Brizard (2009, p.717), and
2245   derived here in the **Appendix** as equation (A-43).
2246

2247   5.2.2.   Requirements for L^* violations
2248
2249   <u>*L* can only be violated if the time variations of the field depend on local time:*</u>

2250 If the time variations of the fields are the same all along the drift contour $(d\varepsilon/dt\,(\boldsymbol{r_o},t) =$
2251 $[d\varepsilon/dt]_D(t)$ for all guiding center locations $\boldsymbol{r_o}$ along the drift contour) then it follows, in a
2252 symmetric field:

$$\frac{dL^*}{dt}(\boldsymbol{r_o},t) = 0 \tag{5-10}$$

2253 This is consistent with the result obtained paragraph **5.2.1.**
2254
2255 *dL*/dt is zero on drift-average along the drift contour:*
2256 The instantaneous rate of change of L^* for a guiding center located at $(\boldsymbol{r_o},t)$ along the drift
2257 contour is proportional to $\big([d\varepsilon/dt]_D(t) - d\varepsilon/dt\,(\boldsymbol{r_o},t)\big)$. Thus, the drift average of the
2258 variations of L^* along $\Gamma(r_o)$ is zero:

$$\left[\frac{dL^*}{dt}\right]_D (t) = 0 \tag{5-11}$$

2259 This result is consistent with the fact that there is no net transport of the third adiabatic invariant
2260 if all guiding centers are homogenously distributed along the drift contour (i.e., it is zero under
2261 the assumption of phase mixing).
2262
2263 *There is a competition between the drift period and the characteristic time for the variation of*
2264 *the fields:*
2265 The general expression of dL^*/dt (equation (5-9)) highlights the competition between the
2266 characteristic time for the variation of the field τ_C and the drift period τ_D of the population
2267 considered. Since the instantaneous rate of change of L^* is proportional to τ_D/τ_C (equation (5-
2268 9)), L^* remains approximately constant if the characteristic time for the variation of the field is
2269 very long in comparison with the drift period : $(\tau_D/\tau_C \ll 1) \Rightarrow (dL^*/dt \ll 1)$. This is in
2270 agreement with the fact that L^* is an adiabatic invariant associated with drift motion.
2271

2272 5.2.3. Challenges
2273
2274 In the most general case, the quantification of dL^*/dt requires:

2275 - to define the drift contour of the population considered at a given instance,
2276 - to evaluate the electric and magnetic fields, together with their total time derivatives – i.e., to
2277   evaluate the total changes as seen by the particles $(d/dt = \partial/\partial t + \boldsymbol{V_D} \cdot \boldsymbol{V})$, over the entire
2278   drift shell, at a given instance.

2279 Since no measurement can provide such information, there is ineluctable uncertainty when
2280 quantifying dL^*/dt. Thus, it is important to approach any work on radial diffusion by
2281 determining the fields chosen, together with the approximation chosen to evaluate dL^*/dt.

2282   In addition, it is important to keep in mind that the proposed framework relies on the frozen field
2283   condition (See also **Section 2.3.1; Appendix**). This requires no electric field component parallel
2284   to the magnetic field direction and a perfectly conducting Earth's surface. In practice, both
2285   assumptions should be examined in the region of interest.
2286

2287   5.3.   Radial diffusion is a formalism
2288

2289   The radial diffusion formalism and the associated Fokker-Planck equation are commonly
2290   assumed to apply *de facto*. Yet, this is incorrect (see also **Section 2.3.2**). The concept of radial
2291   diffusion has been introduced to tackle the degree of randomness in cross drift shell motion. It
2292   provides a simple average description for the dynamics of a given population. In addition to the
2293   derivation of the diffusion equation introduced and discussed **Section 2.3.2**, we review in the
2294   following to compute a radial diffusion coefficient. That way, we highlight the set of
2295   assumptions underlying the radial diffusion formalism.
2296

2297   5.3.1. Derivation of a radial diffusion coefficient
2298

2299   Let us derive a general formulation for the radial diffusion coefficient, starting from the
2300   expression of the instantaneous rate of change of L^* at a location **r** and a time t:

$$V_L(q, M, J; \boldsymbol{r}, t) = \frac{dL^*}{dt}(q, M, J; \boldsymbol{r}, t) \tag{5-12}$$

2301   with dL^*/dt described in the general equation (5-9). V_L is called the the Lagrangian velocity in
2302 L^* of a radiation belt particle with characteristics (q, M, J).
2303

2304   *Integration over a time interval t*
2305   After a time t, the variation in the L^* of a particle (q, M, J) is equal to

$$\Delta L^* = L^*(\boldsymbol{r}(t), t) - L^*(\boldsymbol{r}(0), 0) = \int_0^t V_L(\boldsymbol{r}(u), u)\, du \tag{5-13}$$

2306

2307   *Computation of the expectation value for the mean square displacement*
2308   The expectation value of the square of the displacement is equal to

$$[(\Delta L^*)^2] = \int_0^t \int_0^t [V_L(\boldsymbol{r}(u), u) V_L(\boldsymbol{r}(v), v)]\, du dv \tag{5-14}$$

2309   where [ ] denotes the expectation value. Therefore, it is necessary to compute the
2310   autocorrelation function of the Lagrangian velocity V_L, a function of both time and space, in
2311   order to derive the radial diffusion coefficient.

2312

2313   *Separation of the spatial and temporal dependence for the velocity V_L*
2314   How does one describe the Lagrangian velocity $V_L(\boldsymbol{r}(t), t)$? The traditional assumption is that
2315   the spatial and temporal functions are independent ($V_L(\boldsymbol{r}, t) = \lambda(t)\gamma(\boldsymbol{r})$). In addition, because
2316   the particles are drifting in close shells around Earth, it is considered that the spatial function is a
2317   periodic function in local time, with a periodicity defined by the particle drift period. Because the
2318   radial diffusion formalism assumes small variations for the coordinate of interest, the radial
2319   dependence of the spatial function is often omitted $\left(\gamma(\boldsymbol{r}) = \gamma(\varphi) = \gamma(\Omega t - \varphi_0)\right)$. As a result,
2320   the velocity V_L is rewritten in terms of a product:

$$V_L(\boldsymbol{r}(t), t) = \lambda(t)cos(\Omega t - \varphi_0) \tag{5-15}$$

2321   where λ describes the temporal variations of the Lagrangian velocity, and $cos(\Omega t - \varphi_0)$
2322   represents the particle location at time t (Ω and φ_0 are respectively the angular drift velocity and
2323   the initial drift phase of the particle considered). This formulation could be further elaborated by
2324   rewriting $V_L(\boldsymbol{r}(t), t)$ as a Fourier sum $\sum_n \lambda_n(u)cos\left(n\varphi + \varphi_{0,n}\right)$. For the sake of simplicity, we
2325   only consider the first harmonic $n=1$ in the following. The generalization is straightforward.

2326

2327   *Drift phase averaging*
2328   We compute the expectation value of $V_L(\boldsymbol{r}(u), u)V_L(\boldsymbol{r}(v), v)$ by averaging over multiple
2329   scenarios, and including all possible initial drift phases.
2330   As a result:

$$[V_L(\boldsymbol{r}(u), u)V_L(\boldsymbol{r}(v), v)] = \frac{1}{2}[\lambda(u)\lambda(v)]cos(\Omega(u - v)) \tag{5-16}$$

2331   *Stationary signals*
2332   It is then assumed that the signal λ is stationary in the wide sense (e.g. Taylor 1922). The mean
2333   and the autocovariance of λ do not vary with time. Thus, that the autocorrelation $[\lambda(u)\lambda(v)]$
2334   only depends on the lag between u and v. The integral (5-14) becomes:

$$[(\Delta L^*)^2] = t \int_0^t [\lambda(T)\lambda(T + \tau)]cos(\Omega\tau)\, d\tau \tag{5-17}$$

2335   where $[\lambda(T)\lambda(T + \tau)]$ does not depend on T. Once the time τ becomes longer than the
2336   autocorrelation time of the signal λ, the expectation value of $[\lambda(T)\lambda(T + \tau)]$ becomes zero.
2337   Thus, the integral reaches a finite value once t is large enough.
2338   In that context, the mean square of the displacement will grow linearly with time, and the rate of
2339   change of $[(\Delta L^*)^2]$ will be constant:

$$\frac{d}{dt}([(\Delta L^*)^2]) = \int_0^\infty [\lambda(T)\lambda(T+\tau)]\cos(\Omega\tau)\, d\tau \tag{5-18}$$

2340   It is the magnitude of the rate of change of $[(\Delta L^*)^2]$ that determines the radial diffusion
2341   coefficient (see also **section 2.3**):

$$D_{LL} = \frac{1}{2}\frac{d}{dt}([(\Delta L^*)^2]) \tag{5-19}$$

2342

2343   We identify part of equation (5-17) as being the power spectrum P_λ of the fluctuations λ at the
2344   angular drift velocity Ω:

$$P_\lambda(\Omega) = 4\int_0^\infty [\lambda(t)\lambda(t+\tau)]\cos(\Omega\tau)\, d\tau \tag{5-20}$$

2345   Note that we assume $\lambda(t)$ to be in a way that P_λ is independent on time. With this it results that:

$$D_{LL} = \frac{P_\lambda(\Omega)}{8} \tag{5-21}$$

2346   For instance, if the autocorrelation of the signal λ is described by an exponential function:

$$[\lambda(T)\lambda(T+\tau)] = [\lambda_0^2]\, e^{-\tau/\tau_\lambda} \tag{5-22}$$

2347   where $[\lambda_0^2]$ is the mean square velocity, and the exponential time constant τ_λ represents the
2348   characteristic time over which the signal λ is correlated with its previous values, it results that

$$D_{LL}(\Omega) = \frac{[\lambda_0^2]}{2}\frac{\tau_\lambda}{1+\Omega^2\tau_\lambda^2} \tag{5-23}$$

2349   Thus, if $\tau_\lambda \ll 1/\Omega$, i.e. if the autocorrelation time is very small in comparison with the
2350   population drift period, $D_{LL}(\Omega) = [\lambda_0^2]\tau_\lambda/2$. The diffusion coefficient becomes independent of
2351   energy. It increases when the mean square velocity increases (i.e. when the field fluctuations
2352   increases), and when the autocorrelation time increases (i.e. when the particles are pushed in the
2353   same direction for a longer time). On the other hand, if $\tau_\lambda \gg 1/\Omega$, $D_{LL}(\Omega) = [\lambda_0^2]/(2\Omega^2\tau_\lambda)$, and
2354   the diffusion coefficient decreases with increasing energy. Thus, the variations of the diffusion
2355   coefficient with particles' energy can provide information on the autocorrelation time of the
2356   signal λ, and vice versa.
2357

2358 **5.3.2. Applicability of the concept of diffusion**

2359

2360 *Applicability of the concept of radial diffusion:*
2361 Radial diffusion can be used pragmatically in order to describe planetary environments. It is
2362 important to keep in mind that the concept of radial diffusion is a formalism that trades accuracy
2363 and complexity for expediency and simplicity. Expediency is of practical use when trying to
2364 forecast or "now-cast" space weather. The diffusion coefficient is free from the mathematical
2365 standpoint. It can in principle be tailored to fit observations, therefore allowing good control over
2366 the model solutions, which is not the case for more sophisticated methods like particle tracing.
2367 The simplicity of diffusion can be needed in data starved scenarios, where no multi-point
2368 observations and/or observations of similar locations at different times are available that would
2369 be needed to constrain more sophisticated approaches. While the limitation on data has reduced
2370 at Earth in the recent decades, it is still true for the outer planets. Simplicity and expediency
2371 make diffusion a useful data analysis tool because it allows to change the parameters of the
2372 model and quickly see the outcome of the numerical experiment.

2373

2374 To what extent the diffusion formalism is a realistic description on the actual physics is a
2375 separate question. Radial diffusion is germane to the Fokker-Planck equation, which provides an
2376 average description of the particle dynamics, based on average properties of the field. The
2377 modeled distribution function is a drift averaged function, and information on the drift phase is
2378 lost. Several important assumptions were made in the derivation of the Fokker-Planck equation.
2379 For example, it was assumed that there were many very small fluctuations in L^*, and that the
2380 distribution function was always uniform in longitude. Radial diffusion is the result of many
2381 small uncorrelated perturbations of the particles' drift motion. Since none of these assumptions
2382 holds true during active times in a magnetosphere, the radial diffusion formalism cannot apply to
2383 major events. In particular, it cannot describe the massive injections characteristic of a substorm.
2384 Thus, in addition to the difficulty in proposing and calculating radial diffusion coefficients,
2385 solving the proposed Fokker-Planck equation does not prove that radial diffusion occurs.

2386

2387 Radial diffusion can be more or less adequate, depending on the region that is considered. For
2388 electrons in Earth's outer radiation belt, radial diffusion agrees poorly with the results obtained
2389 by tracking test particles when applied to event analysis (Riley and Wolf 1992; Ukhorskiy et al.
2390 2008, 2009). This can be tested by describing radial motion of trapped equatorial particles in a
2391 time-dependent electric field model (1) by tracking test particles, and (2) by solving the radial
2392 diffusion equation, with the appropriate radial diffusion coefficient calculated from the assumed
2393 electric field characteristics. This shows that:

2394 - The agreement between the simulation results and the diffusion theory predictions is
2395   mediocre when the comparison is performed for one event. Particle tracking results show
2396   much more structure in the particle distribution as a function of time and location. The results
2397   differ depending on the details of the wave (like its phase), even if the statistical wave
2398   parameters (like the average size of its structures) are the same.

2399 - The diffusion formalism describes the average outcome of different wave fields that differ in
2400   their details but share the same statistical parameters. It is also able to bracket the extreme
2401   values covered by the particle tracking results (Ukhorskiy et al. 2009).
2402 - The diffusion formalism does much better in the case of a series of sequential small storms
2403   (Riley and Wolf 1992).

2404 This behavior is similar to a finite 1D random walk process, in which the distribution function
2405 approaches the Gaussian distribution only after a sufficiently large number of steps.

2406
2407 Having said that, there are also cases where radial diffusion appears to be a very adequate
2408 description of both the physics and the measurements. An example are the inner ion belts of
2409 magnetized planets such as Earth's inner proton belt and Saturn's proton belts between the main
2410 rings and the orbit of the moon Tethys. These belts vary only slowly on the timescale of years
2411 (Qin et al. 2015) and are smoothly distributed in space, both of which has been described very
2412 well with models that are based on radial diffusion (Selesnick et al. 2013; Kollmann et al. 2017).
2413 Particularly Saturn's proton belts appear like a prototype for radial diffusion because neither
2414 internal injections nor strong solar events (Roussos et al. 2008) appear to strongly affect their
2415 population.

2416
2417 *A brief discussion on the general concept of diffusion in planetary radiation belts*
2418 Diffusion is not just limited to the radial mode, it can also occur in energy and pitch angle (or
2419 equivalent coordinates) when the first and second invariants are violated. It might be useful to
2420 highlight similarities and differences between models describing the statistical evolution of the
2421 distribution function when the first two adiabatic invariants are violated with that of radial
2422 diffusion. The commonly used formalism to describe statistically the temporal evolution of
2423 particle species experiencing violation of the first two adiabatic invariants in planetary radiation
2424 belts is quasi-linear theory (Sagdeev and Galeev 1969; Kennel and Engelman 1966). Just like
2425 radial diffusion, quasi-linear theory characterizes the evolution of the distribution function in its
2426 respective phase-space in terms of a Fokker-Planck equation. Likewise, a number of crucial
2427 assumptions are also necessary. For instance, for such a formalism to hold, the distribution
2428 function must experience very little change on time scales associated with the motion of the first
2429 and/or second adiabatic invariant. In other words, similarly to radial diffusion, the change in the
2430 action-angle variables have to be very small, i.e. $\Delta J/J \ll 1$, where J stands for one of the first
2431 two adiabatic invariants.
2432 Moreover, requirement of time-stationarity of the turbulent fluctuations responsible for the
2433 violation of the adiabatic invariants and small autocorrelation times are required to reduce the
2434 coupled Vlasov-Maxwell system in terms of a Fokker-Planck diffusion equation. In the presence
2435 of long autocorrelation times, or put differently, if particles can sample the electric and magnetic
2436 field fluctuations, phase-space structures and other nonlinear structures could form in the
2437 distribution function and affect the transport (i.e., diffusion and advection coefficients).
2438 In situ observation of large-amplitude fluctuations and nonlinear phase-space structures in the
2439 Earth's radiation belts (Cattell et al. 2008, Cully et al. 2008, Mozer et al. 2014) indicate that
2440 some caution might be required when applying quasi-linear formalisms to quantify the

2441 energization and losses of charged particles in the Earth's radiation belts. Confirmed by multiple
2442 independent experiments in the last ten years and across a wide range of geomagnetic conditions,
2443 the existence of nonlinear and/or large-amplitude fluctuations put into question the fundamental
2444 assumptions underlying quasi-linear formalisms.
2445

2446

2447 **6.   CONCLUSION: 60 years of radial diffusion research, at Earth and beyond**
2448

2449 6.1.   Summary: Observations and theory
2450

2451 The concept of radial diffusion was introduced in the year following the discovery of the Earth's
2452 radiation belts to explain the existence of the belts. Experimental evidence was found indicating
2453 that magnetically trapped particles of external origin were transported in the outer zone of the
2454 Earth's radiation belts by processes consistent with the conservation of the first two adiabatic
2455 invariants. In the same years, high altitude nuclear explosions evidenced the existence of a radial
2456 diffusion mechanism in the inner belt.
2457

2458 Early theoretical descriptions of cross drift shell motion in a background dipole field showed that
2459 electric and/or magnetic field fluctuations could drive radial diffusion, provided that the
2460 fluctuations depend on local time and occur on a timescale comprised between the bounce and
2461 the drift period of the population considered. Assuming that the field fluctuations are stationary,
2462 and that the spatial and temporal variations of the field are decoupled, the radial diffusion
2463 coefficient is proportional to the power spectrum of the field fluctuations at harmonics of the
2464 population drift frequency. Early estimates of the radial diffusion coefficients based on particle
2465 and/or field measurements showed consistency, suggesting the validity of the underlying
2466 theoretical picture.
2467

2468 There is a variety of physical drivers for the field fluctuations. Electric field fluctuations can be
2469 induced by magnetic field disturbances (due to variations in currents flowing inside or outside of
2470 the planetary magnetosphere). They can be driven from above (by variations in the coupling
2471 between the solar wind and the planetary magnetosphere), or from below (by variations in the
2472 coupling between the thermosphere and the ionosphere, which usually map directly into the
2473 magnetosphere). Ultimately, it is the sum of all these different field fluctuations that drives
2474 radiation belt particle cross drift shell motion.
2475

2476 As the temporal and spatial accuracy for radiation belt observations improved at Earth in the 90s,
2477 the data revealed complex structure and rapid dynamics which challenged the traditional picture
2478 of radiation belt dynamics provided by the Fokker-Planck equation. In particular, it was realized
2479 that relativistic electron fluxes could increase significantly on time scales that were shorter than
2480 expected. It was proposed that the rapid outer belt relativistic electron flux enhancements could
2481 be due to a drift resonant interaction with a monochromatic ULF oscillation in a distorted

2482 magnetic field. From these considerations re-emerged the idea that the asymmetry of the
2483 background magnetic field could drive a form of enhanced radial diffusion in the presence of
2484 multiple ULF frequencies. As a result, new theoretical expressions were developed in order to
2485 characterize radial diffusion in an asymmetric background field. These new formulas diverge
2486 from the traditional ones, even in the absence of asymmetry. This discrepancy indicates that the
2487 new theoretical expressions are unlikely to be fully effective in forwarding our understanding of
2488 radial diffusion. In addition, even current radial diffusion coefficient estimates rely on the
2489 assumption of a background magnetic dipole field, which poses a limit to their accuracy.
2490

2491 6.2.   Summary: physics of radial diffusion
2492

2493 Given the importance of advancing radial diffusion research for further progress in our ability to
2494 understand and to model radiation belt dynamics, it is necessary to clarify and to reassess the sets
2495 of assumptions underlying the theoretical picture of radial diffusion.
2496

2497 The first possible source of confusion associated with radial diffusion is the variable of interest.
2498 It is important to keep in mind that the appropriate coordinate to discuss radial diffusion is L^*.
2499 This adiabatic coordinate allows the separation between adiabatic and non-adiabatic energization
2500 effects in a realistic magnetic field. In the early days of radiation belt science, it was assumed
2501 that the background magnetic field was a dipole, thus, cross drift shell motion merged with radial
2502 motion in the magnetic equatorial plane. We now know that planetary magnetic fields depart
2503 from a dipole field, and that the discrepancy can sometimes be drastic, even at Earth. In the
2504 currently commonly accepted formulas for radial diffusion, the coordinate of reference is the
2505 normalized equatorial radial distance. This inescapably leads to flawed estimates.
2506

2507 Secondly, radial diffusion requires violation of the third adiabatic invariant. In other words, it
2508 requires a variation of the magnetic flux encompassed by the drift contour of a trapped
2509 population. The conditions for the third adiabatic invariant to vary (and for the first two adiabatic
2510 invariants to remain constant) are well known - even though they have been the object of little
2511 attention so far. Violation of the third adiabatic invariant requires field fluctuations that depend
2512 on local time, on timescales comprised between the bounce and the drift period of the population
2513 considered. Drift resonance is not required.
2514

2515 Thirdly, it is important to keep in mind that the concept of radial diffusion is a formalism that
2516 trades accuracy for expediency. It is germane to the Fokker-Planck equation, which provides an
2517 average description of the particle dynamics, based on average properties of the field. The
2518 modeled distribution function is a drift averaged function, and information on the drift phase is
2519 lost. Radial diffusion is the result of many small uncorrelated perturbations of the particles' drift
2520 motion. Therefore, the radial diffusion formalism cannot describe injections. It agrees poorly
2521 with the results obtained by tracking test particles when applied to event analysis. It agrees well
2522 with observations of slowly changing particle populations, like the inner ion belts of Earth and
2523 Jupiter. In summary, the use of the radial diffusion formalism and the associated Fokker-Planck
2524 equation requires caution.

2525

2526   6.3.   Some challenges for the future, near and far

2527

2528   Particles transported through L^*shells via radial diffusion gain or lose kinetic energy from the
2529   fields. Thus radial diffusion is often contrasted to local acceleration processes (that is, processes
2530   that accelerate particles without necessarily transporting them), when it comes to assessing the
2531   most important acceleration mechanism for the Earth's radiation belts. However, radial diffusion
2532   is not the only way to accelerate particles on the macroscale. Slow variations of the magnetic
2533   field and the associated gyro-betatron and drift betatron effects lead to adiabatic and reversible
2534   acceleration. Injections, as they follow substorms or interchange, can in parts lead to transport
2535   consistent with the conservation of the first two adiabatic invariants, and energization similar to
2536   diffusion. Thus, a careful analysis requires differentiating between adiabatic and non-adiabatic
2537   effects, which always depends on the accuracy of the models chosen for the fields.

2538

2539   On the other hand, it may be worth keeping in mind that predictions provided by the radial
2540   diffusion formalism provide mediocre agreement with test particle simulations when doing event
2541   analysis. Thus, a temporary discrepancy between event observations and numerical simulations
2542   relying on the Fokker-Planck equation does not necessary mean that additional processes are
2543   occurring. It may only highlight the limits of radial diffusion formalism.

2544

2545   It is interesting to note that the theoretical picture of violation of the third adiabatic invariant
2546   relies on the assumption that the plasma obeys to the "frozen-field condition". Yet, there are
2547   times and regions where this is not necessarily true. What happens to the trapped population drift
2548   motion in that context is unknown.

2549

2550   It is common practice to break down the global radial diffusion coefficient into a sum of different
2551   components. This approach is based on the assumption that the different sources of cross drift
2552   shell motion are uncorrelated. In practice, the correlation is unknown. A potential correlation
2553   between the different field fluctuations would result in a global radial diffusion coefficient
2554   distinct from the sum of the different contributions.

2555

2556   In addition, the theoretical models for the radial diffusion coefficients rely on idealized field
2557   fluctuations in which the spatial and temporal variations of the fields are decoupled. The extent
2558   to which this assumption is valid is unknown.

2559

2560   In that context, MHD simulations could provide useful information because they can provide
2561   global information on the variations of the field, in particular: on the characteristic times for the
2562   variations of the field, on the spatial and temporal coupling, on the correlation between the field
2563   components, etc.

2564

2565   Let us conclude by mentioning that there is also a need to improve the spatial and temporal
2566   accuracy of the radiation belt simulations, by introducing local time as a 4th dimension in the
2567   codes, and by developing event-specific models (e.g., Shprits et al. 2015). In that case, it is

2568 pivotal to realize the limitations of the Fokker-Planck equation, which originate by design.
2569 Finding a compromise between accuracy (achieved for instance via MHD and test particle
2570 simulations) and expediency (Fokker-Planck diffusion theory) requires a statistical reformulation
2571 of the radiation belt dynamics able to model localized (non-diffusive) radial transport, drift phase
2572 bunching, and drift echoes. Such features are specific to trapped population drift motion. Yet,
2573 they cannot be reproduced by the current numerical simulations that consist of solving a 3D
2574 Fokker-Planck equation.

2575   **APPENDIX**: Derivation for the instantaneous rate of change of the third adiabatic invariant
2576
2577   In this section, we present two different ways to derive the analytic formulation of dL^*/dt that
2578   was used in Section 5.2. Both proofs provide complementary physical insights on the process at
2579   play. The results are then reformulated in more compact ways.
2580

2581   A.1.   Theoretical Framework and Working Hypotheses
2582
2583   In the following proofs, it is assumed that:

2584   -   the frozen-in condition applies;
2585   -   all three adiabatic invariants of the population are well-defined and meaningful (no open drift
2586   shells, Lamor radius small compared to field gradients, etc.);
2587   -   the first two adiabatic invariants are conserved;
2588   -   the characteristic time for the variation of the field τ_C is very long in comparison with the
2589   bounce period of the population considered τ_B, and very short in comparison with the drift
2590   period τ_D:

$$\tau_G \ll \tau_B \ll \tau_C \ll \tau_D \tag{A-1}$$

2591
2592   where τ_G, τ_B, τ_D are respectively the gyration, bounce, and drift periods of the particle
2593   considered, and τ_C is the characteristic time for the variation of the field.
2594
2595   We use an infinitesimal time step dt adapted to this ordering:
2596

$$\tau_G \ll \tau_B \ll dt \approx \tau_C \ll \tau_D \tag{A-2}$$

2597
2598   so that we can track the bounce-averaged drift motions of the particle guiding centers.
2599
2600   In a time varying field, the guiding center drift velocity $\boldsymbol{V_D}$ is:
2601

$$\boldsymbol{V_D} = \frac{\boldsymbol{B}}{qB^2} \times \left(-q\boldsymbol{E} + \frac{m}{2B}\left(v_\perp^2 + 2v_\parallel^2\right)\boldsymbol{\nabla}_\perp B + m\frac{d\boldsymbol{V_D}}{dt} \right) \tag{A-3}$$

2602
2603   where m is the mass of the particle, q is the electric charge, and $v_\perp$ and $v_\parallel$ correspond to the
2604   particle velocities perpendicular and parallel to the magnetic field direction (e.g., Roederer 1970,
2605   eq. 1.29, p.19).
2606   The order of magnitude of the inertia term (last term in the brackets of the equation (A-3)) is
2607   very small:
2608

$$\frac{\left| \frac{m\boldsymbol{B}}{qB^2} \times \frac{d\boldsymbol{V_D}}{dt} \right|}{|\boldsymbol{V_D}|} = \left| \frac{m}{qB} \right| \cdot \frac{\left| \frac{d\boldsymbol{V_D}}{dt} \right|}{|\boldsymbol{V_D}|} = \frac{\tau_G}{\tau_C} \ll 1 \tag{A-4}$$

2609

2610   Thus, the inertia term is omitted and the drift velocity is equal to its bounce-averaged expression
2611   at the magnetic equator for every time step:

2612

$$V_D = \frac{2p\nabla_o I \times e_o}{q\tau_B B_o} + \frac{E_o \times e_o}{B_o} \tag{A-5}$$

2613

2614   where p is the particle momentum, $e_o = B_o/B_o$, B_o is the magnetic field at the magnetic equator
2615   (minimum B surface), E_o is the equatorial electric field (with both induced and electrostatic
2616   components), $I = \int_{s_m}^{s'_m} \sqrt{1 - B(s)/B_m}\,ds$ is the integral function of B_m between the mirror points
2617 s_m and s'_m, and $\nabla_o I$ is the equatorial gradient of the quantity I determined at constant magnetic
2618   field intensity B_m at the mirror points (e.g. Roederer 1970, p.49, eq.(2.41.a)).

2619

2620   Finally, all variations will be expressed as first-order approximations in dt and the total rate of
2621   change of the third invariant during dt will be merged with its instantaneous rate of change:

2622

$$dL^* = \left(\frac{dL^*}{dt}\right) dt \tag{A-6}$$

2623

2624   The objective is to compute the rate of change of the magnetic flux encompassed by the drift
2625   contour of an equatorial particle in a time varying magnetic field, in the absence of electrostatic
2626   fields.

2627

2628   A.2.   Proof #1

2629

2630   Let us track the drift motion of an equatorial particle trapped in a magnetic field. At time t, the
2631   three adiabatic invariants are $(M, J = 0, L^*)$ and the particle's guiding center is located at r_o
2632   along its drift contour $\Gamma(r_o)$. The magnetic field changes during an infinitesimal time step dt.
2633   Due to the magnetic field variation and the resulting induced electric fields, the drift velocity is
2634   altered, and the guiding center move away from its initial drift contour. At $t + dt$, the guiding
2635   center is located at $r_o + dr_o$. The equatorial magnetic field intensity along the new drift contour
2636 $\Gamma(r_o + dr_o)$ is a constant equal to $B(r_o + dr_o, t + dt)$.

2637

2638   The objective of this demonstration is to quantify the difference $d\Phi(r_o, t)$ between the magnetic
2639   flux $\Phi(r_o + dr_o, t + dt)$ encompassed by the drift contour $\Gamma(r_o + dr_o)$ at time $t + dt$, and the
2640   magnetic flux $\Phi(r_o, t)$ encompassed by the drift contour $\Gamma(r_o)$ at time t.

2641

$$d\Phi(r_o, t) = \Phi(r_o + dr_o, t + dt) - \Phi(r_o, t)$$
$$= \iint_{S(r_o+dr_o)} B(r, t + dt) \cdot dS - \iint_{S(r_o)} B(r, t) \cdot dS \tag{A-7}$$

2642

2643   where $S(r_o + dr_o)$ indicates the area encompassed by $\Gamma(r_o + dr_o)$ at time t + dt and $S(r_o)$
2644   indicates the area encompassed by $\Gamma(r_o)$ at time t. They are represented **Fig. 14**.
2645
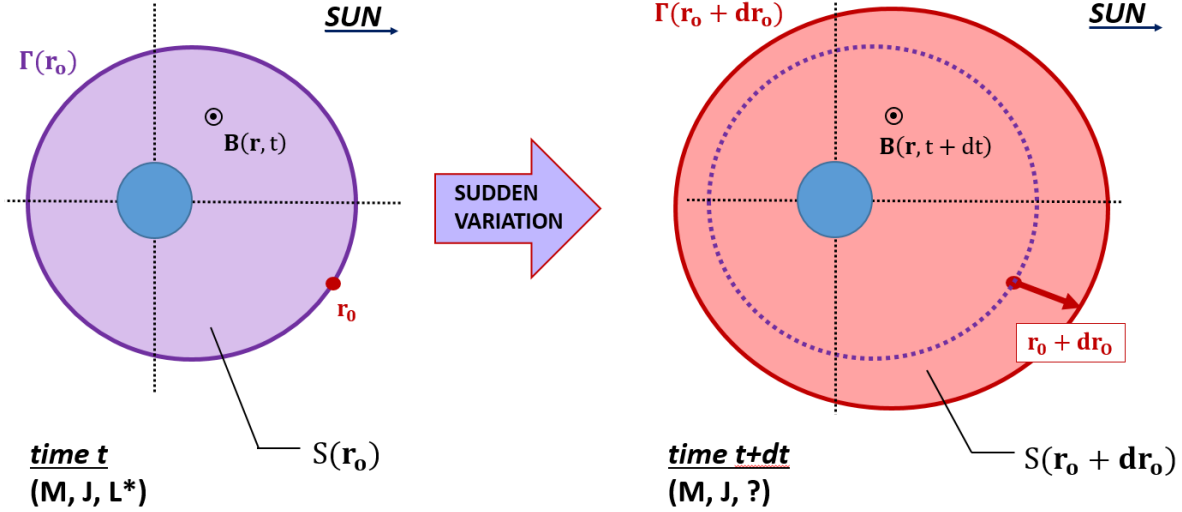
2646
2647   **Fig. 14** Representation of the drift contours $\Gamma(r_o)$ at time t (dark purple line) and $\Gamma(r_o + dr_o)$ at
2648   time $t + dt$ (dark red line), and the associated integrating surface areas $S(r_o)$ at time t (purple
2649   area) and $S(r_o + dr_o)$ at time $t + dt$ (red area)

2650
2651   By adding and subtracting the quantity $\iint_{S(r_o)} \boldsymbol{B}(\boldsymbol{r}, t + dt) \cdot \boldsymbol{dS}$ to the equation (A-7), the
2652   variation of the magnetic flux associated with the guiding center initially located at $\mathbf{r_o}$
2653   can be interpreted as the sum of a spatial contribution and a temporal contribution:

$$d\Phi(\boldsymbol{r_o}, t) = \left(\iint_{S(r_o + dr_o)} \boldsymbol{B}(\boldsymbol{r}, t + dt) \cdot \boldsymbol{dS} - \iint_{S(r_o)} \boldsymbol{B}(\boldsymbol{r}, t + dt) \cdot \boldsymbol{dS} \right)$$
$$+ \left(\iint_{S(r_o)} \boldsymbol{B}(\boldsymbol{r}, t + dt) \cdot \boldsymbol{dS} - \iint_{S(r_o)} \boldsymbol{B}(\boldsymbol{r}, t) \cdot \boldsymbol{dS} \right) \quad \text{(A-8)}$$

2654
2655   The spatial contribution is:

$$d\Phi_A(\boldsymbol{r_o}, t) = \iint_{S(r_o + dr_o)} \boldsymbol{B}(\boldsymbol{r}, t + dt) \cdot \boldsymbol{dS} - \iint_{S(r_o)} \boldsymbol{B}(\boldsymbol{r}, t + dt) \cdot \boldsymbol{dS} \quad \text{(A-9)}$$

2656
2657   It corresponds to the magnetic flux at time t+dt through the strip $A(r_o)$ between $\Gamma(r_o)$ and
2658 $\Gamma(r_o + dr_o)$. The strip is represented in green **Fig. 15**.
2659
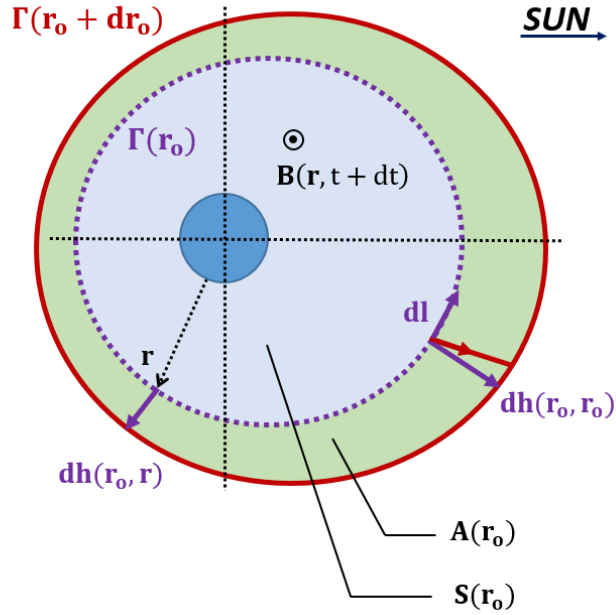
Fig. 15 Definition of the integrating surfaces: the strip $A(r_o)$ is in green, and the initial integrating surface area $S(r_o)$ is in blue. The width of the strip $A(r_o)$ starting from a location $\mathbf{r}$ along $\Gamma(r_o)$ is $dh(\mathbf{r_o}, \mathbf{r})$

The temporal contribution is:

$$d\Phi_T(\mathbf{r_o}, t) = \iint_{S(r_o)} \mathbf{B}(\mathbf{r}, t + dt) \cdot d\mathbf{S} - \iint_{S(r_o)} \mathbf{B}(\mathbf{r}, t) \cdot d\mathbf{S} \qquad \text{(A-10)}$$

This contribution corresponds to the variation of the magnetic field through the initial integrating surface area $S(r_o)$. It results that:

$$d\Phi(\mathbf{r_o}, t) = d\Phi_A(\mathbf{r_o}, t) + d\Phi_T(\mathbf{r_o}, t) \qquad \text{(A-11)}$$

Let us quantify each component individually.

For the spatial component:

$$d\Phi_A(\mathbf{r_o}, t) = \iint_{A(r_o)} \mathbf{B}(\mathbf{r}, t + dt) \cdot d\mathbf{S}$$

$$= \oint_{\Gamma(r_o)} \mathbf{B}(\mathbf{r}, t + dt) \cdot (\mathbf{dh}(\mathbf{r_o}, \mathbf{r}) \times \mathbf{dl}) \qquad \text{(A-12)}$$

For all points along $\Gamma(r_o)$, the width of the strip $dh(\mathbf{r_o}, \mathbf{r})$ is such that

$$B(\boldsymbol{r}, t + dt) - |\nabla B(\boldsymbol{r}, t + dt)|dh(\boldsymbol{r_o}, \boldsymbol{r}) = B(\boldsymbol{r_o} + d\boldsymbol{r_o}, t + dt) \tag{A-13}$$

2673   In addition, for all points along $\Gamma(r_o), B(\boldsymbol{r}, t) = B(\boldsymbol{r_o}, t)$.
2674   Thus, we have that:

$$B(\boldsymbol{r}, t + dt) = B(\boldsymbol{r_o}, t) + \frac{\partial B}{\partial t}(\boldsymbol{r}, t)dt \tag{A-14}$$

2675   As a result, for all points $\boldsymbol{r}$ along $\Gamma(r_o)$

$$dh(\boldsymbol{r_o}, \boldsymbol{r}) = \frac{dt}{|\nabla B(\boldsymbol{r}, t + dt)|}\left(\frac{\partial B}{\partial t}(\boldsymbol{r}, t) - \frac{dB}{dt}(\boldsymbol{r_o}, t)\right) \tag{A-15}$$

2676   Consequently, the spatial component is, to the first order in dt:

$$d\Phi_A(\boldsymbol{r_o}, t) = dt \oint_{\Gamma(r_o)} \frac{B(\boldsymbol{r}, t)}{|\nabla B(\boldsymbol{r}, t)|} \cdot \left(\frac{\partial B}{\partial t}(\boldsymbol{r}, t) - \frac{dB}{dt}(\boldsymbol{r_o}, t)\right) dl \tag{A-16}$$

2677
2678   For the temporal contribution, one can write that:

$$\begin{aligned} d\Phi_T(\boldsymbol{r_o}, t) &= \iint_{S(r_o)} \boldsymbol{B}(\boldsymbol{r}, t + dt) \cdot d\boldsymbol{S} - \iint_{S(r_o)} \boldsymbol{B}(\boldsymbol{r}, t) \cdot d\boldsymbol{S} \\ &= dt \iint_{S(r_o)} \frac{\partial \boldsymbol{B}(\boldsymbol{r}, t)}{\partial t} \cdot d\boldsymbol{S} \end{aligned} \tag{A-17}$$

2679
2680   Thus, using the integral form of the Maxwell-Faraday equation:

$$d\Phi_T(\boldsymbol{r_o}, t) = -dt \oint_{\Gamma(r_o)} \boldsymbol{E_{ind}}(\boldsymbol{r}, t) \cdot d\boldsymbol{l} \tag{A-18}$$

2681
2682   In addition, the projection of the electric field vector $\boldsymbol{E_{ind}}$ onto the local direction of the initial
2683   guiding drift contour is related to the drift velocity ($\boldsymbol{V_D} = -M\nabla B \times \boldsymbol{B}/\gamma q B^2 + \boldsymbol{E_{ind}} \times \boldsymbol{B}/B^2$).
2684   by the relation:

$$\boldsymbol{E_{ind}}(\boldsymbol{r}, t) \cdot d\boldsymbol{l} = -\frac{B(\boldsymbol{r}, t)}{|\nabla B(\boldsymbol{r}, t)|} \boldsymbol{V_D}(\boldsymbol{r}, t) \cdot \nabla B(\boldsymbol{r}, t)dl \tag{A-19}$$

2685

2686   Thus:

$$d\Phi_T(\boldsymbol{r_o}, t) = dt \oint_{\Gamma(r_o)} \frac{B(\boldsymbol{r}, t)}{|\nabla B(\boldsymbol{r}, t)|} \boldsymbol{V_D} \cdot \nabla B(\boldsymbol{r}, t) dl \tag{A-20}$$

2687   Finally, let us note that for all points along $\Gamma(r_o)$

$$\frac{dB}{dt}(\boldsymbol{r}, t) = \frac{\partial B}{\partial t}(\boldsymbol{r}, t) + \boldsymbol{V_D}(\boldsymbol{r}, t) \cdot \nabla B(\boldsymbol{r}, t) \tag{A-21}$$

2688   As a result, the sum of the spatial and temporal contributions to the variation of the magnetic flux
2689   is

$$d\Phi(\boldsymbol{r_o}, t) = d\Phi_A(\boldsymbol{r_o}, t) + d\Phi_T(\boldsymbol{r_o}, t)$$
$$= dt \oint_{\Gamma(r_o)} \frac{B(\boldsymbol{r}, t)}{|\nabla B(\boldsymbol{r}, t)|} \left(\frac{dB}{dt}(\boldsymbol{r}, t) - \frac{dB}{dt}(\boldsymbol{r_o}, t) \right) dl \tag{A-22}$$

2690   Thus:

$$\frac{d\Phi}{dt}(\boldsymbol{r_o}, t) = \oint_{\Gamma(r_o)} \frac{B(\boldsymbol{r}, t)}{|\nabla B(\boldsymbol{r}, t)|} \left(\frac{dB}{dt}(\boldsymbol{r}, t) - \frac{dB}{dt}(\boldsymbol{r_o}, t) \right) dl \tag{A-23}$$

2691   With

$$\frac{dL^*}{L^{*2}} = \frac{d\Phi}{2\pi B_E R_E^2} \tag{A-24}$$

2692   we obtain that

$$\frac{dL^*}{dt}(\boldsymbol{r_o}, t) = \frac{L^{*2}}{2\pi B_E R_E^2} \oint_{\Gamma(r_o)} \frac{B(\boldsymbol{r}, t)}{|\nabla B(\boldsymbol{r}, t)|} \left(\frac{dB}{dt}(\boldsymbol{r}, t) - \frac{dB}{dt}(\boldsymbol{r_o}, t) \right) dl \tag{A-25}$$

2693

2694   A.3.   Proof #2

2695

2696   The second proof consists of tracking the drift motions over all guiding center locations along
2697   the same drift contour $\Gamma(r_o)$. All guiding centers have initially the same three adiabatic
2698   invariants (M, $J=0$, L^*), but they have different drift phases at the time of the perturbation.
2699   This second proof relies on the fact that the magnetic flux through a closed curve moving at
2700 $(\boldsymbol{E_{ind}} \times \boldsymbol{B})/B^2$ is conserved, which is what we will demonstrate as a first step.

2701

2702   A.3.1. Conservation of the magnetic flux through a closed curve moving at $(E_{ind} \times B)/B^2$

2703

2704   Let us consider at time $t+dt$ the closed curve $\tilde{\Gamma}$ formed by all the new guiding center locations

2705   (see also **Fig. 16**).

2706
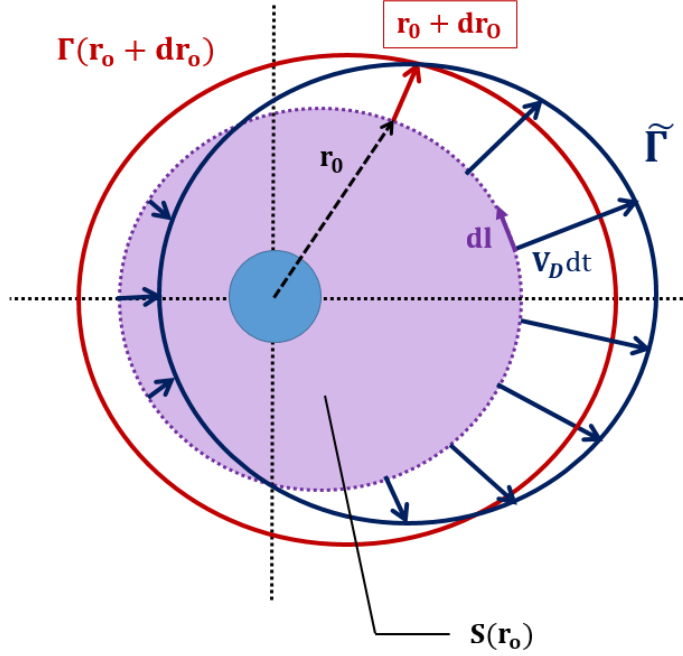
2707   **Fig. 16** Definition of the closed curve $\tilde{\Gamma}$ formed by all the new guiding center locations. Because

2708   the equatorial magnetic field intensity along $\tilde{\Gamma}$ is not necessarily constant, $\tilde{\Gamma}$ is not necessarily a

2709   drift contour. Yet, because $(E_{ind} \times B)/B^2$ is flux preserving, the flux encompassed by $\tilde{\Gamma}$ is equal

2710   to the initial magnetic flux of the population considered

2711

2712   Because the equatorial magnetic field intensity along $\tilde{\Gamma}$ is not necessarily constant, $\tilde{\Gamma}$ is not

2713   necessarily a drift contour. Yet, it is interesting to note that the magnetic flux $\tilde{\Phi}$ encompassed by

2714 $\tilde{\Gamma}$ is equal to the initial magnetic flux through $\Gamma(r_o)$. Indeed:

$$\tilde{\Phi}(t + dt) = \iint_{S(r_o)} B(r, t + dt) \cdot dS + \oint_{\Gamma(r_o)} B(r, t + dt) \cdot (V_D(r, t)dt \times dl) \qquad \text{(A-26)}$$

2715   Because

$$B(r, t + dt) \cdot (V_D(r, t) \times dl) = \big(B(r, t + dt) \times V_D(r, t)\big) \cdot dl = E_{ind}(r, t) \cdot dl \qquad \text{(A-27)}$$

2716   It results that

$$\oint_{\Gamma(r_o)} \boldsymbol{B}(\boldsymbol{r}, t+dt) \cdot (\boldsymbol{V_D}(\boldsymbol{r}, t)dt \times d\boldsymbol{l}) = dt \oint_{\Gamma(r_o)} \boldsymbol{E_{ind}}(\boldsymbol{r}, t) \cdot d\boldsymbol{l} \tag{A-28}$$

2717
2718   Using the integral form of the Maxwell-Faraday equation:
2719

$$dt \oint_{\Gamma(r_o)} \boldsymbol{E_{ind}}(\boldsymbol{r}, t) \cdot d\boldsymbol{l} = -dt \iint_{S(r_o)} \frac{\partial \boldsymbol{B}(\boldsymbol{r}, t)}{\partial t} \cdot d\boldsymbol{S}$$

$$= \iint_{S(r_o)} \boldsymbol{B}(\boldsymbol{r}, t) \cdot d\boldsymbol{S} - \iint_{S(r_o)} \boldsymbol{B}(\boldsymbol{r}, t+dt) \cdot d\boldsymbol{S} \tag{A-29}$$

2720   Thus,

$$\tilde{\Phi}(t+dt) = \iint_{S(r_o)} \boldsymbol{B}(\boldsymbol{r}, t+dt) \cdot d\boldsymbol{S}$$

$$+ \left(\iint_{S(r_o)} \boldsymbol{B}(\boldsymbol{r}, t) \cdot d\boldsymbol{S} - \iint_{S(r_o)} \boldsymbol{B}(\boldsymbol{r}, t+dt) \cdot d\boldsymbol{S} \right) \tag{A-30}$$

2721
2722   We conclude that for all guiding center locations $\boldsymbol{r_o}$ initially along $\Gamma(r_o)$:

$$\Phi(\boldsymbol{r_o}, t) = \tilde{\Phi}(t+dt) \tag{A-31}$$

2723   In other words, the drift contour distorts to conserve the magnetic flux. This is due to the fact that
2724 $(\boldsymbol{E_{ind}} \times \boldsymbol{B})/B^2$ is flux preserving (Newcomb 1958).
2725

2726   A.3.2. Reformulation for the variation of the magnetic flux
2727

2728   We reformulate the variation of the magnetic flux (equation (A-7)) using the fact that the
2729   magnetic flux encompassed by the closed curve $\tilde{\Gamma}$ at $t + dt$ is equal to the initial flux (equation
2730   (A-31)) (see also **Fig. 17**)

$$d\Phi(\boldsymbol{r_o}, t) = \Phi(\boldsymbol{r_o} + d\boldsymbol{r_o}, t+dt) - \Phi(\boldsymbol{r_o}, t)$$

$$= \Phi(\boldsymbol{r_o} + d\boldsymbol{r_o}, t+dt) - \tilde{\Phi}(t+dt) \tag{A-32}$$

$$\Phi(\mathbf{r_o} + d\mathbf{r_o}, t + dt) \qquad \widetilde{\Phi}(t + dt) \qquad d\Phi(\mathbf{r_o}, t)$$
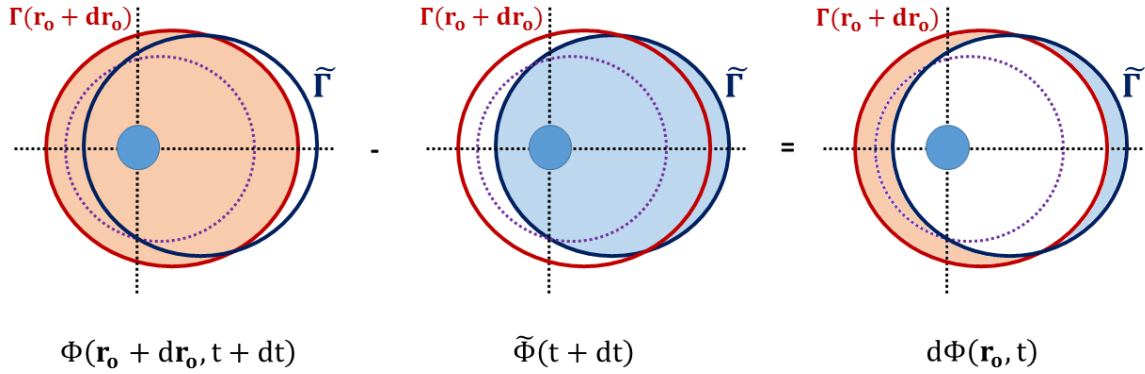
Fig. 17 Representation of the variation of the magnetic flux as the difference between the magnetic flux encompassed by the drift contour $\Gamma(r_o + dr_o)$ at $t+dt$ and the magnetic flux encompassed by the distorted contour $\tilde{\Gamma}$

Combining the equations (A-9) and (A-26), we have that

$$d\Phi(\boldsymbol{r_o}, t) = d\Phi_A(\boldsymbol{r_o}, t) - \oint_{\Gamma(r_o)} \boldsymbol{B}(\boldsymbol{r}, t + dt) \cdot (\boldsymbol{V_D}(\boldsymbol{r}, t)dt \times \boldsymbol{dl}) \qquad \text{(A-33)}$$

From the equation (A-12), we obtain that the variation of the magnetic flux is, to the first order in dt

$$d\Phi(\boldsymbol{r_o}, t) = \oint_{\Gamma(r_o)} \boldsymbol{B}(\boldsymbol{r}, t) \cdot \left((\boldsymbol{dh}(\boldsymbol{r_o}, \boldsymbol{r}) - \boldsymbol{V_D}(\boldsymbol{r}, t)dt) \times \boldsymbol{dl}\right) \qquad \text{(A-34)}$$

This expression is also:

$$d\Phi(\boldsymbol{r_o}, t) = \oint_{\Gamma(r_o)} \boldsymbol{B}(\boldsymbol{r}, t) \cdot \left((\boldsymbol{dh}(\boldsymbol{r_o}, \boldsymbol{r}) - \boldsymbol{dh}(\boldsymbol{r}, \boldsymbol{r})) \times \boldsymbol{dl}\right) \qquad \text{(A-35)}$$

Using the equation (A-15), this result is equivalent to the equation (A-25). A geometric definition for the variation of the magnetic flux according to the equation (A-35) is represented **Fig. 18**.
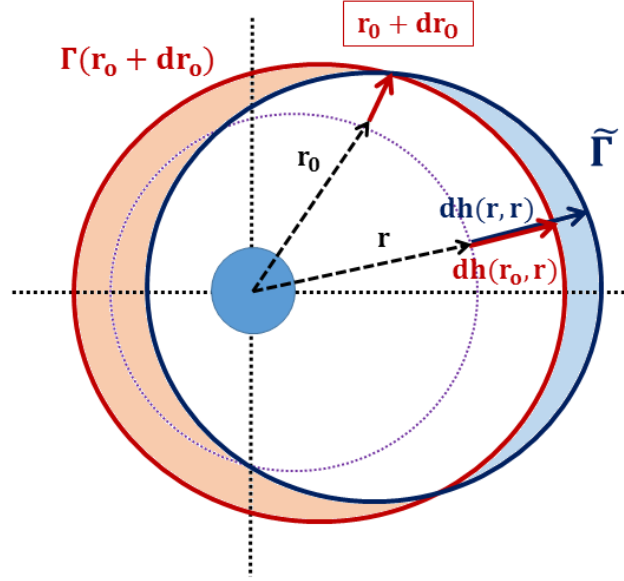
2744
2745 **Fig. 18** Geometric interpretation of the variation of the magnetic flux
2746

2747 A.4. Reformulation in terms of deviation from the average
2748

2749 Noticing that the drift velocity of a guiding center trapped in a magnetic field in stationary
2750 conditions in the absence of electric fields is:

$$V_{D,s}(\boldsymbol{r},t) = -\frac{M}{\gamma q} \frac{\nabla B(\boldsymbol{r},t) \times \boldsymbol{e_o}}{B(\boldsymbol{r},t)} \tag{A-36}$$

2751 And introducing the infinitesimal time step spent along the drift contour $d\tau$ such that

$$|d\tau| = \frac{dl}{|V_{D,s}(\boldsymbol{r},t)|} \tag{A-37}$$

2752 The equation (A-25) becomes:

$$\frac{d\Phi}{dt}(\boldsymbol{r_o},t) = \int_0^{\tau_D} \frac{M}{\gamma q} \left(\frac{dB}{dt}(\boldsymbol{r},t) - \frac{dB}{dt}(\boldsymbol{r_o},t) \right) d\tau \tag{A-38}$$

2753 Let us introduce the linear operator $[\quad]_D$ to denote the spatial drift average along the guiding
2754 drift contour Γ. It is defined by

$$[f]_D(t) = \frac{1}{\tau_D} \int_0^{\tau_D} f(\boldsymbol{r}(\tau),t) d\tau \tag{A-39}$$

2755 This operation determines the spatial average of the quantity f along the drift contour Γ,
2756 weighted by the time spent drifting through each location under stationary conditions.
2757 Thus

$$\frac{d\Phi}{dt}(\boldsymbol{r_o}, t) = \frac{\tau_D}{q}\left(\left[\frac{M}{\gamma}\frac{dB}{dt}\right]_D(t) - \frac{M}{\gamma}\frac{dB}{dt}(\boldsymbol{r_o}, t)\right) \tag{A-40}$$

2758
2759 In the case of an equatorial guiding center trapped in a magnetic field in the absence of
2760 electrostatic fields

$$\frac{M}{\gamma}\frac{dB}{dt} = \frac{d\varepsilon}{dt} \tag{A-41}$$

2761 where ε is the total energy of the guiding center. Thus, we obtain that

$$\frac{d\Phi}{dt}(\boldsymbol{r_o}, t) = \frac{\tau_D}{q}\left(\left[\frac{d\varepsilon}{dt}\right]_D(t) - \frac{d\varepsilon}{dt}(\boldsymbol{r_o}, t)\right) \tag{A-42}$$

2762 This expression is identical to the one derived by Northrop (1963, eq (3.80), p.64). It is valid in
2763 the most general case (e.g., Cary and Brizard 2009, p.717; Lejosne et al. 2012; Lejosne 2013).
2764 As a result,

$$\frac{dL^*}{dt}(\boldsymbol{r_o}, t) = \frac{L^{*2}}{q\Omega B_E R_E^2}\left(\left[\frac{d\varepsilon}{dt}\right]_D(t) - \frac{d\varepsilon}{dt}(\boldsymbol{r_o}, t)\right) \tag{A-43}$$

2765 where $\Omega = 2\pi/\tau_D$ is the population drift frequency.
2766

REFERENCES

A.F. Ali, S.R. Elkington, W. Tu, L.G. Ozeke, A.A. Chan, R.H.W. Friedel, Magnetic field power spectra and magnetic radial diffusion coefficients using CRRES magnetometer data. J. Geophys. Res. Space Physics, 120: 973–995 (2015). https://doi.org/10.1002/2014JA020419

A.F. Ali, D.M. Malaspina, S.R. Elkington, A.N. Jaynes, A.A. Chan, J. Wygant, C.A. Kletzing, Electric and magnetic radial diffusion coefficients using the Van Allen probes data. J. Geophys. Res. Space Physics, 121, 9586–9607 (2016). https://doi.org/10.1002/2016JA023002

M. Andriopoulou, et al., A noon-to-midnight electric field and nightside dynamics in Saturn's inner magnetosphere, using microsignature observations. Icarus, 220, 503–513 (2012). https://doi.org/10.1016/j.icarus.2012.05.010

M. Andriopoulou, et al., Spatial and temporal dependence of the convective electric field in Saturn's inner magnetosphere. Icarus, 229, 57–70 (2014). https://doi.org/10.1016/j.icarus.2013.10.028

A.R. Azari, M.W. Liemohn, X. Jia, M.F. Thomsen, D.G. Mitchell, N. Sergis, et al., Interchange injections at Saturn: Statistical survey of energetic H^+ sudden flux intensifications. J. Geophys. Res. Space Physics, 123, 4692–4711 (2018). https://doi.org/10.1029/2018JA025391

D.N. Baker, S. Kanekal, J.B. Blake, B. Klecker, G. Rostoker, Satellite anomalies linked to electron increase in the magnetosphere, Eos Trans., AGU, 75, 404 (1994). https://doi.org/10.1029/94EO01038

F. Bagenal, R.J. Wilson, S. Siler, W.R. Paterson, W.S. Kurth, Survey of Galileo plasma observations in Jupiter's plasma sheet. J. Geophys. Res. Planets, 121 (2016). https://doi.org/10.1002/2016JE005009

W. Baumjohann, G. Paschmann, H. Lühr, Characteristics of High-Speed Ion Flows in the Plasma Sheet, J. Geophys. Res., 95, A4, 3801-3809 (1990). https://doi.org/10.1029/JA095iA04p03801

T. Beutier, D. Boscher, A three-dimensional analysis of the electron radiation belt by the Salammbô code. J. Geophys. Res., 100 (A8), 14853–14861 (1995). https://doi.org/10.1029/94JA03066

T.J. Birmingham, F.C. Jones, Identification of moving magnetic field lines. J. Geophys. Res., 73, 5505–5510 (1968). https://doi.org/10.1029/JA073i017p05505

T.J. Birmingham, Convection electric fields and the diffusion of trapped magnetospheric radiation. J. Geophys. Res., 74(9), 2169–2181 (1969). https://doi.org/10.1029/JA074i009p02169

T. Birmingham, et al., The electron diffusion coefficient in Jupiter's magnetosphere. J. Geophys. Res, 79, 1, 87-97 (1974). https://doi.org/10.1029/JA079i001p00087

D.H. Brautigam, J.M. Albert, Radial diffusion analysis of outer radiation belt electrons during the October 9, 1990, magnetic storm. J. Geophys. Res., 105(A1), 291–309 (2000). https://doi.org/10.1029/1999JA900344

D.H. Brautigam, G.P. Ginet, J.M. Albert, J.R. Wygant, D.E. Rowland, A. Ling, J. Bass, CRRES electric field power spectra and radial diffusion coefficients. J. Geophys. Res., 110, A02214 (2005). https://doi.org/10.1029/2004JA010612

N. Brice, T.R. McDonough, Jupiter's radiation belts, Icarus, 18, 206–219 (1973). https://doi.org/10.1016/0019-1035(73)90204-2

A.J. Brizard, A.A. Chan, Relativistic bounce-averaged quasilinear diffusion equation for low-frequency electromagnetic fluctuations. Phys. Plasmas, 8(11), 4762–4771 (2001). https://doi.org/10.1063/1.1408623

W.L. Brown, Observations of the Transient Behavior of Electrons in the Artificial Radiation Belts. In: McCormac B.M. (eds) *Radiation Trapped in the Earth's Magnetic Field. Astrophysics and Space Science Library,* vol 5. Springer, Dordrecht (1966). https://doi.org/10.1007/978-94-010-3553-8_44

J.R. Cary, A.J. Brizard, Hamiltonian theory of guiding-center motion. Rev. Mod. Phys., 81, 2, 693-738 (2009). https://link.aps.org/doi/10.1103/RevModPhys.81.693

C. Cattell, et al. Discovery of very large amplitude whistler-mode waves in Earth's radiation belts. Geophys. Res. Lett., 35, L01105 (2008). https://doi.org/10.1029/2007GL032009

S. Chandrasekhar, Stochastic Problems in Physics and Astronomy. Reviews of Modern Physics, 15, 1 (1943). https://doi.org/10.1103/RevModPhys.15.1

Y. Chen, T. W. Hill, A. M. Rymer, R. J. Wilson, Rate of radial transport of plasma in Saturn's inner magnetosphere. J. Geophys. Res., 115, A10211 (2010). https://doi.org/10.1029/2010JA015412

A.F. Cheng, et al., Energetic ion and electron phase space densities in the magnetosphere of Uranus. J. Geophys. Res., 92, A13, 15315-15328 (1987). https://doi.org/10.1029/JA092iA13p15315

A.F. Cheng, et al., Energetic ion phase space densities in Neptune's magnetosphere. Icarus, 99, 420-429 (1992). https://doi.org/10.1016/0019-1035(92)90157-3

2853   G. Clark, C. Paranicas, D. Santos-Costa, S. Livi, N. Krupp, D.G. Mitchell, E. Roussos, W.-L.
2854   Tseng, Evolution of electron pitch angle distributions across Saturn's middle magnetospheric
2855   region from MIMI/LEMMS. Planet. Space Sci., 104, 18–28 (2014).
2856   https://doi.org/10.1016/j.pss.2014.07.004
2857
2858   G. Clark, B.H. Mauk, C. Paranicas, P. Kollmann, H.T. Smith, Charge states of energetic oxygen
2859   and sulfur ions in Jupiter's magnetosphere. J. Geophys. Res. Space Physics, 121, 2264–2273
2860   (2016). https://doi.org/10.1002/2015JA022257
2861
2862   J.F. Cooper, Nuclear cascades in Saturn's rings - Cosmic ray albedo neutron decay and origins of
2863   trapped protons in the inner magnetosphere. J. Geophys. Res., 88, 3945–3954 (1983).
2864   https://doi.org/10.1029/JA088iA05p03945
2865
2866   J.F. Cooper et al., Local time asymmetry of drift shells for energetic electrons in the middle
2867   magnetosphere of Saturn. Adv. Space Res., 21, 11 1479-1482 (1998).
2868   https://doi.org/10.1016/S0273-1177(98)00022-2
2869
2870   J.F. Cooper, S.J. Sturner, Energetic radiation from galactic cosmic ray interactions with Saturn's
2871   main rings. J. Geophys. Res. Space Physics, 123 (2018). https://doi.org/10.1029/2018JA025583
2872
2873   J.M. Cornwall, Diffusion Processes Influenced by Conjugate-Point Wave Phenomena. Radio
2874   Science, 3 (1968). https://doi.org/10.1002/rds196837740
2875
2876   F.V. Coroniti, Energetic Electrons in Jupiter's Magnetosphere. The Astronomical Journal
2877   Supplement Series, 244, 27, 261-281(1974). https://doi.org/10.1086/190296
2878
2879   S. W. H. Cowley, The Causes of Convection in the Earth's Magnetosphere: A Review of
2880   Developments During the IMS, Reviews of Geophysics and Space Physics, 20, 3, 531-565
2881   (1982). https://doi.org/10.1029/RG020i003p00531
2882
2883   S. W. H. Cowley et al., Jupiter's polar ionospheric flows: Theoretical interpretation, Geophys.
2884   Res. Lett., 30(5), 1220 (2003). https://doi.org/10.1029/2002GL016030
2885
2886   S. W. H. Cowley, et al., Saturn's polar ionospheric flows and their relation to the main
2887   auroral oval, Annales Geophysicae, 22: 1379–1394 (2004).
2888   https://doi.org/10.1029/RG020i003p00531
2889
2890   C.M. Cully, J.W. Bonnell, R.E. Ergun, THEMIS observations of long-lived regions of large-
2891   amplitude whistler waves in the inner magnetosphere. Geophys. Res. Lett., 35, L17S16 (2008).
2892   https://doi.org/10.1029/2008GL033643
2893
2894   G.S. Cunningham, V. Loridan, J.-F. Ripoll, M. Schulz, Neoclassical diffusion of radiation-belt
2895   electrons across very low L-shells. J. Geophys. Res. Space Physics, 123, 2884– 2901 (2018).
2896   https://doi.org/10.1002/2017JA024931
2897

L. Davis Jr., D.B. Chang, On the effect of geomagnetic fluctuations on trapped particles. J. Geophys. Res., 67(6), 2169–2179 (1962). https://doi.org/10.1029/JZ067i006p02169

I. De Pater, C.K. Goertz, Radial diffusion models of energetic electrons and Jupiter's synchrotron radiation 2: Time Variability, J. Geophys. Res., 99, A1, 2271-2287 (1994). https://doi.org/10.1029/93JA02097

I. De Pater, et al., Outburst of Jupiter's synchrotron radiation after the impact of comet Shoemaker-Levy 9, Science, 268, 5219, 1879-1883 (1995). https://doi.org/10.1126/science.11536723

A.J. Dessler, R. Karplus, Some effects of diamagnetic ring currents on Van Allen radiation, J. Geophys. Res., 66(8), 2289–2295 (1961). https://doi.org/10.1029/JZ066i008p02289

A.Y. Drozdov, Y.Y. Shprits, N.A. Aseev, A.C. Kellerman, G.D. Reeves, Dependence of radiation belt simulations to assumed radial diffusion rates tested for two empirical models of radial transport. Space Weather, 15, 150–162 (2017). https://doi.org/10.1002/2016SW001426

M. Dumont et al., Jupiter's equatorward auroral features: Possible signatures of magnetospheric injections, J. Geophys. Res. Space Physics, 119, 10,068–10,077 (2014). https://doi.org/10.1002/2014JA020527

J.W. Dungey, Effects of Electromagnetic Perturbations on Particles Trapped in the Radiation Belts, Space Sci. Rev., 4, 199 (1965). https://doi.org/10.1007/BF00173882

S.R. Elkington, M.K. Hudson, A.A. Chan, Acceleration of relativistic electrons via drift-resonant interaction with toroidal-mode Pc-5 ULF oscillations. Geophys. Res. Lett. (1999). https://doi.org/10.1029/1999GL003659

S.R. Elkington, M.K. Hudson, A.A. Chan, Resonant acceleration and diffusion of outer zone electrons in an asymmetric geomagnetic field. J. Geophys. Res., 108, 1116, A3 (2003). https://doi.org/10.1029/2001JA009202

C.-G. Fälthammar, Effects of time-dependent electric fields on geomagnetically trapped radiation. J. Geophys. Res., 70(11), 2503–2516 (1965). https://doi.org/10.1029/JZ070i011p02503

C.-G. Fälthammar, On the transport of trapped particles in the outer magnetosphere. J. Geophys. Res., 71(5), 1487–1491 (1966). https://doi.org/10.1029/JZ071i005p01487

C.-G. Fälthammar, Radial diffusion by violation of the third adiabatic invariant, in *Earth's Particles and Fields*, edited by B. M. McCormac, pp. 157–169, Reinhold, New York (1968).

C.-G. Fälthammar, F. S. Mozer, On the concept of moving magnetic field lines. Eos Trans. AGU, 88 (2007). https://doi.org/10.1029/2007EO150002

T.A. Farley, Radial diffusion of electrons at low L values. J. Geophys. Res., 74(1), 377–380 (1969a). https://doi.org/10.1029/JA074i001p00377

T.A. Farley, Radial diffusion of starfish electrons. J. Geophys. Res., 74(14), 3591–3600 (1969b). https://doi.org/10.1029/JA074i014p03591

Y. Fei, A.A. Chan, S.R. Elkington, M.J. Wiltberger, Radial diffusion and MHD particle simulations of relativistic electron transport by ULF waves in the September 1998 storm. J. Geophys. Res., 111, A12209 (2006). https://doi.org/10.1029/2005JA011211

R.W. Fillius, C.E. McIlwain, Adiabatic betatron acceleration by a geomagnetic storm. J. Geophys. Res., 72(15), 4011–4015 (1967). https://doi.org/10.1029/JZ072i015p04011

R.W. Fillius, et al., Radiation belts of Jupiter: A second look. Science, 188, 4187, 465-467 (1974). https://doi.org/10.1126/science.188.4187.465

L.A. Frank, J.A. Van Allen, H. K. Hills, A study of charged particles in the Earth's outer radiation zone with explorer 14. J. Geophys. Res., 69(11), 2171–2191 (1964). https://doi.org/10.1029/JZ069i011p02171

L.A. Frank, Inward radial diffusion of electrons of greater than 1.6 million electron volts in the outer radiation zone. J. Geophys. Res., 70(15), 3533–3540 (1965). https://doi.org/10.1029/JZ070i015p03533

S.A. Glauert, R.B. Horne, N.P. Meredith, Three-dimensional electron radiation belt simulations using the BAS Radiation Belt Model with new diffusion models for chorus, plasmaspheric hiss, and lightning-generated whistlers. J. Geophys. Res. Space Physics, 119, 268–289 (2014). https://doi.org/10.1002/2013JA019281

S.A. Glauert, R.B. Horne, N.P. Meredith, A 30-year simulation of the outer electron radiation belt. Space Weather, 16, 1498–1522 (2018). https://doi.org/10.1029/2018SW001981

T.I. Gombosi, D.N. Baker, A. Balogh, et al., Anthropogenic Space Weather. Space Sci Rev 212: 985 (2017). https://doi.org/10.1007/s11214-017-0357-5

T. Gold, Motions in the magnetosphere of the Earth. J. Geophys. Res., 64, 9 (1959). https://doi.org/10.1029/JZ064i009p01219

J.C. Green, M.G. Kivelson, Relativistic electrons in the outer radiation belt: Differentiating between acceleration mechanisms. J. Geophys. Res., 109, A03213 (2004). https://doi.org/10.1029/2003JA010153

2985
2986 J.C. Green, J. Likar, Y. Shprits, Impact of space weather on the satellite industry. Space Weather,
2987 15, 804–818 (2017). https://doi.org/10.1002/2017SW001646
2988
2989 S. Han et al., Investigating solar wind-driven electric field influence on long-term dynamics
2990 of Jovian synchrotron radiation. Journal of Geophysical Research: Space Physics, 123, 9508–
2991 9516 (2018). https://doi.org/ 10.1029/2018JA025849
2992
2993 T.W. Hill, Inertial Limit on Corotation. J. Geophys. Res., 84, A11 (1979).
2994 https://doi.org/10.1029/JA084iA11p06554
2995
2996 T.W. Hill, Longitudinal asymmetry of the Io plasma torus. Geophys. Res. Lett., 10: 969-972
2997 (1983). https://doi.org/10.1029/GL010i010p00969
2998
2999 T.W. Hill, et al., Evidence for rotationally driven plasma transport in Saturn's magnetosphere.
3000 Geophys. Res. Lett.,, 32, L14S10 (2005). https://doi.org/10.1029/2005GL022620
3001
3002 R.H. Holzworth, F. S. Mozer, Direct evaluation of the radial diffusion coefficient near L=6 due
3003 to electric field fluctuations. J. Geophys. Res., 84(A6), 2559–2566 (1979).
3004 https://doi.org/10.1029/JA084iA06p02559
3005
3006 L.L. Hood, Radial diffusion in Saturn's radiation belts - A modeling analysis assuming satellite
3007 and ring E absorption. J. Geophys. Res., 88, 808–818 (1983).
3008 https://doi.org/10.1029/JA088iA02p00808
3009
3010 R.B. Horne, S.A. Glauert, N.P. Meredith, D. Boscher, V. Maget, D. Heynderickx, D. Pitchford,
3011 Space weather impacts on satellites and forecasting the Earth's electron radiation belts with
3012 SPACECAST. Space Weather, 11, 169– 186 (2013). https://doi.org/10.1002/swe.20023
3013
3014 R.B. Horne, D. Pitchford, Space Weather Concerns for All-Electric Propulsion Satellites. Space
3015 Weather, 13, 430– 433 (2015). https://doi.org/10.1002/2015SW001198
3016
3017 R.B. Horne, M.W. Phillips, S.A. Glauert, N.P. Meredith, A.D.P. Hands, K. Ryden, W. Li,
3018 Realistic worst case for a severe space weather event driven by a fast solar wind stream. Space
3019 Weather, 16, 1202–1215 (2018). https://doi.org/10.1029/2018SW001948
3020
3021 C.-L. Huang, H.E. Spence, M.K. Hudson, S.R. Elkington, Modeling radiation belt radial
3022 diffusion in ULF wave fields: 2. Estimating rates of radial diffusion using combined MHD and
3023 particle codes. J. Geophys. Res., 115, A06216 (2010). https://doi.org/10.1029/2009JA01491
3024
3025 M.K. Hudson, S.R. Elkington, J.G. Lyon, C.C. Goodrich, T.J. Rosenberg, Simulation of
3026 Radiation Belt Dynamics Driven by Solar Wind Variations. In Sun-Earth Plasma Connections
3027 (eds J.L. Burch, R.L. Carovillano and S.K. Antiochos) (1999).
3028 https://doi.org/10.1029/GM109p0171
3029

S.A. Jacques, L. Davis Jr., Diffusion Models for Jupiter's Radiation Belt. NASA/Caltech technical report N75-15574, Report Number: NASA-CR-141967, Document ID: 19750007502, (1972). http://hdl.handle.net/2060/19750007502

A.N. Jaynes, D. Malaspina, A.A. Chan, S.R. Elkington, A.F. Ali, M. Bruff, H. Zhao, D.N. Baker, X. Li, S. Kanekal, Battle Royale: VLF-driven local acceleration vs ULF driven radial transport. AGU Fall Meeting Abstracts (2018a). https://agu.confex.com/agu/fm18/meetingapp.cgi/Paper/369848

A.N. Jaynes, A.F. Ali, S.R. Elkington, D.M. Malaspina, D.N. Baker, X. Li, et al., Fast diffusion of ultrarelativistic electrons in the outer radiation belt: 17 March 2015 storm event. Geophys. Res. Lett., 45, 10,874–10,882 (2018b). https://doi.org/10.1029/2018GL079786

S. Jurac, J.D. Richardson, A self-consistent model of plasma and neutrals at Saturn: Neutral cloud morphology. J. Geophys. Res., 110, A09220 (2005). https://doi.org/10.1029/2004JA010635.

P.J. Kellogg, Possible explanation of the radiation observed by Van Allen at high altitudes in satellites. Nuovo cimiento, [10] 11, 48 (1959a). https://doi.org/10.1007/BF02724906

P.J. Kellogg, Van Allen Radiation of Solar Origin. Nature, Lond. 183, 1295-7 (1959b). https://doi.org/10.1038/1831295a0.

C. F. Kennel, F. Engelmann, Velocity space diffusion from weak plasma turbulence in a magnetic field. The Physics of Fluids, 9(12), 2377-2388 (1966). https://doi.org/10.1063/1.1761629

H.-J. Kim, A.A. Chan, Fully adiabatic changes in storm time relativistic electron fluxes. J. Geophys. Res., 102(A10), 22107–22116 (1997). https://doi.org/10.1029/97JA01814

K.C. Kim, Y. Shprits, D. Subbotin, B. Ni, Understanding the dynamic evolution of the relativistic electron slot region including radial and pitch angle diffusion. J. Geophys. Res., 116, A10214 (2011). https://doi.org/10.1029/2011JA016684

P. Kollmann et al., Energetic particle phase space densities at Saturn: Cassini observations and interpretations. J.Geophys. Res., 116, A05222 (2011). https://doi.org/10.1029/2010JA016221

P. Kollmann, E. Roussos, C. Paranicas, N. Krupp, D. K. Haggerty, Processes forming and sustaining Saturn's proton radiation belts. Icarus, 222, 323–341 (2013). https://doi.org/10.1016/j.icarus.2012.10.033

P. Kollmann, E. Roussos, A. Kotova, C. Paranicas, N. Krupp, The evolution of Saturn's radiation belts modulated by changes in radial diffusion. Nature Astronomy 1, 872–877 (2017). https://doi.org/10.1038/s41550-017-0287-x

P. Kollmann, E. Roussos, C.P. Paranicas, E.E. Woodfield, B.H. Mauk, G. Clark, D.C. Smith, J. Vandegriff, Electron acceleration to MeV energies at Jupiter and Saturn. J. Geophys. Res. Space Phys, 123, 9110– 9129 (2018). https://doi.org/10.1029/2018JA025665

H. Korth, M.F. Thomsen, J.E. Borovsky, D.J. McComas, Plasma sheet access to geosynchronous orbit. J. Geophys. Res., 104(A11), 25047– 25061 (1999). https://doi.org/10.1029/1999JA900292

N. Krupp et al., Dynamics of the Jovian Magnetosphere. In: *Jupiter. The Planet, Satellites and Magnetosphere* (2005). Cambridge University Press. ISBN: 0-521-81808-7

H.R. Lai et al., Transport of magnetic flux and mass in Saturn's inner magnetosphere, J. Geophys. Res. Space Physics, 121, 3050–3057 (2016). https://doi.org/10.1002/2016JA022436

L.J. Lanzerotti, C.G. Maclennan, M. Schulz, Radial diffusion of outer-zone electrons: An empirical approach to third-invariant violation. J. Geophys. Res., 75(28), 5351–5371 (1970). https://doi.org/10.1029/JA075i028p05351

L.J. Lanzerotti, C.G. Maclennan, M. Schulz, Reply [to "Comments on 'Radial diffusion of outer-zone electrons'"]. J. Geophys. Res., 76(22), 5371–5373 (1971). https://doi.org/10.1029/JA076i022p05371

L.J. Lanzerotti, C.G. Morgan, ULF geomagnetic power near L = 4: 2. Temporal variation of the radial diffusion coefficient for relativistic electrons. J. Geophys. Res., 78(22), 4600–4610 (1973). https://doi.org/10.1029/JA078i022p04600

L.J. Lanzerotti, D.C. Webb, C.W. Arthur, Geomagnetic field fluctuations at synchronous orbit 2. Radial diffusion. J. Geophys. Res., 83(A8), 3866–3870 (1978). https://doi.org/10.1029/JA083iA08p03866

S. Lejosne, Modélisation du phénomène de diffusion radiale au sein des ceintures de radiation terrestres par technique de changement d'échelle. PhD thesis, Université de Toulouse, France (2013). https://hal.archives-ouvertes.fr/tel-01132913/document

S. Lejosne, Analytic expressions for radial diffusion. Journal of Geophysical Research: Space Physics, 124 (2019). https://doi.org/10.1029/2019JA026786

S. Lejosne, D. Boscher, V. Maget, G. Rolland, Bounce-averaged approach to radial diffusion modeling: From a new derivation of the instantaneous rate of change of the third adiabatic invariant to the characterization of the radial diffusion process. J. Geophys. Res., 117, A08231 (2012). https://doi.org/10.1029/2012JA018011

S. Lejosne, D. Boscher, V. Maget, G. Rolland, Deriving electromagnetic radial diffusion coefficients of radiation belt equatorial particles for different levels of magnetic activity based on

magnetic field measurements at geostationary orbit. J. Geophys. Res. Space Physics, 118, 3147–3156 (2013). https://doi.org/10.1002/jgra.50361

Z. Li, M. Hudson, M. Patel, M. Wiltberger, A. Boyd, D.Turner, ULF wave analysis and radial diffusion calculation using a global MHD model for the 17 March 2013 and 2015 storms, J. Geophys. Res. Space Physics, 122, 7353– 7363 (2017). https://doi.org/10.1002/2016JA023846

A.J. Lichtenberg, M.A. Lieberman, *Regular and Chaotic Dynamics*, Second edition, Applied Mathematical Sciences, Springer-Verlag, New York (1992). https://doi.org/10.1007/978-1-4757-2184-3

W.W. Liu, G. Rostoker, D. N. Baker, Internal acceleration of relativistic electrons by large-amplitude ULF pulsations. J. Geophys. Res., 104(A8), 17391–17407 (1999). https://doi.org/10.1029/1999JA900168

W. Liu, W. Tu, X. Li, T. Sarris, Y. Khotyaintsev, H. Fu, H. Zhang, Q. Shi, On the calculation of electric diffusion coefficient of radiation belt electrons with in situ electric field measurements by THEMIS. Geophys. Res. Lett., 43, 1023–1030 (2016). https://doi.org/10.1002/2015GL067398

L. Lorenzato, A. Sicard, S. Bourdarie, A physical model for electron radiation belts of Saturn. J. Geophys. Res. Space Physics 117, A08214 (2012). https://doi.org/10.1029/2012JA017560

X. Ma et al., Flux tube entropy and specific entropy in Saturn's magnetosphere. Journal of Geophysical Research: Space Physics, 124, 1593–1611 (2019). https://doi.org/10.1029/2018JA026150

V. Maget, S. Bourdarie, D. Boscher, R.H.W. Friedel, Data assimilation of LANL satellite data into the Salammbô electron code over a complete solar cycle by direct insertion. Space Weather, vol. 5, no. S10003 (2007). https://doi.org/10.1029/2007SW000322

V. Maget, S. Bourdarie, D. Boscher, Direct data assimilation over solar cycle time-scales to improve proton radiation belt models. IEEE Trans. Nucl. Sci., vol. 55, no. 4, pp. 2188–2196 (2008). https://doi.org/10.1109/TNS.2008.921928

I.R. Mann, et al., Explaining the dynamics of the ultra-relativistic third Van Allen radiation belt. Nature Phys 12:978–983 (2016). https://doi.org/10.1038/nphys3799

I.R. Mann, et al. Reply to 'The dynamics of Van Allen belts revisited'. Nature Physics, 14(2), 103–104 (2018). https://doi.org/10.1038/nphys4351

R.A. Mathie, I.R. Mann, A correlation between extended intervals of Ulf wave power and storm-time geosynchronous relativistic electron flux enhancements. Geophys. Res. Lett.,27, 3261 (2000). https://doi.org/10.1029/2000GL003822

3163 B.H. Mauk, et al., Fundamental Plasma Processes in Saturn's Magnetosphere, In: Saturn from
3164 Cassini-Huygens, Springer Science+Business Media B.V. (2009). https://doi.org/10.1007/978-1-
3165 4020-9217-6_11
3166
3167 B.H. Mauk, Comparative investigation of the energetic ion spectra comprising the
3168 magnetospheric ring currents of the solar system, J. Geophys. Res. Space Physics, 119 (2014).
3169 https://doi.org/10.1002/2014JA020392
3170
3171 G.D. Mead, Deformation of the geomagnetic field by the solar wind. J. Geophys. Res., 69(7),
3172 1181– 1195 (1964). https://doi.org/10.1029/JZ069i007p01181
3173
3174 G.D. Mead, W.N. Hess, Jupiter's radiation belts and the sweeping effect of its satellites, J.
3175 Geophys. Res., 78(16), 2793– 2811 (1973). https://doi.org/10.1029/JA078i016p02793
3176
3177 D.G. Mitchell, et al., Injection, Interchange, and Reconnection: Energetic particle observations in
3178 Saturn's magnetosphere, In: *Magnetotails in the Solar System*, John Wiley & Sons Inc. (2015).
3179 ISBN 9781118842324. https://doi.org/10.1002/9781118842324.ch19
3180
3181 A. Mogro-Campero, Absorption of radiation belt particles by the inner satellites of Jupiter, In:
3182 *Jupiter: Studies of the interior, atmosphere, magnetosphere, and satellites*. The University of
3183 Arizona Press, ISBN 0-8165-530-6 (1976). http://adsabs.harvard.edu/abs/1976jsia.coll.1190M
3184
3185 F.S. Mozer, Power spectra of the magnetospheric electric field. J. Geophys. Res., 76(16), 3651–
3186 3667 (1971). https://doi.org/10.1029/JA076i016p03651
3187
3188 F.S. Mozer, et al., Direct observation of radiation-belt electron acceleration from electron-volt
3189 energies to megavolts by nonlinear whistlers. Physical review letters, 113(3), 035001 (2014).
3190 https://doi.org/10.1103/PhysRevLett.113.035001
3191
3192 M.P. Nakada, G. D. Mead, Diffusion of protons in the outer radiation belt. J. Geophys.
3193 Res., 70(19), 4777–4791 (1965). https://doi.org/10.1029/JZ070i019p04777
3194
3195 M.P. Nakada, J.W. Dungey, W.N. Hess, On the origin of outer-belt protons: 1..J. Geophys. Res.,
3196 70(15), 3529–3532 (1965). https://doi.org/10.1029/JZ070i015p03529
3197
3198 Q. Nénon, A. Sicard, S. Bourdarie, A new physical model of the electron radiation belts of
3199 Jupiter inside Europa's orbit. J. Geophys. Res Space Physics, 122, 5148– 5167 (2017).
3200 https://doi.org/10.1002/2017JA023893
3201
3202 Q. Nénon, A. Sicard, P. Kollmann, H.B. Garrett, S.P.A. Sauer, C. Paranicas, A physical model of
3203 the proton radiation belts of Jupiter inside Europa's orbit. J. Geophys. Res. Space Physics, 123,
3204 3512–3532 (2018). https://doi.org/10.1029/2018JA025216
3205
3206 W.A. Newcomb, Motion of magnetic lines of Force. Annals of Physics, 3, 347-385 (1958).
3207 https://doi.org/10.1016/0003-4916(58)90024-1
3208

3209 L.L. Newkirk, M. Walt, Radial diffusion coefficient for electrons at $1.76 < L < 5$. J. Geophys.
3210 Res., 73(23), 7231–7236 (1968a). https://doi.org/10.1029/JA073i023p07231
3211
3212 L.L. Newkirk, M. Walt, Radial diffusion coefficient for electrons at low L values. J. Geophys.
3213 Res., 73(3), 1013–1017 (1968b). https://doi.org/10.1029/JA073i003p01013
3214
3215 T.G. Northrop, *The Adiabatic Motion of Charged Particles*. Wiley-
3216 Interscience, Hoboken, N. J. ISBN-13: 978-0470651391 (1963).
3217
3218 T.G. Northrop, E. Teller, Stability of the adiabatic motion of charged particles in the Earth's
3219 field. Phys. Rev., 117, 215–225 (1960). https://doi.org/10.1103/PhysRev.117.215
3220
3221 T.P. O'Brien, J.E. Mazur, T.B. Guild. What the Satellite Design Community Needs From the
3222 Radiation Belt Science Community. In *Dynamics of the Earth's Radiation Belts and Inner*
3223 *Magnetosphere* (eds D. Summers, I. R. Mann, D.N. Baker and M. Schulz) (2013).
3224 https://doi.org/10.1029/2012GM001316
3225
3226 T.P. O'Brien, Breaking all the invariants: Anomalous electron radiation belt diffusion by pitch
3227 angle scattering in the presence of split magnetic drift shells. Geophys. Res. Lett., 41, 216– 222
3228 (2014). https://doi.org/10.1002/2013GL058712
3229
3230 T.P. O'Brien et al., Changes in AE9/AP9-IRENE Version 1.5, in *IEEE Transactions on Nuclear*
3231 *Science*, vol. 65, no. 1, pp. 462-466 (2018). https://doi.org/10.1109/TNS.2017.2771324
3232
3233 L. Olifer, I.R. Mann, L.G. Ozeke, I.J. Rae, S.K. Morley, On the relative strength of electric and
3234 magnetic ULF wave radial diffusion during the March 2015 geomagnetic storm. J. Geophys.
3235 Res. Space Physics, 124, 2569– 2587 (2019). https://doi.org/10.1029/2018JA026348
3236
3237 L.G. Ozeke, I.R. Mann, I.J. Rae, Mapping guided Alfvén wave magnetic field amplitudes
3238 observed on the ground to equatorial electric field amplitudes in space. J. Geophys. Res., 114,
3239 A01214 (2009). https://doi.org/10.1029/2008JA013041
3240
3241 L.G. Ozeke, et al., ULF wave derived radiation belt radial diffusion coefficients. J. Geophys.
3242 Res., 117, A04222 (2012). https://doi.org/10.1029/2011JA017463
3243
3244 L.G. Ozeke, I.R. Mann, K.R. Murphy, I.J. Rae, D.K. Milling, Analytic expressions for ULF
3245 wave radiation belt radial diffusion coefficients. J. Geophys. Res. Space Physics, 119, 1587–
3246 1605 (2014). https://doi.org/10.1002/2013JA019204
3247
3248 M.K. Öztürk, R.A. Wolf, Bifurcation of drift shells near the dayside magnetopause. J. Geophys.
3249 Res., 112, A07207 (2007). https://doi.org/10.1029/2006JA012102
3250
3251 M. Paonessa, Voyager observations of ion phase space densities in the Jovian magnetosphere. J.
3252 Geophys. Res., 90, A1, 521-525 (1985). https://doi.org/10.1029/JA090iA01p00521
3253

3254 C. Paranicas, et al., Effects of radial motion on interchange injections at Saturn. Icarus 264, 342–
3255 351 (2016). https://doi.org/10.1016/j.icarus.2015.10.002
3256
3257 E.N. Parker, Geomagnetic fluctuations and the form of the outer zone of the Van Allen radiation
3258 belt. J. Geophys. Res., 65(10), 3117–3130 (1960). https://doi.org/10.1029/JZ065i010p03117
3259
3260 K.L. Perry, M.K. Hudson, S.R. Elkington, Incorporating spectral characteristics of Pc5 waves
3261 into three-dimensional radiation belt modeling and the diffusion of relativistic electrons. J.
3262 Geophys. Res., 110, A03215 (2005). https://doi.org/10.1029/2004JA010760
3263
3264 K.L. Perry, M.K. Hudson, S.R. Elkington, Correction to "Incorporating spectral characteristics of
3265 Pc5 waves into three-dimensional radiation belt modeling and the diffusion of relativistic
3266 electrons". J. Geophys. Res., 111, A11228 (2006). https://doi.org/:10.1029/2006JA012040
3267
3268 D.H. Pontius Jr., T.W. Hill, Rotation driven plasma transport: The coupling of macroscopic
3269 motion and microdiffusion. J. Geophys. Res, 94, A11, 15041-15053 (1989).
3270 https://doi.org/10.1029/JA094iA11p15041
3271
3272 D.H. Pontius Jr., R.A. Wolf, Transient Flux Tubes in the terrestrial magnetosphere, Geophys.
3273 Res. Lett., 17, 1, 49-52 (1990). https://doi.org/10.1029/GL017i001p00049
3274
3275 M. Qin, X. Zhang, B. Ni, H. Song, H. Zou, Y. Sun, Solar cycle variations of trapped proton flux
3276 in the inner radiation belt. J. Geophys. Res. Space Physics, 119, 9658–9669 (2014).
3277 https://doi.org/10.1002/2014JA020300
3278
3279 J.D. Richardson, A Quantitative Model of Plasma in Neptune's Magnetosphere. Geophys. Res.
3280 Lett., 20, 14, 1467-1470 (1993). https://doi.org/10.1029/93GL01353
3281
3282 P. Riley, R.A. Wolf, Comparison of diffusion and particle drift descriptions of radial transport in
3283 the Earth's inner magnetosphere. J. Geophys. Res., 97(A11), 16865–16876
3284 (1992). https://doi.org/10.1029/92JA01538
3285
3286 J.G. Roederer, On the adiabatic motion of energetic particles in a model magnetosphere. J.
3287 Geophys. Res., 72(3), 981– 992 (1967). https://doi.org/10.1029/JZ072i003p00981
3288
3289 J.G. Roederer, *Dynamics of Geomagnetically Trapped Radiation*. New York: Springer (1970).
3290 https://doi.org/10.1007/978-3-642-49300-3
3291
3292 J.G. Roederer, Geomagnetic field distortions and their effects on radiation belt particles. Rev.
3293 Geophys., 10(2), 599–630 (1972). https://doi.org/10.1029/RG010i002p00599
3294
3295 J.G. Roederer, M. Schulz, Effect of shell splitting on radial diffusion in the magnetosphere. J.
3296 Geophys. Res., 74(16), 4117– 4122 (1969). https://doi.org/10.1029/JA074i016p04117
3297
3298 J.G. Roederer, M. Schulz, Splitting of drift shells by the magnetospheric electric field. J.
3299 Geophys. Res., 76, 4, 1055-1059 (1971). https://doi.org/10.1029/JA076i004p01055

3300

3301 J.G. Roederer, H.H. Hilton, M. Schulz, Drift shell splitting by internal geomagnetic multipoles.
3302 J. Geophys. Res., 78, 133-144 (1973). https://doi.org/10.1029/JA078i001p00133

3303

3304 J.G. Roederer, H. Zhang, *Dynamics of Magnetically Trapped Particles, Foundations of the*
3305 *Physics of Radiation Belts and Space Plasmas*, Astrophysics and Space Science Library, vol.
3306 403, Springer-Verlag, Berlin, Heidelberg (2014). https://doi.org/10.1007/978-3-642-41530-2

3307

3308 J.G. Roederer, S. Lejosne, Coordinates for representing radiation belt particle flux. J. Geophys.
3309 Res. Space Physics, 123, 1381–1387 (2018). https://doi.org/10.1002/2017JA025053

3310

3311 G. Rostoker, S. Skone, D.N. Baker, On the origins of relativistic electrons in the magnetosphere
3312 associated with some geomagnetic storms. Geophys. Res. Lett., 25, 3701 (1998).
3313 https://doi.org/10.1029/98GL02801

3314

3315 E. Roussos, et al., Electron microdiffusion in the Saturnian radiation belts: Cassini
3316 MIMI/LEMMS observations of energetic electron absorption by the icy moons. J. Geophys. Res.
3317 (Space Physics), 112, 6214 (2007). https://doi.org/862 10.1029/2006JA012027

3318

3319 E. Roussos, et al., Discovery of a transient radiation belt at Saturn. J. Geophys. Res., 35, L22106
3320 (2008). https://doi.org/10.1029/2008GL035767

3321

3322 E. Roussos, et al., Energetic electron microsignatures as tracers of radial flows and dynamics in
3323 Saturn's innermost magnetosphere. J. Geophys. Res., 115, A03202 (2010).
3324 https://doi.org/10.1029/2009JA014808

3325

3326 E. Roussos, et al., The variable extension of Saturn's electron radiation belts. Planetary and
3327 Space Science, 104 ,3-17 (2014). https://doi.org/10.1016/j.pss.2014.03.021

3328

3329 E. Roussos, et al., Evidence for dust-driven, radial plasma transport in Saturn's inner radiation
3330 belts, Icarus, 274, 272–283 (2016). http://doi.org/10.1016/j.icarus.2016.02.054

3331

3332 E. Roussos, et al., A radiation belt of energetic protons located between Saturn and its rings.
3333 Science, 362(6410) (2018). https://doi.org/10.1126/science.aat1962

3334

3335 E. Roussos, et al., Drift-resonant, relativistic electron acceleration at the outer planets: Insights
3336 from the response of Saturn's radiation belts to magnetospheric storms. Icarus, 305, 160 – 173
3337 (2018b). https://doi.org/10.1016/j.icarus.2018.01.016

3338

3339 R.Z. Sagdeev, A.A, Galeev, *Nonlinear Plasma Theory* (edited by T. M. O'Neil and D. L. Book),
3340 W. A. Benjamin, New York (1969).

3341

3342 D. Santos-Costa, S.A. Bourdarie, Modeling the inner Jovian electron radiation belt including
3343 non-equatorial particles. Planetary and Space Science, Volume 49, Issues 3–4, 2001, Pages 303-
3344 312, ISSN 0032-0633 (2001). https://doi.org/10.1016/S0032-0633(00)00151-3

3345

D. Santos-Costa, M. Blanc, S. Maurice, S.J. Bolton, Modeling the electron and proton radiation belts of Saturn. Geophys. Res. Lett., 30, 2059 (2003). https://doi.org/10.1029/2003GL017972

D. Sawyer, J. Vette, AP-8 trapped proton environment for solar maximum and solar minimum. National Space Science Data Center, Report 76-06, Greenbelt, Maryland (1976).

M. Schulz, Drift-shell splitting at arbitrary pitch angle. J. Geophys. Res., 77(4), 624–634 (1972). https://doi.org/10.1029/JA077i004p00624

M. Schulz, The Magnetosphere, in *Geomagnetism*. Academic Press, J.A. Jacobs, Pages 87-293, ISBN 9780123786746 (1991). https://doi.org/10.1016/B978-0-12-378674-6.50008-X.

M. Schulz, Particle drift and loss rates under strong pitch angle diffusion in Dungey's model magnetosphere. J. Geophys. Res., 103, A1, 61-67 (1998). https://doi.org/10.1029/97JA02042

M. Schulz, A. Eviatar, Diffusion of equatorial particles in the outer radiation zone. J. Geophys. Res., 74(9), 2182–2192 (1969). https://doi.org/10.1029/JA074i009p02182

M. Schulz, and L.J. Lanzerotti, *Particle Diffusion in the Radiation Belts*. Springer-Verlag Berlin Heidelberg (1974). https://doi.org/10.1007/978-3-642-65675-0

R.S. Selesnick, E.C. Stone, Energetic electrons at Uranus: Bimodal diffusion in a satellite limited radiation belt. J. Geophys. Res., 96, A4, 5651-5665(1991). https://doi.org/10.1029/90JA02696

R.S. Selesnick, E.C. Stone, Radial diffusion of relativistic electrons in Neptune's magnetosphere. Geophys. Res. Lett., 21, 15, 1579-1582 (1994). https://doi.org/10.1029/94GL01357

R.S. Selesnick, M.D. Looper, R.A. Mewaldt, A theoretical model of the inner proton radiation belt. Space Weather, 5, S04003 (2007). https://doi.org/10.1029/2006SW000275

R.S. Selesnick, M.K. Hudson, B.T. Kress, Direct observation of the CRAND proton radiation belt source. J. Geophys. Res. Space Physics, 118, 7532–7537 (2013). https://doi.org/10.1002/2013JA019338

R.S. Selesnick, Y.-J. Su, J.B. Blake, Control of the innermost electron radiation belt by large-scale electric fields. J. Geophys. Res. Space Physics, 121 (2016). https://doi.org/10.1002/2016JA022973

V.A. Sergeev, V. Angelopoulos, J.T Gosling, C.A. Cattell, C. A., C.T. Russell, Detection of localized, plasma-depleted flux tubes or bubbles in the midtail plasma sheet. J. Geophys. Res., 101, A5, 10817-10825 (1996). https://doi.org/10.1029/96JA00460

Y.Y. Shprits et al., Unusual Stable Trapping of the Ultra-Relativistic Electrons in the Van Allen Radiation Belts. Nature Phys., 9, 699–703 (2013). https://doi.org/10.1038/NPHYS2760

Y.Y. Shprits et al., Combined convective and diffusive simulations: VERB-4D comparison with 17 March 2013 Van Allen Probes observations, Geophys. Res. Lett., 42, 9600–9608 (2015). https://doi.org/10.1002/2015GL065230

Y.Y. Shprits et al., The dynamics of Van Allen belts revisited. Nature Physics, 14, 102–103 (2018). https://doi.org/10.1038/nphys4350

S.F. Singer, Trapped albedo theory of the radiation belt. *Phys. Rev. Lett., 1*, 181 (1958). https://doi.org/10.1103/PhysRevLett.1.300

G.L. Siscoe, D. Summers, Centrifugally driven diffusion of iogenic plasma. J. Geophys. Res., 86, A10, 8471-8479 (1981a). https://doi.org/10.1029/JA086iA10p08471

G.L. Siscoe, et al., Ring current impoundment of the Io plasma torus. J. Geophys. Res., 86, A10, 8480-8484 (1981b). https://doi.org/10.1029/JA086iA10p08480

E.C. Sittler, et al., Ion and neutral sources and sinks within Saturn's inner magnetosphere: Cassini results. Planetary and Space Science, 56, 3–18 (2008). https://doi.org/10.1016/j.pss.2007.06.006

D.J. Southwood, M.G. Kivelson, Magnetospheric interchange instability. J. Geophys. Res., 92(A1), 109– 116 (1987). https://doi.org/10.1029/JA092iA01p00109

D.J. Southwood, M.G. Kivelson, Magnetospheric interchange motions. J. Geophys. Res., 94 (A1), 299– 308 (1989). https://doi.org/10.1029/JA094iA01p00299

E.C. Stone, The physical significance and application of L, Bo, and Ro to geomagnetically trapped particles. J. Geophys. Res., 68(14), 4157–4166 (1963). https://doi.org/10.1029/JZ068i014p04157

Z. Su, F. Xiao, H. Zheng, S. Wang, STEERB: A three-dimensional code for storm-time evolution of electron radiation belt. J. Geophys. Res., 115, A09208 (2010). https://doi.org/10.1029/2009JA015210

Z. Su, et al., Ultra-low-frequency wave-driven diffusion of radiation belt relativistic electrons. Nature Communications, 6, 10096 (2015). https://doi.org/10.1038/ncomms10096

D.A. Subbotin, Y.Y. Shprits, Three-dimensional modeling of the radiation belts using the Versatile Electron Radiation Belt (VERB) code. Space Weather, 7 :10001 (2009). https://doi.org/10.1029/2008SW000452

D. A. Subbotin, Y.Y. Shprits. Three-dimensional radiation belt simulations in terms of adiabatic invariants using a single numerical grid. J. Geophys. Res., 117, A05205 (2012). https://doi.org/10.1029/2011JA017467

3436   D. Summers, C. Ma, Rapid acceleration of electrons in the magnetosphere by fast-mode MHD
3437   waves. J. Geophys. Res., 105(A7), 15887–15895 (2000). https://doi.org/10.1029/1999JA000408
3438
3439   D. Summers, G.L. Siscoe, Coupled low-energy - ring current plasma diffusion in the Jovian
3440   magnetosphere. J. Geophys. Res. 90, A, 2665-2671 (1985).
3441   https://doi.org/10.1029/JA090iA03p02665
3442
3443   G.I. Taylor. Diffusion by continuous movements. Proc. London Math. Soc., 2, 196-211 (1922).
3444   https://doi.org/10.1112/plms/s2-20.1.196
3445
3446   M.F. Thomsen, C.K. Goertz, J.A. Van Allen, On Determining Magnetospheric Diffusion
3447   Coefficients From the Observed Effects of Jupiter's Satellite Io. J. Geophys. Res., 82, 35 (1977).
3448   https://doi.org/10.1029/JA082i035p05541
3449
3450   M.F. Thomsen, J.A. Van Allen, Motion of trapped electrons and protons in Saturn's inner
3451   magnetosphere. J. Geophys. Res., 85, 5831–5834 (1980).
3452   https://doi.org/10.1029/JA085iA11p05831
3453
3454   M.F. Thomsen, et al., Saturn's inner magnetospheric convection pattern: Further evidence. J.
3455   Geophys. Res., 117, A09208 (2012). https://doi.org/10.1029/2011JA017482
3456
3457   R.M. Thorne, Radiation belt dynamics: The importance of wave-particle interactions. Geophys.
3458   Res. Lett., 37, L22107 (2010). https://doi.org/10.1029/2010GL044990
3459
3460   A.D. Tomassian, T.A. Farley, A.L. Vampola, Inner-zone energetic-electron repopulation by
3461   radial diffusion. J. Geophys. Res., 77(19), 3441–3454 (1972).
3462   https://doi.org/10.1029/JA077i019p03441
3463
3464   F. Tsuchiya et al., Short-term changes in Jupiter's synchrotron radiation at 325 MHz: Enhanced
3465   radial diffusion in Jupiter's radiation belt driven by solar UV/EUV heating. J. Geophys. Res.,
3466   116, A09202 (2011). https://doi.org/10.1029/2010JA016303
3467
3468   W. Tu, et al., Quantifying radial diffusion coefficients of radiation belt electrons based on global
3469   MHD simulation and spacecraft measurements. J. of Geophys. Res., 117, A10210 (2012).
3470   https://doi.org/10.1029/2012JA017901
3471
3472   W. Tu, et al., Modeling radiation belt electron dynamics during GEM challenge intervals with
3473   the DREAM3D diffusion model. J. Geophys. Res. Space Physics, 118, 6197–6211 (2013).
3474   https://doi.org/10.1002/jgra.50560
3475
3476   A.Y. Ukhorskiy, M.I. Sitnov, Radial transport in the outer radiation belt due to global
3477   magnetospheric compressions. J. Atmos. Sol.-Terr. Phys. 70, 1714 (2008).
3478   https://doi.org/10.1016/j.jastp.2008.07.018
3479

3480 A.Y. Ukhorskiy, M.I. Sitnov, K. Takahashi, B.J. Anderson, Radial transport of radiation belt
3481 electrons due to stormtime pc5 waves. Ann. Geophys. 27, 2173 (2009).
3482 https://doi.org/10.5194/angeo-27-2173-2009

3484 J.A. Van Allen, L.A. Frank, Radiation Around the Earth to a Radial Distance of 107,400 km.
3485 Nature, volume 183, pages 430–434 (1959). https://doi.org/10.1038/183430a0

3487 J.A. Van Allen, et al., Sources and Sinks of Energetic Electrons and Protons in Saturn's
3488 Magnetosphere, J. Geophys. Res., 85, A11, 5679-5694 (1980a).
3489 https://doi.org/10.1029/JA085iA11p05679

3491 J.A. Van Allen, et al., The Energetic Charged Particle Absorption Signature of Mimas. J.
3492 Geophys. Res., 85, A11, 5709-5718 (1980b). https://doi.org/10.1029/JA085iA11p05709

3494 J.A. Van Allen, Energetic particles in the inner magnetosphere of Saturn. In: *Saturn*, The
3495 University of Arizona Press, ISBN 0-8165-0829-1 (1984).

3497 A. Varotsou, et al., Three dimensional test simulations of the outer radiation belt electron
3498 dynamics including electron-chorus resonant interactions, J. Geophys. Res., 113, A12212 (2008).
3499 https://doi.org/10.1029/2007JA012862.

3501 S.N. Vernov, et al., Possible mechanism of production of terrestrial corpuscular radiation under
3502 the action of cosmic rays. Soviet Phys., Doklady,4,154 (1959).

3504 J. Vette, The AE-8 trapped electron model environment. National Space Science Data
3505 Center, Report 91-24, Greenbelt, Maryland (1991).

3507 L.S. Waldrop et al., Three-dimensional convective flows of energetic ions in Jupiter's equatorial
3508 magnetosphere. J. Geophys. Res. Space Physics, 120, 10,506– 10,527 (2015).
3509 https://doi.org/10.1002/2015JA021103

3511 M. Walt, Radial diffusion of trapped particles and some of its consequences. Rev. Geophys.,
3512 9(1), 11–25 (1971a). https://doi.org/10.1029/RG009i001p00011

3514 M. Walt, The radial diffusion of trapped particles induced by fluctuating magnetospheric fields.
3515 Space Sci. Rev., 12: 446 (1971b). https://doi.org/10.1007/BF00171975

3517 M. Walt, L.L. Newkirk, Comments [on "Radial diffusion of outer-zone electrons"]. J. Geophys.
3518 Res., 76(22), 5368–5370 (1971). https://doi.org/10.1029/JA076i022p05368

3520 M. Walt, *Introduction to geomagnetically trapped radiation*. Cambridge University Press
3521 (1994). https://doi.org/10.1017/CBO9780511524981

3523 M. Walt, Source and loss processes for radiation belt particles. in *Radiation Belts: Models and*
3524 *Standards*, vol. 97, edited by J.F. Lemaire, D. Heynderickx, and D.N. Baker, p.1, AGU,
3525 Washington D.C. (1996). https://doi.org/10.1029/GM097p0001

H. I. West Jr., R.M. Buck, G.T. Davidson, The dynamics of energetic electrons in the Earth's outer radiation belt during 1968 as observed by the Lawrence Livermore National Laboratory's Spectrometer on Ogo 5. J. Geophys. Res., 86(A4), 2111–2142 (1981). https://doi.org/10.1029/JA086iA04p02111

R.J. Wilson et al., Evidence from radial velocity measurements of a global electric field in Saturn's inner magnetosphere, J. Geophys. Res. Space Physics, 118, 2122–2132 (2013). https://doi.org/10.1002/jgra.50251

E.E. Woodfield, et al., The origin of Jupiter's outer radiation belt. J. Geophys. Res. Space Physics, 119, 3490–3502 (2014). https://doi.org/10.1002/2014JA019891

E.E. Woodfield, et al., Formation of electron radiation belts at Saturn by Z-mode wave acceleration. Nature Communications,5062, 9, 1, 2041-1723 (2018). https://doi.org/10.1038/s41467-018-07549-4

M. A. Xapsos, P. M. O'Neill and T. P. O'Brien, Near-Earth Space Radiation Models. in *IEEE Transactions on Nuclear Science*, vol. 60, no. 3, pp. 1691-1705 (2013). https://doi.org/10.1109/TNS.2012.2225846